9

Jupiter's Thermosphere and Ionosphere

R. V. Yelle
University of Arizona

S. Miller
University College, London

9.1 INTRODUCTION

Jupiter's upper atmosphere forms the boundary between the lower atmosphere and interplanetary space. As the topmost layer, the thermosphere absorbs solar extreme ultraviolet (EUV) radiation and charged particles from the magnetosphere that cause dissociation and ionization of thermospheric molecules. Subsequent chemistry establishes the ionosphere and the densities of minor, photo- and electrochemically produced constituents. Densities are low in the upper atmosphere and the mean free path between collisions is large, varying from 10 cm near 1 μbar at the base of the thermosphere to 150 km near 2.5 pbar at the exobase, the top of the thermosphere. Because of this large mean free path, molecular diffusion becomes dominant over convective mixing and thermal conduction becomes an important term in the energy balance equation. The low collision rates also imply that the population of molecular energy levels may depart from their local thermodynamic equilibrium (LTE) values.

Jupiter shares all of the characteristics mentioned above with other upper atmospheres, but there are important differences between the upper atmosphere of Jupiter and those of the terrestrial planets. Because the main atmospheric constituent, H_2, is light, molecular diffusion sequesters most species at lower altitudes making the composition of the thermosphere relatively pure. Moreover, the second most abundant species in the jovian atmosphere, He, is inert and plays a very minor role in atmospheric chemistry. Thus, chemistry in the thermosphere of Jupiter is relatively simple. In addition, Jupiter's heliocentric distance and giant magnetosphere suggest that auroral processes may be far more important on Jupiter than they are on the Earth. Finally, H^+ in the jovian ionosphere does not react readily with H_2, leading to large densities of this long-lived ion, in contrast to terrestrial ionospheres where O^+ reacts with O_2 to produce O_2^+, which quickly recombines.

Many of the interesting phenomena observed in Jupiter's upper atmosphere are also seen on Saturn, Uranus, and Neptune, though often less vigorously. The remarkably high thermospheric temperatures discovered on Jupiter are seen on Saturn, Uranus, and Neptune as well. Saturn, Uranus, and possibly Neptune display aurora, though none as intense as Jupiter's. The physical processes suspected to be responsible for Jupiter's enigmatic ionosphere may also operate on the other giant planets. As the most accessible of the giant planets, Jupiter can be thought of as a laboratory in which we can study physical processes important throughout the solar system and perhaps in other solar systems.

Jupiter's upper atmosphere has been an object of scientific study for a little over 30 years, beginning with speculation about its structure (Gross and Rasool 1964, Shimizu 1966, Hunten 1969, Wallace and Hunten 1973) and the first UV measurements with sounding rockets (Moos *et al.* 1969, Giles *et al.* 1976) and spacecraft (Judge and Carlson 1974). As is customary in planetary science, many of the early ideas have proved incorrect; while others that were thought to be incorrect have recently been revived. We give an overview of these developments, emphasizing both solid results from observations and models and those areas where our understanding remains less than adequate. The first half of the chapter concentrates on observations with a discussion of interpretation only when it is straightforward. The second half concentrates on models and interpretation. This organization reflects the fact that many aspects of the jovian thermosphere and ionosphere can only be understood through a synthesis of many observations.

9.2 OBSERVATIONS

Jupiter's upper atmosphere has been observed at wavelength from X-ray to mid-IR and many of the observations contain both spectral and imaging information. In addition, the upper atmosphere has been studied through occultations of stars in the UV, visible and near infrared and through occultations of radio signals emitted by spacecraft as they pass behind Jupiter. Finally, the Atmospheric Structure Instrument (ASI) on the *Galileo* Probe made in situ measurements of the density in the upper atmosphere. Out of necessity, we concentrate on those observations that have provided definitive information on atmospheric structure or bear on the many open questions regarding the jovian thermosphere and ionosphere.

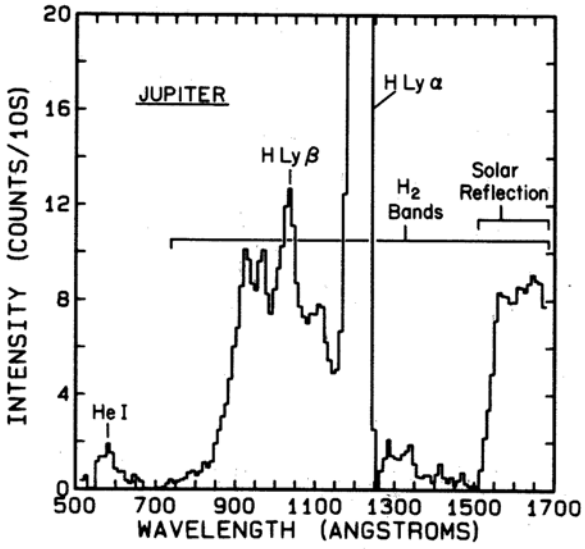

Figure 9.1. The EUV/FUV spectrum of Jupiter as measured by the *Voyager* 2 UVS. Emissions due to H Lyman α, H Lyman β, HeI, and H_2 electronic bands, as well as Rayleigh scattered emissions are indicated on the figure (from Yelle *et al.* 1987).

9.2.1 UV and X-ray Emissions

UV emissions from Jupiter extend from the HeI resonance line at 58.4 nm to beyond 170 nm where emissions from the Lyman electronic band system blend with Rayleigh scattered light from the stratosphere. (Figure 9.1). The UV emissions from Jupiter are non-thermal because temperatures are far too low to populate electronically excited states of atoms or molecules. The emissions are produced by a combination of fluorescence of solar UV radiation and collisional excitation by energetic electrons. The strongest feature in the UV range is the H Lyα line, but other Lyman Rydberg series lines are present, as well as numerous lines from H_2 electronic band systems, and the HeI resonance line.

Non-Auroral Lyα Emissions

Observations of H Lyα from Jupiter have been made from sounding rockets, Earth-orbiting satellites and interplanetary spacecraft. With the exception of one or two early measurements, there is general agreement on the brightness and morphology of the Lyα emissions. There are gradual variations over time scales of years in the emission intensity and abrupt variations over time scales of days in both brightness and morphology. These characteristics have led to several theories about the Lyα excitation mechanism and have impeded efforts to deduce the H density, yet they have revealed previously unexpected temperature and velocity structure in the upper atmosphere.

Figure 9.2 shows a contour plot of jovian H Lyα brightness obtained with the UVS on *Voyager* 1 (Dessler *et al.* 1981). Outside the auroral regions the Lyα intensity is ∼10-20 kR. Variations across the disc are gradual, as expected for an upper atmosphere, but there is a pronounced brightening in the equatorial region from ∼70 to 170° West longitude (System III). This phenomenon, commonly called the Lyα bulge, was discovered nearly simultaneously by Clarke *et al.*

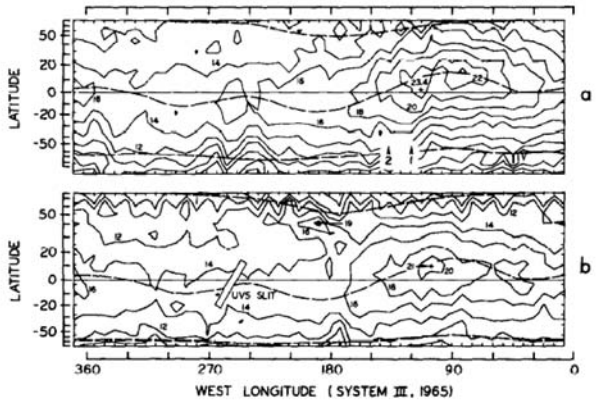

Figure 9.2. A contour plot of the H Lyman α emissions from Jupiter as measured by the *Voyager* 1 UVS. The H Lyman α brightness ranges from 12 to 24 kR and has a maximum along the magnetic dip equator at a system III longitude of ∼100° (from Dessler *et al.* 1981).

(1980) and Sandel *et al.* (1980). The bulge is fixed in System III longitude (the rotation period of Jupiter's magnetic field) and follows the magnetic dip equator rather than the spin equator (Sandel *et al.* 1980, Dessler *et al.* 1981). The bulge also appears on the nightside of Jupiter (McConnell *et al.* 1980).

Subsequent to the intensity measurements by *Voyager* and IUE, Clarke *et al.* (1991) succeeded in using the high resolution mode of IUE to obtain high-quality line profiles in the bulge and non-bulge regions of Jupiter (Figure 9.3). They found that the bulge profile was broader than the non-bulge profile by an amount just sufficient to explain the intensity variations and that it was the Doppler core of the line that increased in width rather than the Lorentzian wings. This result has implications for the nature of the bulge and excitation mechanisms that we discuss below. In fact, Cochran and Barker (1979) had shown earlier that brightness variations seen in *Copernicus* observations were correlated with changes in line width. This observation was made before the characteristics of the bulge were understood and it is possible that Cochran and Barker (1979) observed variations due to the presence of the bulge. Observations with GHRS/HST by Emerich *et al.* (1996) confirm the existence of an anomalously broad line profile from the bulge region and also show that the line shape is complex. For a gas whose kinetic modes are in thermal equilibrium the core of the line profile should be gaussian, yet the observed profiles are decidedly non-gaussian. Further observations are needed to fully characterize this complex line shape and its variations.

Because the solar Lyα flux varies with solar cycle, the jovian Lyα emissions are expected to vary even if the atmosphere is static. A careful study by Skinner *et al.* (1988) shows that jovian Lyα emissions are tightly correlated with solar Lyα during the descending phase of solar cycle 21. The aperture-averaged emission intensity outside of the bulge varied from ∼12 kR near solar maximum (1979) to ∼8 kR near solar minimum (1987). All observations were made with the IUE, with similar observing geometry, and were analyzed in a consistent fashion and are therefore directly comparable. The intensities observed by IUE in 1979 are comparable to

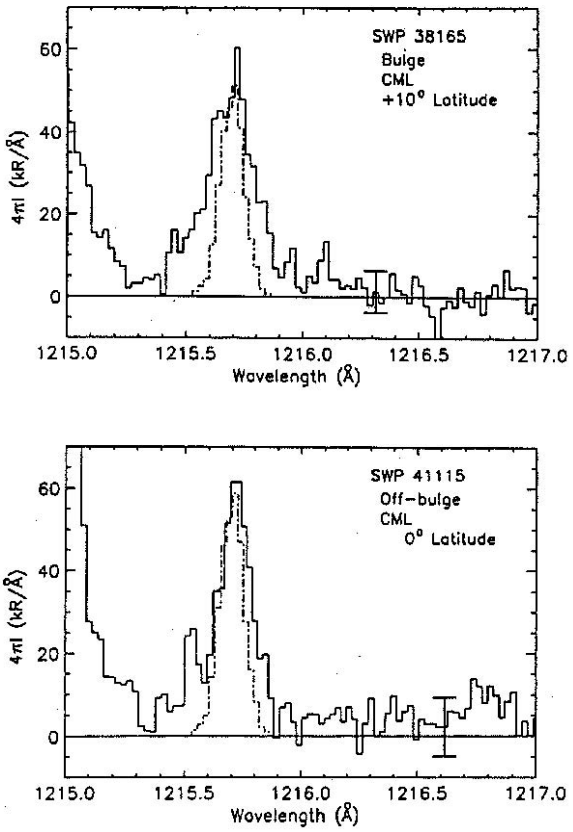

Figure 9.3. The H Lyman α line profile from Jupiter in the bulge and non-bulge regions of Jupiter's atmosphere. Both profiles were obtained with the IUE small aperture on the central meridian. Observations that produced the top profile were centered on a latitude of 10° N and System III longitude $\lambda_{III} = 75 - 170°$ and those that produced the bottom profile were centered on a latitude of 0° and longitude $\lambda_{III} = 264 - 336°$ (adapted from Clarke *et al.* 1991).

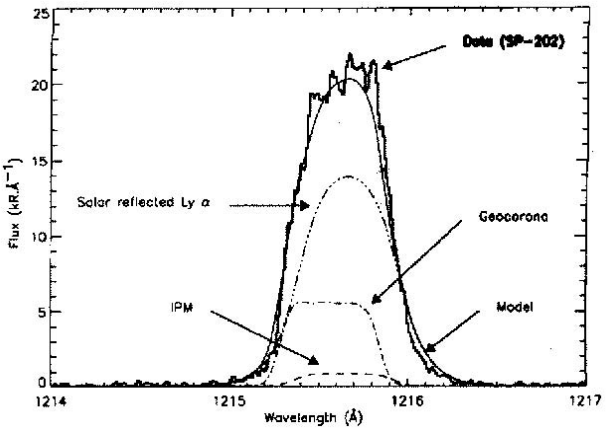

Figure 9.4. Observations and a model of the H Lyman α line shape based on scattering of Lyα from the Sun and interplanetary medium. An excellent fit is obtained for an H column of $1{\times}10^{21}$ m^{-2} (from Rego *et al.* 2001).

those measured by *Voyager* during the same period within the absolute calibration uncertainties of the two instruments (Skinner *et al.* 1988). The Lyα bulge was observed to be present at all times, but exhibited more short term variability than the non-bulge atmosphere (Skinner *et al.* 1988).

Jovian Lyα is also correlated with solar activity during the ascending phase of cycle 21, but the variation appears to be stronger (Shemansky and Judge, 1988). For example, the *Copernicus* measurements in 1976, near solar minimum, find a Lyα brightness in the range of 3-4 kR (Bertaux *et al.* 1980). However, this is not directly comparable to the IUE measurements at the solar minimum in 1987 for two reasons. First, the *Copernicus* slit is 0.3" by 39" and was inclined 45 degrees to the Jupiter spin axis whereas the Skinner *et al.* (1988) data represents an average over an area of 8".9 x15".1 centered on the jovian disc; thus, the IUE measurements are weighted much more heavily toward the bright equatorial region. As pointed out by McGrath (1991), Lyα emission from the equatorial region is enhanced at all longitudes, not just in the bulge. Second, geocoronal emission represents a 10-20% contamination of the jovian signal in the IUE measurements and removal of this contribution does not introduce serious inaccuracies to the analysis. However, jovian Lyα is strongly blended with a much brighter geocoronal line in the *Copernicus* data and separation of the two is difficult. Unfortunately, the published *Copernicus* data have been smoothed to facilitate the separation and this makes it difficult to infer the actual signal-to-noise ratio (SNR) and uncertainty of the observations. Giles *et al.* (1976) also detected weak Lyα emissions from Jupiter, but the field of view for these observations included the whole planet and comparison with more recent measurements is even more difficult. Finally, we note that *Pioneer* 10 observed a much weaker signal than any other measurement. This appears to be due to calibration: Shemansky and Judge (1988) find a factor of 4.4 difference between *Pioneer* 10 and *Voyager* 1 from a comparison of interstellar medium observations. In summary, jovian Lyα exhibits a clear 50% decrease during the descending phase of solar cycle 21. There is evidence for a factor of 3 increase during the ascending phase of solar cycle 21, but considering the difficulty of the observations and the fact that the variability rests on comparison of observations by different instruments, it may be unwise to ascribe too much significance to this result.

Jovian Lyα emissions also exhibit short term variations. Skinner *et al.* (1988) notes that the variance in brightness of the bulge is larger than the variance in the non-bulge region and further reports a 30% change in a period of 2 days, though this is of marginal statistical significance. The first definitive evidence for large changes in bulge Lyα emissions were presented by McGrath (1991), who observed on several days in 1989 and 1991 that the bulge brightened and grew in longitude so that it encompassed nearly the entire equatorial region while the peak brightness moved from 110° longitude to 40°. Subsequently, Emerich *et al.* (1996) have reported observations with the GHRS/HST that show variations in the Lyα profile in the bulge region on the time scale of minutes.

Despite early debates, it now seems clear that the jovian Lyα emissions are caused by resonance scattering of the solar Lyα line, with a small contribution from scattering of Lyα emissions from the interplanetary medium. Ben Jaffel (1993) shows that the Lyα line intensity and profile

outside the bulge region is well fit by a resonance scattering model with a column abundance of H above the absorbing hydrocarbons of 1×10^{21} m^{-2}. Similar results were obtained by Rego *et al.* (2001) and are shown in Figure 9.4. Moreover, Clarke *et al.* (1991) showed that the enhancement in Lyα brightness in the bulge is caused by an increase in the line width, which makes H more efficient at scattering solar Lyα. This correlation of measured line width and intensity is a direct indication of the dominance of resonance scattering, even if the details of the line profile in the bulge region are not understood.

The alternative to solar scattering is electron impact excitation. Shemansky (1985) postulated that the excess Lyα emissions in the bulge region derive from a reservoir of H(2s) atoms, created by electron impact excitation, that subsequently suffer preferential collisional transfer to H(2p), followed by emission of a Lyα photon. The direct cause for the bulge is asymmetric conditions in the ionosphere, presumably caused by the magnetosphere, that make the bulge region especially efficient in causing the H(2s)→ H(2p) reaction. Shemansky (1985) adopted this complex hypothesis in part because he rejected earlier explanations that relied on resonance scattering and required order-of-magnitude variations in the H abundance to explain the Lyα bulge. However, we now know that the bulge is not caused by a variation in H density but a variation in line width, and there seems to be little reason to hypothesize a large contribution to H Lyman α emissions from electron excitation.

D Lyα Emissions

Observation of deuterium Lyα from Jupiter has been reported by Ben Jaffel *et al.* (1998). Though this emission is weak relative to H Lyman α, Ben Jaffel *et al.* were able to detect it by observing just off the limb of Jupiter where the increased column abundance gives a relative enhancement to D Lyα, because its optical depth is less than H Lyman α. Ben Jaffel *et al.* derive a D/H ratio of $5.9\pm1.4\times10^{-5}$ from analysis of these data. The error bar includes uncertainties related to the atmospheric model, the eddy diffusion coefficient, and the solar Lyα flux. This result is higher than the D/H values of $2.6\pm0.7\times10^{-5}$ and $2.25\pm0.35\times10^{-5}$ determined by the GCMS on the *Galileo* probe (Mahaffy *et al.* 1998) and inferred from analysis of infrared measurements by the ISO spacecraft (Lellouch *et al.* 2001). Parkinson *et al.* (1999) claims that the Ben Jaffel *et al.* detection of D Lyα, off Jupiter's limb may be spurious, though few details are given on the errors, and further suggest that the signature of D Lyα may be present in the Emerich *et al.* (1996) line Lyα profiles of the jovian disc. Model calculations presented by Parkinson *et al.* (1999) show that the D abundance in the thermosphere is sensitive to the vibrational chemistry in the upper atmosphere, but detailed comparison of these models with observations have yet to be carried out.

HeI 58.4 nm Emissions

Jovian emissions from the helium resonance line at 58.4 nm have been observed by the *Voyager* UVS and EUVE. The *Voyager* data were first analyzed by McConnell *et al.* (1981), who inferred a brightness that varied with longitude from 2 to 5 R. McConnell *et al.* (1981) also found that the HeI brightness was anti-correlated with the Lyα brightness, being dimmer in the bulge region, and suggested that this might be due to absorption by an enhanced H column. The HeI emissions were observed to be limb darkened, as expected, since the He lies beneath an absorbing column of H_2. Shemansky (1985) reanalyzed these data and determined an average brightness of 4.1 R and further claimed that the HeI emissions were constant in longitude. Vervack *et al.* (1995) attempted to sort out the issue with a careful reanalysis of the UVS data, including a determination of measurement uncertainties, an issue neglected by Shemansky (1985). These authors verified the McConnell *et al.* detection of longitudinal variation in brightness anti-correlated with the Lyα bulge, but find that it is of marginal statistical significance. Vervack *et al.* determined an average HeI brightness of 4.4 and 4.5 R for *Voyager* 1 and 2.

Gladstone *et al.* (1995) reports EUVE observations of Jupiter at 58.4 nm on several dates. Observations made in April of 1993 detected no 58.4 nm emissions but established a 2σ upper limit of 1.8 R. Subsequent observations in July of 1994, shortly before the SL9 impacts, did detect 58.4 nm emissions with a brightness of 2.9±0.9 R. This is smaller than the brightness inferred from *Voyager* observations, but the *Voyager* observations were made at solar maximum and the EUVE observations at solar minimum and, in addition, the EUVE observations encompassed more of the jovian disc than the *Voyager* observations. Thus, the EUVE and *Voyager* observations appear to be consistent within uncertainties.

Non-Auroral H_2 Electronic Band Systems

Figure 9.5 shows high-resolution observations of Jupiter's UV spectrum at low latitudes obtained with the Hopkins Ultraviolet Telescope (HUT) on the Astro 1 mission in December of 1990 (Feldman *et al.* 1993). The numerous lines belong to the Lyman ($B\,^1\Sigma_u^+ \rightarrow X\,^1\Sigma_g^+$) and Werner ($C\,^1\Pi_u \rightarrow X\,^1\Sigma_g^+$) band systems of H_2. Emissions from the $B'\,^1\Sigma_u^+ \rightarrow X\,^1\Sigma_g^+$, $B''\,^1\Sigma_u^+ \rightarrow X\,^1\Sigma_g^+$, $D\,^1\Pi_u \rightarrow X\,^1\Sigma_g^+$, and $D'\,^1\Pi_u \rightarrow X\,^1\Sigma_g^+$ band systems are present as well. The integrated intensity in the H_2 band emissions is estimated to be 2.3 kR (Feldman *et al.* 1993), which is lower than the value of 3 kR estimated from *Voyager* UVS observations (Shemanksy 1985). Further analysis of HUT observations on Astro 1 and new analysis of observations on Astro 2 in March of 1995 by Morrissey *et al.* (1995) found integrated H_2 band intensity from 145 to 185 nm of 0.8±0.4 kR and < 0.4 kR, respectively, but the total H_2 band emissions were not discussed. The decrease in brightness from 1990 to 1995 could be a solar cycle effect.

Compared with Lyα, the H_2 emissions are well behaved. They show no variations with longitude and, in particular, display no change in the region of the Lyα bulge (Shemansky 1985). The emissions are present everywhere on the dayside of the planet, but absent on the dark side (McConnell *et al.* 1981). The brightness of the H_2 emissions is also proportional to the amount of sunlight incident upon the atmosphere (Yelle *et al.* 1987). H_2 emissions are present on all of the outer planets and their brightness varies roughly as the inverse square of heliocentric distance (Yelle *et al.* 1987).

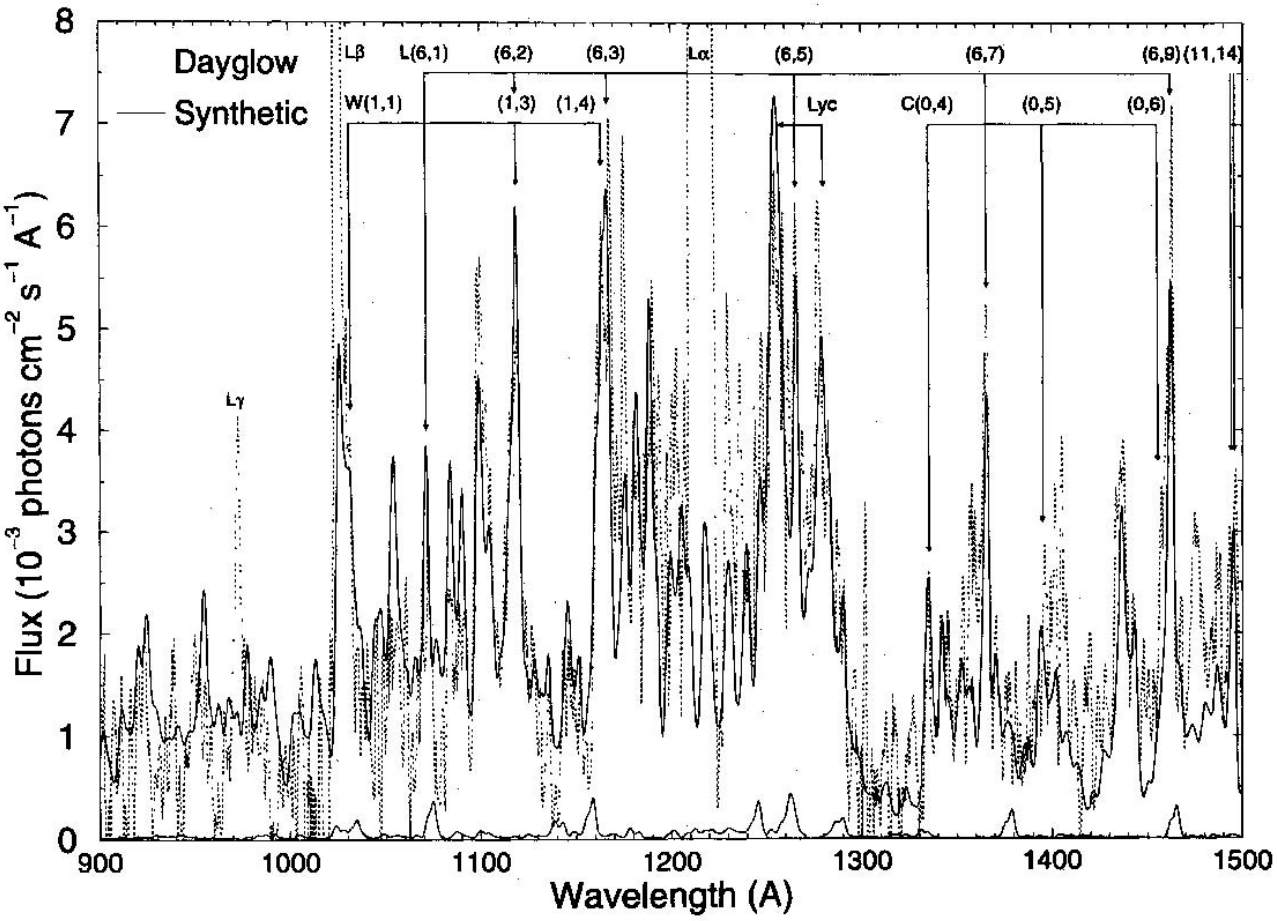

Figure 9.5. The EUV/FUV dayglow spectrum of Jupiter as measured by the HUT spectrometer on the Astro-1 mission. Also shown is a fit to the spectrum based on solar scattering and photo-electron excitation. The spectrum clearly shows a strong contribution from solar fluorescence. (From Liu and Dalgarno 1996a)

In all aspects, the H_2 emissions are tightly correlated with solar insolation.

Despite the relationship between H_2 emission morphology and solar insolation, there has been a debate over the importance of solar fluorescence to the excitation of the H_2 electronic bands. Shemansky (1985) shows that excellent fits to the shape of the *Voyager* UVS spectra can be obtained with electron excitation models. However, the observed emission rate is a factor of several higher than can be explained by photoelectrons. Shemansky advances no theories to explain this anomalous electron excitation but argues that it is present on all the outer planets (Shemansky and Ajello 1983, Shemansky and Smith 1986), and in some instances it is given the name "electroglow" (Broadfoot *et al.* 1986). Without a theory to constrain the properties of the electrons, Shemansky (1985) treats them empirically and adjusts the characteristics of the excitation to fit the observations. The free parameters in his models are the flux and energy distribution of the exciting electrons, the relative densities of H and H_2, the foreground abundance of H and H_2, and the H_2 temperature. Shemansky (1985) also uses the pre-flight calibration of the UVS instrument, which differs substantially from the in-flight calibration (Holberg *et al.* 1982). UV spectrometers are highly sensitive to impurities and radiation damage on the mirrors and post-launch changes in calibration are expected; thus, use of pre-flight calibration is suspect. This fact, combined with the number of free parameters in the electron excitation models and the relatively low resolution of the UVS, makes the good agreement between the electron excitation models and the UVS observations less compelling than it might otherwise appear.

Yelle *et al.* (1987) argued that the correlation of H_2 emission intensity with solar energy depostion rates strongly suggested that they were, in fact, due to scattering of solar radiation. Yelle *et al.* (1987) also show that fluorescence of solar radiation is a strong source for the Lyman and Werner bands, capable of producing the roughly 3 kR of emissions observed by *Voyager*. Yelle *et al.*'s estimates of the emission intensity are much higher than the earlier estimates by Carlson and Judge (1971) because they used a higher H_2 column density in Jupiter's upper atmosphere, consistent with the location of the homopause inferred from the UVS occultation experiment (Festou *et al.* 1981). Yelle (1988) shows that the *Voyager* UVS spectra of Jupiter can be adequately fit with models based on solar fluorescence and the expected levels of photoelectron excitation, though subsequent authors have criticized, with some justification, the solar spectrum used by Yelle (1988) in his calculations

(Liu and Dalgarno, 1996a). On the other hand, the thermospheric temperature profile of Festou *et al.* (1981) used by Yelle (1988) is now known to be too cold and this probably caused an underestimate of the emission intensity. The point is, given that the morphology of the H_2 emissions is identical to that expected for solar scattered emissions and that the sum of solar scattering and photoelectron excitation is capable of explaining the bulk of the emissions, it hardly seems worthwhile to postulate a new category of excitation process that might disappear with an adjustment of the solar UV spectrum or the jovian upper atmospheric model.

Solar scattering and electron excitation should produce very different spectra, but the *Voyager* UVS resolution of 3 nm is insufficient to provide a rigorous test of competing models based on the spectra shape alone. Attempts to provide this discrimination with IUE were also not conclusive, although they favored electron excitation (McGrath *et al.* 1988). The situation was finally resolved with the HUT observations shown in Figure 9.5. These data have a resolution of 0.3 nm and clearly show the presence of solar fluorescence through the prominence of lines connected to the $v' = 6$ level of the B state, which is pumped by solar Lyman beta (Feldman and Fastie 1973). An analysis by Liu and Dalgarno (1996a) finds that roughly 1.3 kR of the emissions are due to solar fluorescence and 1 kR to photoelectron excitation for a total of 2.3 kR in agreement in shape and magnitude with that observed with HUT. There is little room left for other sources of excitation, as originally suggested by Yelle *et al.* (1987). Thus, there seems to be no need for anomalous electron excitation. The HUT spectrum was obtained in the equatorial region of Jupiter and it is to this region that these constraints on anomalous electron excitation apply.

The spectral resolution of HUT was sufficient to isolate individual rotational lines and Liu and Dalgarno (1996a) were able to deduce a rotational temperature of 540 K from the H_2 spectrum. Their analysis assumed an isothermal, homogeneous atmosphere, so the inferred temperature should refer roughly to the base of the thermosphere. The value of 540 K is much higher than temperatures inferred from the UVS stellar occultation by Festou *et al.* (1981), which was used in the earlier calculations by Yelle (1988). The higher temperature causes H_2 to be more efficient at scattering photons. Perhaps more importantly, the Liu and Dalgarno analysis demonstrated that the atmospheric temperature could be determined from the H_2 spectrum. We will return to this point in Section 9.2.3.

Auroral Lyα Emissions

Lyman alpha emissions from the auroral zones are produced by a combination of electron excitation and solar scattering. The characteristics of the auroral Lyα emissions are discussed in detail in the chapter by Clarke *et al.* We concentrate here on the aspects of the emissions that are relevant for the structure of the auroral atmosphere. As with low-latitude Lyα, the line shape has provided the most interesting information on the atmosphere.

Analysis of the H Lyα line shape indicates that the emissions are generated beneath a vertical H column of $1.3\times10^{20}\,\mathrm{m}^{-2}$ (Rego *et al.* 2001). This is much smaller than the vertical column of $\sim1\times10^{21}\,\mathrm{m}^{-2}$ inferred for H in the non-auroral zones by these same authors. Rego *et al.* (2001) conclude that the H abundance in the auroral regions is less than in equatorial regions, which seems odd considering the tremendous production of H in aurorae. Rego *et al.* argued that the emissions cannot simply be produced higher in the atmosphere, where the overhead H column is smaller, because the CH_4 absorption required to fit the spectrum is similar to that required for equatorial models, implying production at similar altitudes. Unfortunately it is difficult to evaluate these arguments because Rego *et al.* (2001) presented no information on the sensitivity of the profile to either the H or CH_4 column densities. In any event, Rego *et al.* (2001) did not consider uncertainties in the solar Lyα line profile or the atmospheric temperature profile, both of which could affect the line profile. Moreover, the plane-parallel assumption commonly used to calculate auroral Lyα line profiles may be inadequate if the auroral oval is narrow (cf. Gladstone 1992). These effects need to be considered in more detail before the extraordinary claim that H densities decrease in the auroral region is accepted.

Prangé *et al.* (1997) present GHRS observations of Lyα line profiles which show them to be asymmetric. The authors suggest that the asymmetry is caused by H winds of several kilometers per second, at or above the sound speed. Though this seems reasonable, the line profiles have yet to be analyzed in detail and precise values for the wind speed have not been determined. Neutral winds of a kilometer per second are consistent with the highest wind speeds determined from measurements of the H_3^+ emissions, as discussed in the next section.

Clarke *et al.* (1994) has reported high resolution Lyα observations that exhibit very broad wings, extending out to $\sim$0.15 nm from line center in roughly symmetrical fashion. These Doppler shifts correspond to line-of-sight velocities of $\sim$450 $\mathrm{km\,s^{-1}}$. Earlier reports of IUE observations that showed line profiles with a net Doppler shift of $30\,\mathrm{km\,s^{-1}}$ (Clarke *et al.* 1989) are not confirmed by the HST/GHRS observations and Doppler shifts do not appear after reprocessing the IUE data with more recent and improved reduction software (J. Clarke, personal communication 2002). Bisikalo *et al.* (1996) examined the effects of energetic H fragments created by electron-induced dissociation of H_2 in the jovian aurora. The authors found that the hot H fragments contributed strongly to the line profile within 0.05 nm from line center, but the very broad wings could not be explained. Clarke *et al.* (1989) suggested that the very high Doppler shifts could be explained by acceleration of protons in the ionosphere followed by charge exchange to produce fast neutral H.

Auroral H_2 Electronic Band Systems

The jovian aurorae are very bright with typical intensities in the Lyman and Werner band systems of hundreds to thousands of kilorayleighs. The observed intensities imply energy deposition rates far above solar EUV levels, suggesting that the aeronomy of the auroral regions is driven primarily by energetic particle input. In order to understand the aeronomical consequences of the aurora, we discuss some aspects of the spectral analysis that have a direct bearing on the atmospheric structure in the auroral region.

The energy spectrum of precipitating electrons is a critical factor in auroral-driven aeronomy. Early investigations

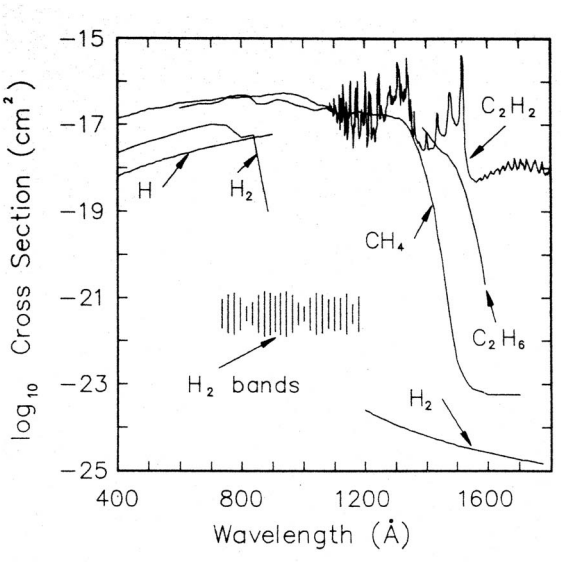

Figure 9.6. UV absorption cross sections for the main species in Jupiter's upper atmosphere. The variation of cross section with wavelength allows the identification and measurement of species in an absorptive occultation experiment. Absorption due to H_2 bands is only roughly indicated. (From Herbert *et al.* 1987).

into the structure of the jovian auroral zones such as those of Gerard and Singh (1982) and Waite *et al.* (1983) had little information on the auroral zones or jovian magnetosphere and therefore assumed a variety of energetic electron distributions in parametric studies of auroral aeronomy. Typically, energies of several keV were assumed and fluxes of order $10\,\mathrm{mW\,m^{-2}}$. These assumptions became relatively standard and persisted for fifteen years (Achilleos *et al.* 1998, Perry *et al.* 1999). However, recent analysis of auroral spectra have indicated a more complex energy distribution than first assumed, while images of the aurora indicate a narrow width (chapter by Clarke *et al.*), implying larger emission rates and precipitating fluxes than previously thought. The reader is referred to Perry *et al.* (1999) for an overview of early contributions to the field. Here, we concentrate on the new information.

Constraints on the energy spectrum of precipitating electrons has come from analysis of *Galileo* and HUT auroral spectra. Ajello *et al.* (2001) analyze a number of H_2 spectra obtained by the *Galileo* UV spectrometers as well as the HUT auroral observations (Wolven and Feldman 1998), using the latest electron excitation cross sections, and a model that includes self-absorption of H_2 band emissions and absorption by hydrocarbons. Ajello *et al.* find evidence for two components in the aurora: a "hard" spectrum produced by high-energy electrons and a "soft" spectrum produced by low-energy electrons. The hard electrons produce auroral emissions from relatively deep levels, near the base of the thermosphere. A useful measure of the depth of penetration of electrons is the color ratio, originally defined by Yung *et al.* (1982) and now taken as the ratio flux in the 155-162 nm band to the 123-130 nm band. The short wavelength band is absorbed by CH_4, whereas the long wavelength band is not (see Figure 9.6); consequently, emission that are generated near or below the homopause have a high color ratio while those generated at high altitude have a low color ratio. According to Ajello *et al.* (2001) emissions with no CH_4 absorption have a color ratio of 0.9. They calculate a color ratio of 2.1 for the HUT auroral spectrum. Ajello *et al.* estimate that a flux of roughly 50–100 $\mathrm{mW\,m^{-2}}$ of electrons with energy > 25 keV are required to produce the hard component of the observed emissions.

Evidence for the soft electron flux comes from the fact that both the *Galileo* and HUT spectra contain emission lines connected to the $v'' = 0$ level in the ground electronic state. The self-absorption cross section for these lines is large, implying that excitation must occur high in the atmosphere for these lines to be seen, *i.*e. the emissions must be optically thin. Ajello *et al.* (2001) calculate that the emissions must be generated close to the exobase and therefore the energy of the precipitating electrons must be in the range of 2-200 eV. The emission rate from this soft electron aurora is 16% of the hard electron aurora discussed above (Ajello *et al.* 2001). We note that Ajello *et al.* assume that photons absorbed in H_2 bands are lost, when they actually have some probability of being re-emitted at nearby wavelengths. For example, a photon absorbed in the (6,0) Lyman band has an 8% probability of being re-emitted in the (6,0) band. Though the approximation employed by Ajello *et al.* (2001) may be adequate for a deep aurora, special care is needed when studying the properties of a weak high-altitude aurora overlying a strong low-altitude aurora and analysis with more accurate scattering calculations such as those of Yelle (1988) or Wolven and Feldman (1998) might prove interesting.

Analysis of emissions from the H_2 electronic band systems also reveals the temperature of the atmosphere through the strength of ro-vibration lines. The technique was first applied by Trafton *et al.* (1994) who analyzed observations made in February 1992 with the Goddard High Resolution Spectrograph (GHRS) on HST. Trafton *et al.* compared the spectra with a model for electron excitation of H_2 and found a best fit for temperatures of 500-550 K. A similar analysis was performed by Clarke *et al.* (1994) who analyzed 6 observations obtained with the GHRS/HST on 3 nights in May/June 1993. For spectra obtained on May 28 and June 3, 1993, Clarke *et al.* (1994) retrieved a temperature of 400-450 K, whereas the temperature retrieved from the June 1, 1993 observations was 700-750 K. The observations are of different longitudes so it is unclear if the aurora varied in time or longitude. Clarke *et al.* (1994) note that temperature variations could reflect changes in the altitude of the aurora.

There are significant discrepancies between the observations and synthetic spectra calculated by Trafton *et al.* (1994), Clarke *et al.* (1994) and Kim *et al.* (1995). In particular, spectral lines at 158.01, 158.07, 158.37, and 158.74 nm are much brighter in the observations than the models, while a spectral feature at 122.83 nm is brighter in the models than the observations. Liu and Dalgarno (1996b) show that these discrepancies are due to deficiencies in the models and obtain better fits by computing models with improved molecular parameters. The earlier analyses relied upon line transition probabilities calculated from the band transition probabilities of Allision and Dalgarno (1970) and Honl-London factors, whereas Liu and Dalgarno (1996b) utilized the line transition probabilities calculated by Abgrall *et al.* (1993a,

1993b). Liu and Dalgarno (1996b) obtained best fits to spectra in the 157.2-160.7 nm and 158.6-162.1 nm regions with temperatures of 450 and 430 K respectively, and the 120.4-124.1 nm and 125.2-128.8 nm regions with temperatures of 500 and 690 K. The temperatures derived for the longer wavelengths are lower than derived by Trafton *et al.* (1994), but higher than Kim *et al.* (1995), while temperatures for the shorter wavelengths are higher than derived by Clarke *et al.* (1994). Liu and Dalgarno (1996b) find no evidence for the correlation between temperature and absolute brightness suggested by Kim *et al.* (1995).

The calculations mentioned above are based on homogeneous model atmospheres, but the variation of derived temperature with wavelength are consistent with a non-isothermal atmosphere. Emissions at short wavelengths must be generated at altitudes above the homopause to escape absorption by CH_4, but emissions at long wavelengths can occur below the homopause. Thus, the higher temperatures inferred from the short wavelength spectra indicate a positive temperature gradient, as expected for the auroral thermosphere. These considerations prompted Kim *et al.* (1997) to make nearly simultaneous observations in short (125.7-129.3 nm) and long (158.7-162.1 nm) wavelength bands. Kim *et al.* (1997) use the short wavelength band to determine CH_4 column density and the long wavelength band to determine temperature. The analysis of these observations, using updated molecular parameters consistent with Liu and Dalgarno (1996b), shows a clear trend of increasing temperature with decreasing CH_4 column density. Kim *et al.* (1997) show that their results for CH_4 column density and temperature imply that the temperature gradient in the vicinity of the homopause is larger than that inferred at equatorial latitudes (Seiff *et al.* 1998) or from hydrocarbon emissions at auroral latitudes (Drossart *et al.* 1993).

Dols *et al.* (2000) followed a slightly different approach and obtained GHRS spectra from 121.4 to 122.0 nm at a resolution of 0.007 nm, followed by spectra from 119. to 174. nm at 0.5 nm resolution. In addition, FUV images were obtained with WFPC2 on nearby orbits. The high resolution spectra were used to determine the H_2 temperature, the low resolution spectra to determine the column density of hydrocarbon absorbers, and the images to provide context for interpretation of the spectroscopy. Dols *et al.* (2000) also took the analysis a step further and combined a two-stream electron transport model with a realistic model atmosphere to compute synthetic spectra. The inferred CH_4 column densities range from 1 to 30×10^{20} m^{-2}. These authors also find absorption features at 148 and 152 nm, indicating the presence of C_2H_2. The spectral fits are improved by inclusion of C_2H_6, though this lacks the distinctive absorption features that make C_2H_2 easy to identify (Figure 9.6). The high resolution spectra indicate temperatures several hundred degrees hotter than at equatorial latitudes, confirming previous conclusions that the auroral atmosphere is warmer than the equatorial atmosphere.

The analyses summarized above rely upon hydrocarbon absorption to define the altitude of the H_2 emissions and the inferred altitudes depend upon the assumed hydrocarbon distribution. Kim *et al.* (1995, 1997) relied upon the atmospheric model of Atreya *et al.* (1981) and Festou *et al.* (1981), whereas Dols *et al.* (2000) relied upon the Gladstone *et al.* (1996) NEB model, which was fit to the Festou *et al.* (1981) CH_4 densities. However, a reanalysis of the *Voyager* UVS data by Yelle *et al.* (1996) finds that CH_4 is mixed to higher levels in the atmosphere than claimed by Festou *et al.* (1981). A separate analysis by Drossart *et al.* (1998), based on CH_4 fluorescence emissions, agrees with the results of Yelle *et al.* (1996) and therefore is also in disagreement with the results of Festou *et al.* (1981). Use of the Yelle *et al.* (1996) or Drossart *et al.* (1998) CH_4 profiles in the auroral spectral analysis would raise the altitude of the inferred emission region to levels where the temperature is higher and the disagreement between the inferred temperatures and the equatorial temperature profile would be less.

Auroral X-rays

Jovian X-rays were first detected by Metzger *et al.* (1983) using the *Einstein* observatory. An emission rate of 4×10^9 W with energies of 0.2 to 3.0 keV were measured from both auroral zones. Metzger *et al.*'s analysis showed that these X-rays could not be due to bremsstrahlung from precipitating electrons as the required input flux would be between 10^{14} and 10^{15} W, about an order of magnitude higher than the measured EUV auroral emission could support. Instead, these workers argued for K-shell emission from highly charged oxygen and sulfur ions, with energies between 0.3 and 4.0 MeV per ion. The problem with this hypothesis was that precipitating ions would also produce more EUV emission than had been detected. Waite *et al.* (1988) suggested that the bulk of EUV emission was produced by 10-100 keV electrons precipitating above the CH_4 homopause, while the X-ray emission was produced below it by ions with energies greater than 0.3 MeV. As a result, EUV emission associated with the ion precipitation would be mostly absorbed by the overlying hydrocarbons, but the X-rays would pass through the atmosphere unabsorbed.

Further measurements of jovian X-rays was provided by ROSAT (Waite *et al.* 1994). Emissions in the 0.1 to 2.1 keV range were measured at between 1.3 and 2.1×10^9 W in April 1991; the discrepancy in emission level was attributed to the sensitivity of the *Einstein* observatory to energies > 2.1 keV. The cause of the emission was ascribed to the precipitation of O(VII) and/or S(VII) or higher ionization states. Emission from the northern auroral zone was enhanced around $\lambda_{III} = 200^\circ$. Modeling of the ROSAT data by Cravens *et al.* (1995) showed that an input flux of 10^{12} W of O^{5+}, O^{6+} and O^{7+} ions within the energy range 0.3 MeV $< E_{ion} <$ 1 MeV could produce 10^8W and that the predicted spectrum fitted the ROSAT data well. More recent work by Liu and Schultz (1999) also finds that the X-ray emissions are likely due to energetic oxygen ions.

Non-Auroral X-rays

Non-auroral X-ray emission has also been observed from Jupiter. Waite *et al.* (1997) analyzed ROSAT observations of non-auroral latitudes and determined an emitted power of $\sim10^9$ W of X-rays. They found that there was a correlation of emission rate with lower magnetic field locations and also brightening near the sunlit limb of the planet. By analogy with the auroral emission, Waite *et al.* (1997) suggested

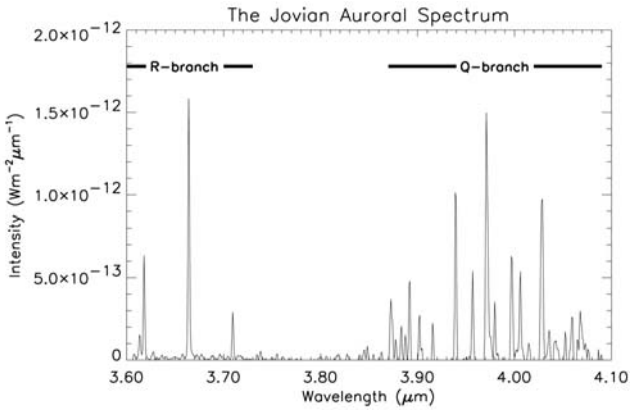

Figure 9.7. An example of an H_3^+ spectrum from the jovian auroral region.

that precipitation of ions with energies of 0.3 MeV and above could be responsible, the eastward drift accounting for the correlation with low B values. The observed emission rate of 0.4 mW m^{-2} could be reproduced with an energy input of 1.3×10^{13} W. Subsequent analysis by Maurellis and coworkers (Maurellis *et al.* 2000) have emphasized the importance of scattering of solar X-rays. These authors show that solar scatter contributes 50% or more of the observed brightness and point out that solar scattering is a natural explanation for observed limb brightening. The latest emission level from the jovian non-auroral disk is 2.3×10^9 W, measured by the Chandra observatory (Gladstone *et al.* 2002). Interestingly, the variation over the jovian disc is uniform and in particular shows no correlation with magnetic field strength as did the ROSAT data analyzed by Waite *et al.* (1997). This argues for the solar scattering rather than ion precipitation explanation for the emissions (T. Cravens, personal communication, 2002).

9.2.2 Infrared Emissions

Infrared emissions from H_3^+, H_2, and hydrocarbons have been detected from Jupiter. These emissions are produced as a consequence of the steady-state distribution of excited energy levels of the molecules and, unlike the UV and X-ray emissions, there are no uncertainties about the excitation mechanism. However, the emissions are very temperature sensitive, and since they are produced by minor species, provide constraints on both the temperature profile and chemistry of the atmosphere.

H_3^+ Emissions

H_3^+ emissions from the jovian atmosphere were discovered by Drossart *et al.* (1989), although Trafton *et al.* (1987, 1989) had detected similar features but did not identify them. Although H_3^+ was predicted to be an present in the jovian ionosphere, the brightness of the emissions was a surprise and is partly due to the unusual spectral properties of H_3^+. This floppy molecule has a series of an-harmonic vibrations, that result in an overtone spectrum that is much more intense than is the case for normal molecules (Majewski *et al.* 1989). A more recent measurement of the H_3^+ spectrum from the jovian auroral zones is shown in Figure 9.7.

At equilibrium, the H_3^+ molecule is geometrically an equilateral triangle, with D3h symmetry (Oka, 1980). As such, it has no permanent dipole, and thus no allowed pure rotational spectrum. Only a weak forbidden rotational spectrum, due to the centrifugal distortion of the molecule under rotation, can exist, and this is as yet unmeasured (Pan and Oka, 1986; Miller and Tennyson, 1988). The symmetric ν_1 stretching vibration maintains the D_{3h} molecular symmetry, and is likewise forbidden. This leaves the only dipole allowed asymmetric stretch/bend vibration, ν_2, as an observable band. The fundamental $\nu_2 = 1$ band is centered in the infrared L window, at 4 μm. Typical values of the Einstein A-coefficient for spontaneous emission are 100 s^{-1}. The overtone $\nu_2 = 2$ band is centered around 2 μm; once more, typical A values are $\sim$100 s^{-1}. These high values mean that individual H_3^+ ro-vibrational transitions are 10^9 stronger than those of H_2. The Jupiter observations represented the first observations of overtone H_3^+ transitions and led to the assignment of many previously baffling laboratory spectra (Majewski *et al.* 1989). Drossart *et al.* (1989) also realized that the H_3^+ emissions could be used to probe the physical conditions in the jovian thermosphere and ionosphere. Analysis of the rotational lines made it possible to determine a temperature of 1100 K for the southern auroral region in September 1988.

Jovian emissions in the H_3^+ fundamental band near 4 μm were first observed and studied in 1990 (Maillard *et al.* 1990, Miller *et al.* 1990, Oka & Geballe 1990). Ro-vibrational temperatures ranging from 650 K (Oka and Geballe, 1990) to 1100 K (Maillard *et al.*, 1990; Miller *et al.*, 1990) were determined for the auroral ionosphere. A similar vibrational temperature determined by Miller *et al.* (1990) led to the conclusion that H_3^+ was in "quasi-thermal" equilibrium, a conclusion borne out by Drossart *et al.*'s (1993) measurement of a translational temperature of 1150 K from the individual line profiles. Derived column densities, accompanying these measurements ranged from a few x 10^{16} m^{-2} to a few x 10^{17} m^{-2}. These measurements were, however, limited to several auroral locations, and it was not clear whether the differences were due to temporal or spatial variations. In order to obtain global pictures of the H_3^+ distribution, therefore, two types of imaging have been used.

The first is direct imaging, making use of narrow ($\lambda/\Delta\lambda$ $\sim$100) circular variable filters (CVF's) or custom narrow band filters, with wavelengths set to image the planet in H_3^+ emission. Kim *et al.* (1991) and Baron *et al.* (1991) both used the ProtoCAM facility instrument on NASA's Infrared Telescope Facility (IRTF) to image Jupiter at wavelengths around 3.4-3.55 μm. These were chosen because in this range CH_4 in the jovian stratosphere is an extremely efficient absorber of solar radiation, making the planet extremely dark, except for the H_3^+ emission. Baron *et al.*'s (1991) analysis showed that the jovian auroral oval occurred at higher latitudes than had previously been proposed. Conventional wisdom had the oval corresponding to the magnetic footprint of the Io plasma torus; the new results meant that the oval was located at the footprint of magnetic field lines that connected out into the middle magnetosphere equatorial plasmasheet. Connerney *et al.* (1993) confirmed this relocation of the oval by demonstrating that there was a distinct footprint from Io itself, well separated from and

equatorward of the main oval. Since then, Connerney and Satoh and their co-workers have carried out a series of imaging studies of Jupiter's auroral/polar regions. These have shown that the polar region itself has a "ying-yang" structure, with a dark, dawn-to-noon sector and a bright, noon-to-dusk sector (Satoh *et al.* 1996). There may be evidence of solar-wind control over the overall auroral brightness (Baron *et al.* 1996). And it is clear that there is considerable structure within the auroral/polar region that can be used to refine magnetic field models (Satoh and Connerney, 1999).

The second technique is spectral imaging, employing long slit spectrometers at moderate or high resolution to map an individual line or group of lines across the planet. The disadvantage of this technique is that it is not possible to image the entire visible hemisphere simultaneously; the advantage is that spectral imaging is better able to discriminate between weak H_3^+ emission arising from the non-auroral ionosphere (at lower latitudes) and sunlight reflected by the lower atmosphere. The first such spectral mapping was undertaken by Lam and co-workers (Lam *et al.* 1997, Miller *et al.* 1997) using the CGS4 spectrometer on the United Kingdom Infrared Telescope (UKIRT) on Mauna Kea. A map of derived temperature H_3^+ and column density from Miller *et al.* (1997) is reproduced in Figure 9.8. This work was carried out at relatively low spatial resolution, $3'' \times 3''$, corresponding to 10,000 km x 10,000 km. The spectral resolution was moderate, with $\lambda/\Delta\lambda \sim 1200$. Thus Lam *et al.* were not able to resolve any auroral structure, but they were able to make good measurements of the non-auroral regions. Their study showed that the auroral polar regions were emitting a few milliwatts per square meter, equivalent to 6.5×10^{12} W integrated over both hemispheres. Typical auroral/polar values of ro-vibrational temperature ranged between 850 K and 1050 K. They also showed that there was a latitudinal temperature structure, with temperatures dropping to 700-800 K in the mid-latitudes, before rising again to 750-1000 K at the equator. H_3^+ emission levels from the non-auroral, mid-to-low (MTL) latitude region fell toward the (magnetic) equator to $\sim 0.1\,\mathrm{mW\,m^{-2}}$, and the overall emission in this region appeared to correlate with a pattern concordant with the magnetic field determination.

Lam et al. (1997) typically found auroral values of the vertical column density of H_3^+ of $2.5\times10^{16}\mathrm{m}^{-2}$ to $12.5\times10^{16}\mathrm{m}^{-2}$, at a latitude of $\sim$60 degrees, with values for the total emission, $E^* \simeq 1\,\mathrm{mW\,m^{-2}}$ averaged over 2π steradians. Grodent *et al.* (2001) estimated a pixel filling factor of 20% to reinterpret these results, increasing them by a factor of 5. Later work by Stallard et al. (2002) made use of east-west cuts across the auroral/polar regions. This enabled them to identify four regions: a Rising Auroral Oval (ROA); a Dark Polar Region (DPR); a Bright Polar Region (BPR); and a Setting Auroral Oval (SAO). They found H_3^+ column densities that varied from $3\times10^{15}\mathrm{m}^{-2}$ in the DPR to $1.4\times10^{16}\mathrm{m}^{-2}$ in the SAO. E^* values ranged from $0.6\,\mathrm{mW\,m^{-2}}$ in the darkest regions of the DPR to $3.1\,\mathrm{mW\,m^{-2}}$ in the brightest SAO, each value being given over 2π steradians. That is to say, the emission rate can vary by a factor of $\sim$6 within the auroral/polar region.

The most recent study of the auroral/polar infrared emission (Stallard *et al.* 2001), shows considerable structure in that region. Stallard *et al.*'s DPR and BPR are similar to Satoh and Connerney's (1996) ying-yang structure, but the DPR is still at least 50% as bright as the BPR. Vibrational temperatures measured by dividing a $\nu_2 = 2 \rightarrow \nu_2 = 1$ hot band line to the $\nu_2 = 1 \rightarrow \nu_2 = 0$ spectrum show considerable structure, mirroring the emission intensity. The values of vibrational temperature varied from 900 to 1250 K, with higher values on the auroral oval and BPR, and lower values on the DPR.

Kim *et al.* (1992) examined the statistical equilibrium of vibrationally excited levels of H_3^+ and concluded that they may be underpopulated compared with an LTE distribution as a result of the large A values, which meant that radiative de-excitation occurred on timescales not much longer than collisional excitation. If H_3^+ vibrational levels are subthermally populated, it could mean that attempts to extrapolate from emission in a relatively small spectral region to the total emission from this molecule may be intrinsically flawed. The original investigation of the vibrational level distribution of H_3^+ by Miller *et al.* (1990) did indicate that the ratio between the $\nu_2 = 2$ and $\nu_2 = 1$ levels was close to that expected from a thermal distribution. They termed this quasi-thermal-LTE (QTE). This result has been borne out by a further study by Stallard *et al.* (2002), which shows that one would have to postulate extremely high ($\sim$1500 K) thermospheric temperatures to explain the relative $\nu_2 = 2/\nu_2 = 1$ populations by anything other than QTE. But that is not to say that the ground state population is not greater than might be expected from true LTE; to date, no one has measured ground state emission from H_3^+.

Two questions arise: Could the relative $\nu_2 = 2/\nu_2 = 1$ populations be in QTE, while still having a Ground State not in LTE? What effect would this have on extrapolating H_3^+ total emission rates? The answer to the first question is "yes", if the $\nu_2 = 2$ states were being preferentially populated, just enough to make up for radiative depopulation, by the following near resonance interaction:

$$H_3^+ + H_2(v=1) \rightarrow H_3^+(\nu_2 = 2) + H_2(v=0) \qquad (1)$$

This reaction is included in Kim *et al.*'s (1992) model, and leads to (almost) QTE ($\nu_2 = 2$) / ($\nu_2 = 1$) relative populations. Stallard *et al.* (2002), however, found no evidence of this process occurring. The answer to the second question is very little. This is because the major part of all H_3^+ emission (at least 90%) originates from the $\nu_2 = 1$ level. Since there is no dipole-allowed rotation spectrum, almost no emission comes from the ground state, unless the overpopulation is several orders of magnitude larger than that consistent with LTE. And, because dipole transition moments for rotational transitions within a vibrational level are extremely small (Miller and Tennyson, 1988), the rotational levels are thermally populated within that vibrational level. Thus, the physical and chemical conditions within the upper atmosphere of Jupiter do allow H_3^+ to be a useful and reliable probe of the energetics of the coupled thermosphere and ionosphere.

H_2 Quadrupole Emissions

The hydrogen molecule has very weak emission in the infrared region because, as a symmetric diatomic molecule, there is no permanent dipole and no induced dipole when the

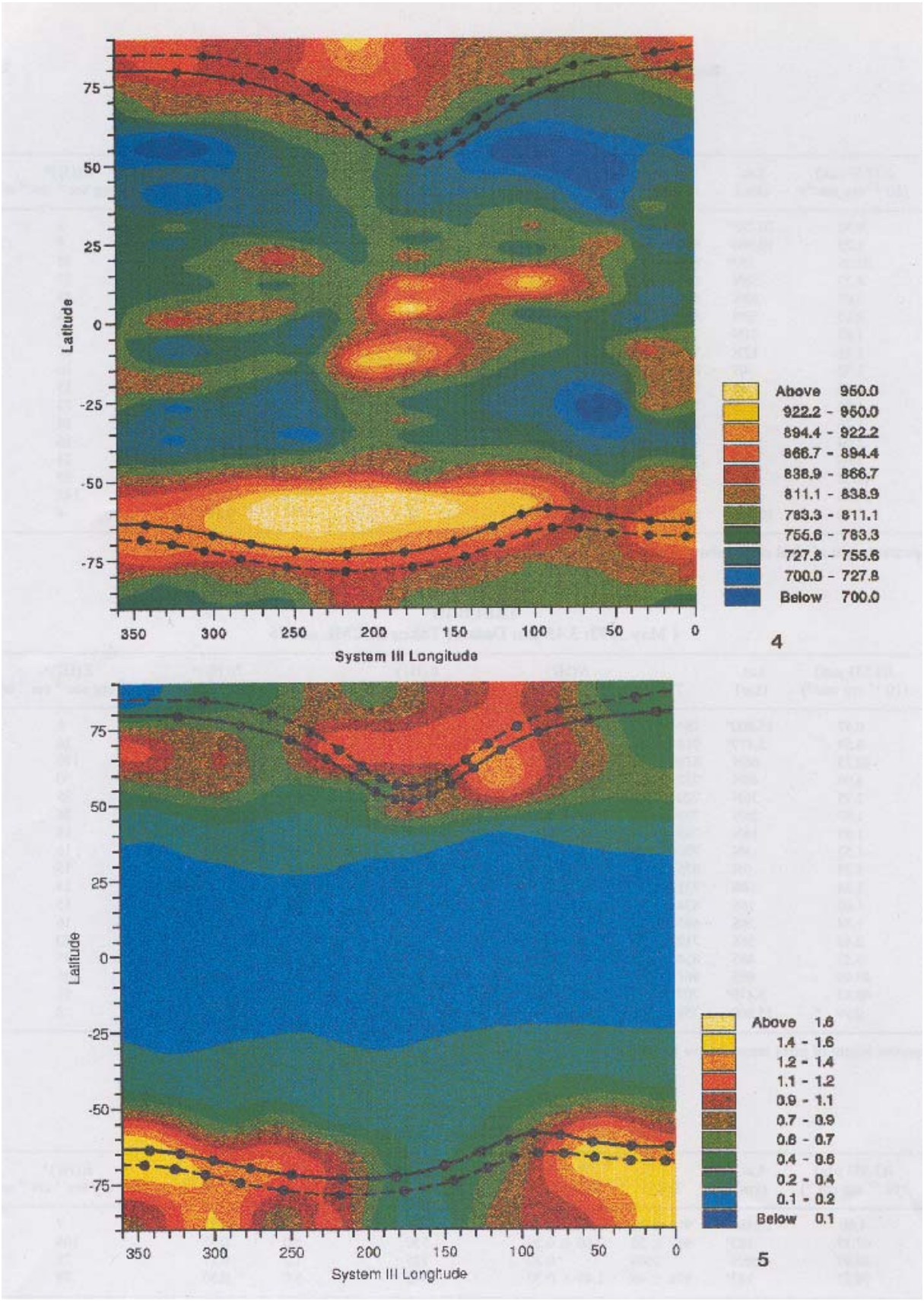

Figure 9.8. Temperature and H_3^+ column density maps derived from spectral mapping of Jupiter. Enhancements in temperature and density in the auroral regions, as well as structure in the temperature field in equatorial regions, is clearly seen. The H_3^+ column density is in units of $10^{16}\,\mathrm{m}^{-2}$ (from Miller *et al.*, 1997).

molecule vibrates. Thus any emission or absorption resulting from H_2 comes from quadrupole allowed ro- vibrational transitions. Typically, these have Einstein A coefficients of $\sim 10^{-7}$ to $10^{-6} s^{-1}$, which is about eight orders of magnitude lower than the H_3^+ ro-vibrational transitions. The H_2 fundamental vibration gives rise to the S(1) $v = 1 \rightarrow 0$ transition in the K atmospheric window near 2 μm and a pressure broadened absorption feature is evident in the the spectrum of reflected sunlight from Jupiter. Kim and Maguire (1986) first modeled the expected H_2 quadrapole emission from Jupiter, prompting Trafton *et al.* (1987) to search for it in the auroral regions, with a possible detection of the S(1) line, followed by confirmation (Trafton *et al.* 1989). The S(1) line was also seen at high resolution by Drossart *et al.* (1989). Analysis of their data indicate a temperature of 730^{+490}_{-200} K (Kim *et al.* 1990). According to the model of Grodent *et al.* (2001) the emission must originate from between the 1 mbar and 0.01 mbar pressure levels, about 50 to 100 km below the main H_3^+ emission peak.

Given the high column densities of H_2 on Jupiter, the hydrogen molecule dimer has been a target of observations. This was first detected by *Voyager* (Frommhold *et al.* 1984; McKellar 1984). Ground-based high resolution observations using the UKIRT picked up tell-tale infrared absorptions in the 2.100 to 2.125 μm due to the H_2-H_2 dimer from the jovian equator (Kim *et al.* 1995). Later auroral dimer emission was detected by Trafton and Watson (1992).

Hydrocarbon Emissions

Enhanced emissions from hydrocarbon species in the mid-IR were first detected from the jovian auroral zones by Caldwell *et al.* (1980). These emissions are thermal in character and therefore are not generated directly by precipitating particles, but indirectly by thermal effects associated with the aurora. Kim *et al.* (1985) discovered auroral enhancements in C_2H_2, C_2H_4, and C_2H_6 in *Voyager* IRIS data and Drossart *et al.* (1986) detected a large enhancement in C_2H_2 emission with high resolution ground-based observations. These mid-IR enhancements in the northern aurora are generally confined to longitudes of $180^\circ < \lambda_{III} < 200^\circ$ while a similar phenomenon in the southern aurora appears more variable (Caldwell *et al.* 1983).

Kim *et al.* (1985) interpreted the enhanced emissions as a temperature increase of 30 K near 1 mbar. However, Drossart *et al.* (1993) points out that it is more likely that the temperature perturbation grows with altitude, with small values in the millibar region and larger values in the microbar region, near the homopause, eventually connecting to the high temperatures in the thermosphere inferred from H_3^+ emissions. Drossart *et al.* (1993) show that the *Voyager* data can be explained with models that have a large temperature gradient from 1 to 50 μbar with the 10-20 μbar region being the most important. The pressure scale depends on the location of CH_4 diffusive separation. So either the strong temperature gradient in the auroral hot spot region is more than an order of magnitude deeper in pressure than at low latitudes, or CH_4 is mixed to higher altitudes in the auroral hot spot than in the low-latitude models adopted for the analysis.

Ion Winds

High resolution H_3^+ observations reveal winds in addition to temperature and column density. In 1997, Rego and coworkers (1999b) detected Doppler shifted H_3^+ emission lines using the NASA IRTF high resolution spectrometer, CSHELL. Their measurements, taken on the northern auroral ansa, showed an anti-rotational (clockwise) ion wind with a velocity $\sim 2\,km\,s^{-1}$, of the same order of the local speed of sound. This appears to be a fortuitous measurement of ion winds during a particularly strong auroral event. In 1998, Stallard *et al.* (2001) measured H_3^+ winds across the entire northern auroral polar region and also found electrojet winds, but at a weaker level than those measured by Rego *et al.* (1999b). Measured velocities in 1998 varied between $\sim 0.5\,km\,s^{-1}$ and $> 1\,km\,s^{-1}$. Thus, although the winds are variable, they have been present with significant velocities in all observations. Inside of the auroral oval, there was evidence for slower blue-shifted winds in the BPR (Stallard *et al.* 2001), possibly coinciding with the inner auroral arcs often seen in UV images (Clarke *et al.* 1998, Pallier and Prangé 2001).

The fastest winds seen in 1998 were in the DPR. Stallard *et al.* (2001) measured Doppler shifts indicating poleward winds with velocities typically in excess of $2\,km\,s^{-1}$. This was interpreted as the result of the solar wind dragging field lines across the polar cap, also seen on Earth (Dungey, 1961). This is the first evidence of direct input from the solar wind into the jovian upper atmosphere, though previously, solar wind control of overall auroral brightness had been proposed by Baron *et al.* (1996). The 1998 H_3^+ observations also showed that the auroral/polar region as a whole brightened and heated up by $\sim$100 K over a five-day period from September 7 to September 11. Coincident with this, electrojet wind speeds increased by approximately a factor of two. These results may also indicate the effects of solar-wind pressure: Cowley and Bunce (2001) and Kivelson and Southwood (2001) have independently proposed that, over relatively short time scales, decreasing solar-wind pressure may lead to enhanced auroral activity as field lines corresponding to the auroral oval migrate outward through the plasmasheet to regions of lower and lower percentages of co-rotation, leading to increased currents and voltages.

9.2.3 Occultations

Jupiter's atmosphere has been probed by occultations in the UV, visible, and radio spectral regions. These 3 techniques provide different but complementary information on the atmosphere and we discuss each in turn. Table 9.1 lists observational parameters for the occultations discussed in this chapter. The reader is referred to the article by Smith and Hunten (1990) for a general review of the theory of occultations.

Voyager UV Occultations

The *Voyager* UV occultations probed Jupiter's upper atmosphere by measuring the transmission of star or sunlight as the spacecraft passed behind the planet. *Voyager* 1 observed a solar occultation and *Voyager* 2 an occultation by the star Alpha Leo (Broadfoot *et al.* 1981). Stellar and solar occultations provide different information because absorption of

Table 9.1. Occultation Observational Parameters

Label	Experiment	Direction	Type	Spectral Range	Date	Latitude	Longitude
-	*Voyager* 1/Solar	Ingress	UV	50-90 nm	5 March 1979		
-	*Voyager* 2/Stellar	Ingress	UV	90-170 nm	9 July 1979	14.5° N	
-	Groundbased	Egress	Visible	broad band	13 December 1989	8° N	
-	*Pioneer* 10	Ingress	Radio	S band	4 December 1973	28° N	45° W
-	*Pioneer* 10	Egress	Radio	S band	4 December 1973	58° N	260° W
-	*Pioneer* 11	Ingress	Radio	S band	3 December 1974	79° S	263°
-	*Pioneer* 11	Egress	Radio	S band	3 December 1974	20° N	61° W
-	*Voyager* 1	Ingress	Radio	S and X band	5 March 1979	12° S	63° W
-	*Voyager* 1	Egress	Radio	S and X band	5 March 1979	1° N	314° W
V2N	*Voyager* 2	Ingress	Radio	S and X band	9 July 1979	67° S	255° W
V2X	*Voyager* 2	Egress	Radio	S and X band	9 July 1979	50° S	148° W
G0N	*Galileo*/Orbit=0	Ingress	Radio	S band	8 December 1995	24° S	292° E
G0X	*Galileo*/Orbit=0	Egress	Radio	S band	8 December 1995	43° S	332° E
G3N	*Galileo*/Orbit=3	Ingress	Radio	S band	8 November 1996	28° S	102° E
G4N	*Galileo*/Orbit=4	Ingress	Radio	S band	21 December 1996	23° S	264° E
G4X	*Galileo*/Orbit=4	Egress	Radio	S band	22 December 1996	25° S	167° E

starlight by interstellar H removes radiation shortward of 91.1 nm. As shown in Figure 9.6, absorption by H_2 in its ionization continuum occurs shortward of 80.4 nm; thus, attenuation due to this absorption is only measurable in the solar occultation. H_2 absorbs photons in its electronic band systems out to 110 nm, but this opacity is much weaker and only provides information on the lower thermosphere. Only the solar occultation measures the primary atmospheric constituent in the upper thermosphere.

Absorptive occultations measure the altitude profile of the horizontal column density, which, for the major constituent, can be converted to a pressure-temperature profile with the assumption of hydrostatic equilibrium. The *Voyager* UVS solar occultation experiment was complicated by the fact that the projected diameter of the Sun was 800 km, much larger than the atmospheric scale height of ∼200 km. Atreya *et al.* (1981) derived a temperature of 1000 ± 200 K, but later analysis revised this downward slightly to 1000 K (McConnell *et al.* 1982). Because of the large projected size of the Sun, these values represent an average over several scale heights centered on the 2×10^{-6} μbar pressure level (Festou *et al.* 1981). Variations in EUV emissions over the face of the Sun represent an additional uncertainty, but subsequent measurements indicate that the UVS results are essentially correct.

The UV occultations measure absorption by hydrocarbon species at wavelengths longward of 110 nm. The hydrocarbons are confined to the lower thermosphere by diffusive equilibrium. Measurement of the hydrocarbon distribution in this region, principally CH_4, can be used to determine the degree of vertical mixing and the location of the homopause (Broadfoot *et al.* 1979). The Jupiter solar occultation is not appropriate for this task because its vertical resolution is larger than a CH_4 scale height, but the stellar occultation is well suited to the job. Festou *et al.* (1981) analyzed the stellar occultation data and derived a CH_4 mixing ratio of $2.3^{+3}_{-2}\times10^{-5}$ at a pressure of 1 μbar. Yelle *et al.* (1996) analyzed the same data set and derived a CH_4 mole fraction of 1-2×10^{-4} at a pressure of $0.2^{+0.2}_{-0.1}$ μbar. The Yelle *et al.* (1996) result is consistent with determination of the CH_4 density through analysis of CH_4 emissions by Drossart (1999). The difference between the Yelle *et al.* and Festou *et al.* analysis is not understood but could be due to improvements in data reduction or different assumptions about the temperature profile in the lower thermosphere (Yelle *et al.* 1996).

Occultation measurements of attenuation in the H_2 Lyman and Werner band systems in the 90-110 nm spectral region can be used to constrain the H_2 density and temperature profile in the lower thermosphere. The first analysis of this spectral region in the UVS stellar occultation was presented by Festou *et al.* (1981). These authors derive a temperature profile with a nearly constant gradient 0.5 K/km, connecting the upper stratosphere with a temperature of 200 K to the hot upper thermosphere.

Ground-based Stellar Occultations

Ground-based stellar occultations also probe Jupiter's lower thermosphere. Attenuation in these occultations is due to defocussing of starlight caused by the refractivity gradient in the atmosphere rather than absorption as in UV occultations. The most recent occultation of Jupiter was of the star SAO 78505 in June of 1989. Analysis of these data by Hubbard *et al.* (1995) yielded a temperature of 176±12 K, if an isothermal atmosphere were assumed. A numerical inversion, using the Festou *et al.* (1981) results to define the upper boundary temperature yielded a profile that was consistent with the isothermal analysis in that temperatures were roughly 180 K.

Yelle *et al.* (1996) pointed out that the temperature of 500-600 K determined by Liu and Dalgarno (1996a) from analysis of the H_2 emission spectrum was much hotter than predicted by the Festou *et al.* (1981) temperature profile. In addition, a reanalysis of the UVS stellar occultation data showed that the data are consistent with a temperature gradient of ∼3 K/km, much larger than found by Festou *et al.* (1981), but consistent with the Liu and Dalgarno (1996a) data point. Yelle *et al.* (1996) also showed that a large temperature gradient was consistent with the groundbased occultation date. It is well known that inversion of refractive occultations is sensitive to the assumptions required for the upper boundary. In fact, the measurements determine not a

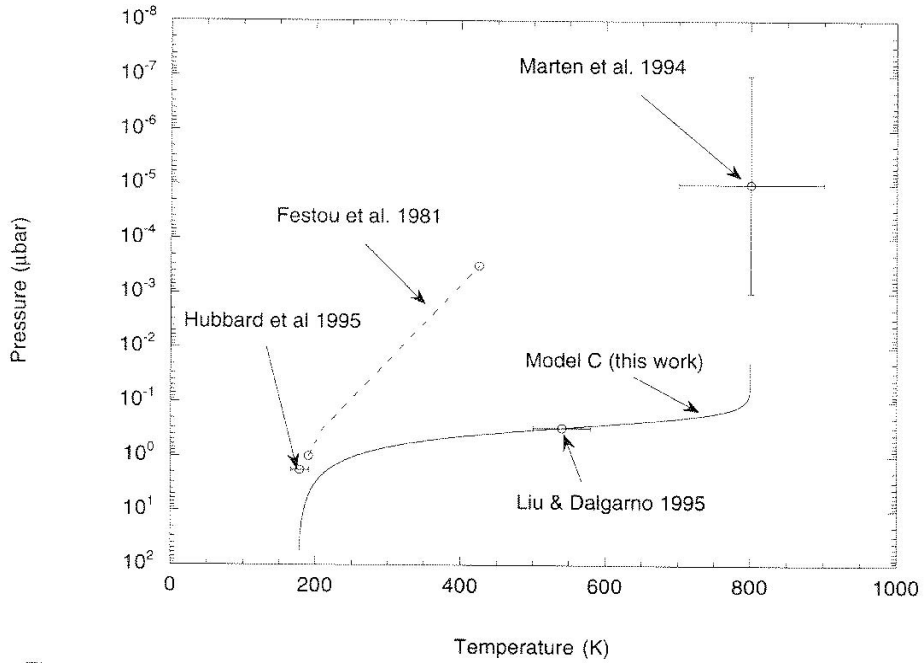

Figure 9.9. A prediction for the temperature profile in Jupiter's upper atmosphere along with earlier estimates and constraints based on UV and ground-based occultations, H_2 band emissions, and H_3^+ emissions (from Yelle *et al.* 1996).

unique temperature profile but a family of profiles characterized by different temperatures at their upper boundary. Yelle *et al.* (1996) showed that the SAO 78505 occultation data was also well fit by the same temperature profile that matched the UVS stellar occultation, the Liu and Dalgarno (1996a) H_2 emission temperature and reached an asymptotic temperature in the upper thermosphere consistent with the H_3^+ emissions. The data and models are presented in Figure 9.9. Thus, according to Yelle *et al.* (1996), all available data were consistent with the existence of a large temperature gradient in Jupiter's lower thermosphere. This conclusion was subsequently confirmed by *Galileo* probe measurements (Sieff *et al.* 1997, 1998), to be discussed in Section 9.2.4 below.

Spacecraft Radio Occultations

In radio occultations the spacecraft itself emits the signal and it is received by large radio telescopes on the ground. The properties of the atmosphere are inferred from the dimming of the radio signal as the spacecraft passes behind the planet. The dimming is caused by refractive defocussing as in the ground-based visible occultations rather than true absorption as in the UV occultations. Radio occultations probe both the lower atmosphere where refraction is caused by the neutral atmosphere and the ionosphere where refraction is caused by free electrons. Information on the lower atmosphere derived from radio occultations is discussed in the chapter by Moses *et al.*. Here, we review what radio occultations tell us about the ionosphere.

Figures 9.10a,b show results from analysis of the *Voyager*, and *Galileo* radio occultation experiments. The *Voyager* 1 data were obtained from Eshleman *et al.* (1979), the *Voyager* 2 data from Hinson *et al.* (1998), and *Galileo* data from Hinson *et al.* (1997) and D. P. Hinson (personal communication,2002). *Galileo* conducted 12 occultations of Jupiter, but only the 5 shown in Figure 9.8 have been fully reduced and archived. *Voyager* employed S and X band links and a radiation resistant oscillator, greatly improving data quality relative to the first *Pioneer* measurements (not shown). *Galileo*, it should be remembered, had to rely upon a back-up low gain antenna that could transmit only an S band signal at a much reduced SNR, rather than the high-power, dual-frequency experiment originally planned. Nevertheless, because of the high quality oscillator and improvements in data reduction techniques, the *Galileo* data appear to be of high fidelity.

The original analyses of *Pioneer* and *Voyager* radio occultation data were based on the geometrical optics approximation to ray propagation (Fjeldbo *et al.* 1975, 1976, Eshleman *et al.* 1979). Though adequate in the upper ionosphere where electron density gradients are mild, the technique fails in the lower ionosphere where numerous narrow ionization levels provide multiple paths for radio signals to reach Earth with similar diminution. Karayel and Hinson (1997) and Hinson *et al.* (1997) developed a technique, based on scalar diffraction theory, that is capable of dealing with multi-path propagation for analysis of the *Galileo* occultations and subsequently applied this to the *Voyager* 2 occultation measurements (Hinson *et al.* 1998). This new analysis technique has greatly improved the data quality, leading to, for example, the appearance of an ionospheric peak in the *Voyager* 2 ingress data and proper characterization of numerous sharp layers beneath the peak (Hinson *et al.* 1998).

The profiles in Figure 9.10 can be grouped into three broad categories. Most of the profiles have an electron density peak of 0.5-2$\times 10^{11}$ m^{-3} at an altitude of 1500-2000 km. However, the V2N and G0N profiles have an ionospheric

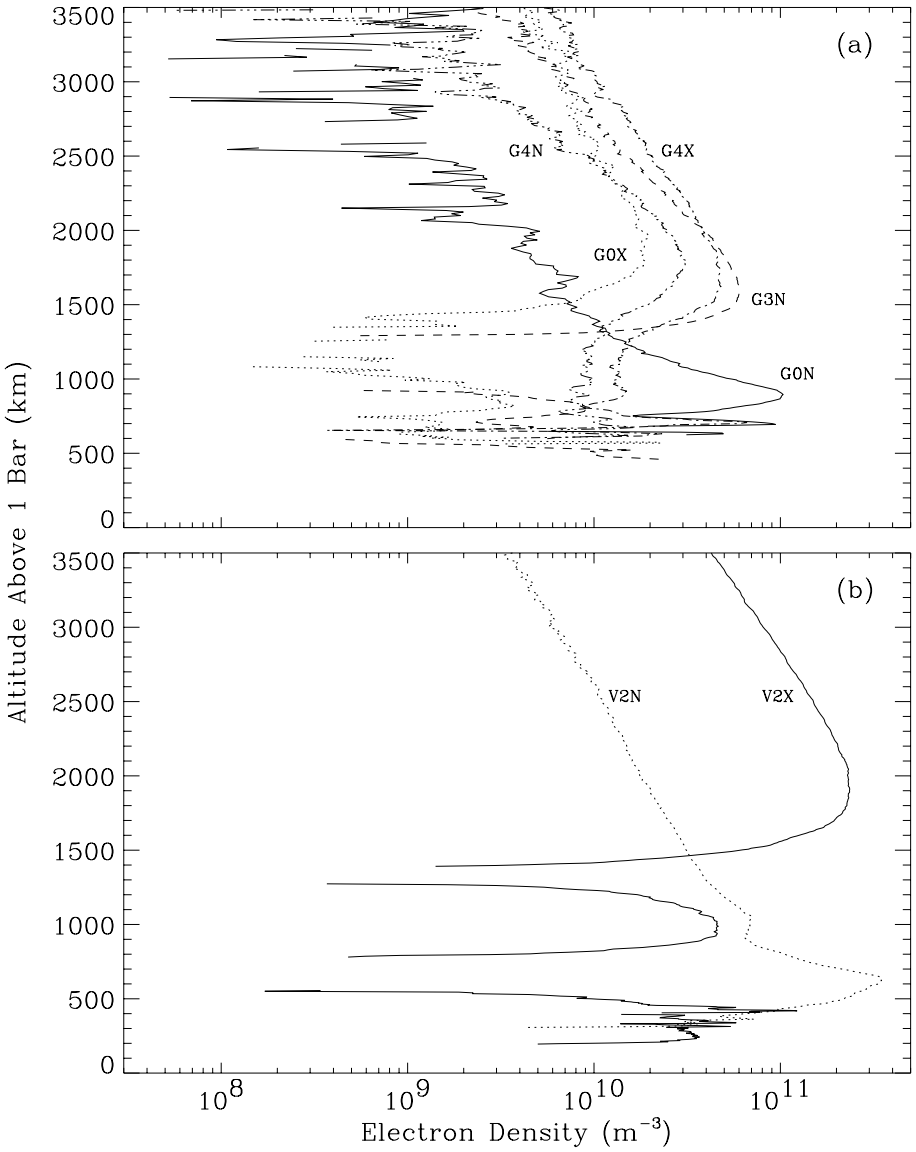

Figure 9.10. Electron density profiles in the jovian ionosphere as measured by *Voyager* (panel a) and *Galileo* (panel b). See Table 9.1 for the observation characteristics.

peak below 1000 km. On the other hand, the G0X profile has a peak density of only $\sim 2\times10^{10}\,\mathrm{m}^{-3}$ at an altitude of roughly 2000 km. The *Voyager* 2 and *Galileo*/0 ingresses occur at dusk and the egresses at dawn, so we could postulate that the low altitude peaks, when they occur, occur at dusk, and the low density profiles, when they occur, occur at dawn. This makes physical sense because recombination during the jovian night should deplete the low altitude peak if it is composed primarily of H_3^+, but the *Galileo*/3 and 4 profiles do not exhibit such behavior. There is no obvious correlation with latitude or local time that organizes the profiles. Most of these peculiar features were recognized prior to the *Galileo* mission and have proved difficult to understand with ionospheric models (McConnell *et al.* 1982). Thus, even with the addition of the *Galileo* profiles, we find that, as first noted by McConnell *et al.* (1982), the characteristics of the electron density profiles do not correlate with any obvious geophysical parameters.

The electron density scale height above the ionospheric peak indicates plasma temperatures, defined as the average of the ion and electron temperature, that range from 800 to 1570 K. Calculations by Nagy *et al.* (1976) show that the plasma temperatures should be equal to the neutral temperatures up to altitudes just above the ionospheric peak and increase slowly at higher altitudes. This led several investigators to consider models for Jupiter's thermosphere with high neutral temperatures (Hunten 1976, Atreya and Donahue 1976, Hunten and Dessler 1977). The high temper-

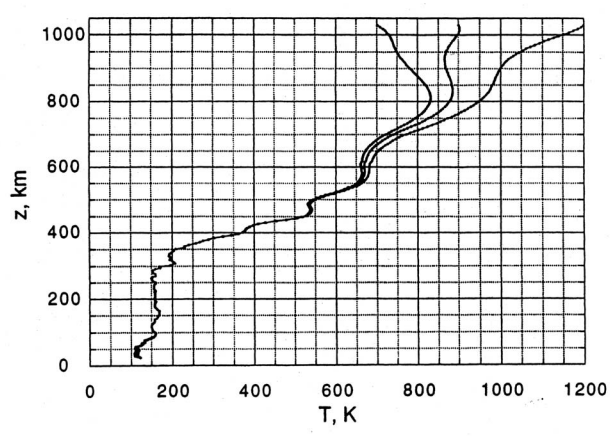

Figure 9.11. The temperature profile in Jupiter's upper atmosphere measured by the ASI experiment on the *Galileo* probe. Results are shown for 3 different assumptions about the temperature at the upper boundary. (From Sieff *et al.* 1998).

atures were subsequently confirmed by *Voyager* UVS occultation measurements, analysis of the H_3^+ emission spectrum, and measurements made by the Atmosphere Structure Instrument (ASI) on the *Galileo* probe.

9.2.4 *Galileo* Probe

Analysis of data from the ASI experiment on the *Galileo* probe determined the density profile in the upper jovian atmosphere by measuring the deceleration caused by atmospheric drag on the probe. The deceleration was measured by 4 accelerometers: two measured accelerations along the probe flight path, and two in an orthogonal direction to define the angle of attack. Measurements from the along-track accelerometers were made every 0.625 seconds with the two sensors interleaved to provide higher resolution. A complete description of the experiment is given in Sieff *et al.* (1998).

The temperatures derived from the ASI measurements are shown in Figure 9.11. The altitude resolution varies from 2.25 km at the top of the atmosphere to 0.11 km just before chute deployment. Propagation of uncertainties from the accelerometer measurements implies an accuracy of 0.12 K for the temperature determination, except in the upper thermosphere where an unknown boundary condition causes additional uncertainty. Determination of temperatures also requires knowledge of the mean molecular weight of the atmosphere and so depends on the mole fractions of H_2, He, CH_4, and to a lesser degree, H. This is only of consequence in the lower thermosphere because the upper thermosphere is essentially pure H_2. Sieff *et al.* (1998) calculate the mean molecular mass from a model for the diffusive separation of constituents using the eddy diffusion coefficient derived by Yelle *et al.* (1996).

The ASI results exhibit a number of interesting characteristics. The profile has a large temperature gradient in the lower thermosphere, as originally deduced by Yelle *et al.* (1996). The temperature gradient peaks at a value of 2.9 K/km at an altitude of 357 km, where the pressure is 0.3 μbar (Young *et al.* 1997). The gradient persists to the upper thermosphere where the temperature is of order 1000 K, consistent with the UVS occultation measurements and the H_3^+ emission measurements. As mentioned above, the temperature in the upper thermosphere is sensitive to assumptions made about the conditions at the upper boundary and Sieff *et al.* (1998) present results for upper boundary temperatures of 700, 900, and 1200 K. These boundary effects disappear by 700 km, where the temperature is 740 K and the pressure 7.8 nbar. An upper boundary temperature of 700 K produces a negative temperature gradient in the uppermost thermosphere, that Sieff *et al.* view as improbable because it implies an energy flow out of the atmosphere. The upper boundary temperature of 1200 K implies a positive temperature gradient in the uppermost thermosphere implying some source of heating above 1 nbar. Thus, Sieff *et al.* (1998) adopt as their preferred solution an upper boundary temperature of 900 K, although other solutions are possible.

Table 9.2. Derived Gravity Wave Properties

	Wave 1	Wave 2
$z_\circ$ (km)	430	710
$2\pi/k_{z,obs}$ (km)	91	288
$A_\circ$ (Kelvins)	38	41
c (km/s)	0.186-0.205	0.18-0.43
ω (s^{-1})	9.9×10^{-5}	1.6×10^{-3}
$2\pi/k_h$ (km)	12,693	773
$2\pi/k_z$ (km)	92	149
$\epsilon F(z_\circ)$ (mWm^{-2})	0.19	0.21

For c=0.2 km s^{-1} and $\epsilon = 0.65$; for other values of c, use $\omega \propto c^{-3}$, $k_h \propto c^{-4}$, $k_z \propto c^{-1}$, and $F \propto c^{-2}$

Periodic temperature variations are present at all altitudes in the ASI profile and these have been interpreted as the signature of buoyancy waves. Young *et al.* (1997) analyzed the temperature perturbations under this assumption to derive characteristics of the waves. The temperature perturbations are shown in Figure 9.12 and the derived properties are reproduced in Table 9.2. The analysis employed a WKB approximation for the vertical propagation of the wave,

$$\delta T = A(z)\exp\left(k_x x + k_y y - \omega t + \int k_z z\right) \tag{2}$$

where the vertical wavenumber k_z is given by

$$k_z^2 = \frac{N^2-\omega^2}{\omega^2}k_h^2 - \frac{1}{4H^2}. \tag{3}$$

N is the Brunt-Väisälä frequency, ω the wave frequency, H the scale height for the density ρ, and $k_h^2 = k_x^2 + k_y^2$ is the square of the horizontal wave vector. Young *et al.* (1997) assumed that the waves would be damped by molecular viscosity and derived the following equation for the variation of amplitude with altitude:

$$A(z) = A_\circ\sqrt{\frac{T^2N^3/\rho}{T_\circ^2N_\circ^3/\rho_\circ}}\exp\frac{-1}{\tilde{H}}\int_{z_\circ}^{z}\frac{\nu N^3}{\nu_\circ N_\circ^3}dz \tag{4}$$

where ν is the coefficient of kinematic viscosity, $\tilde{H} = \partial ln(T^2N^3/\rho)/\partial z$ is very nearly the scale height, and the subscript $\circ$ indicates that quantities are calculated at a reference altitude, which Young *et al.* (1997) took as the lo-

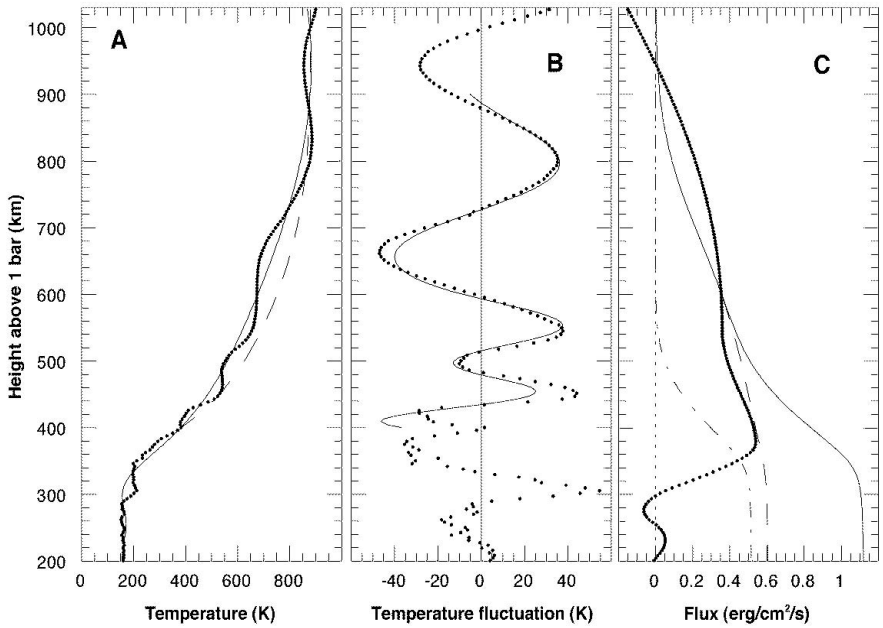

Figure 9.12. The wave structure in Jupiter's upper atmosphere. (From Young *et al.* 1997).

cation of maximum amplitude. The observed perturbations imply the presence of two waves, one with a large vertical wavelength that is damped high in the thermosphere and the other with a smaller vertical wavelength that is damped low in the thermosphere. Both waves are characterized by maximum amplitudes of roughly 40 K. The implication of these waves for the energetics of the thermosphere is discussed in Section 9.3.3.

9.3 MODELS

The previous sections have summarized a broad range of data on the jovian upper atmosphere. We now turn to the question of what can be deduced from these data about the composition, thermal structure, and dynamics of the upper atmosphere, and what basic processes establish these characteristics.

9.3.1 Composition

Diffusive separation confines heavy constituents to lower altitudes, near or below the homopause at ∼0.1-1.0 μbar, and makes the chemistry of Jupiter's upper thermosphere relatively simple. Molecular hydrogen and helium are the only molecules present in more than trace amounts. The chemistry consists of reactions among these species and their derivative ions and molecules. Thus, the list of species considered in chemical models includes H_2, He, H, H^+, H_2^+, H_3^+, He^+, and HeH^+. The primary neutral species produced by ionospheric chemistry is H, and the primary ions are H^+ and H_3^+. Closer to the homopause, hydrocarbons introduce a complex network of reactions, which we do not consider in detail here (see, Strobel & Atreya 1983, Atreya & Donahue 1986, or Wong *et al.* 2000 for reviews of the most important reactions). There are at present no observational constraints on the hydrocarbon ion chemistry.

Reactions

H_2, He, and H are ionized at wavelengths shortward of 80.4, 50.4 and 91.1 nm. In addition to its direct products, photoionization produces energetic electrons that can increase the net ionization and dissociation rates by 10-20% and can penetrate to deeper levels than solar photons. Photoelectrons also play an important role in creating vibrational excitation, in heating the atmosphere, and in excitation of UV emissions. The peak altitude for absorbing EUV photons is between 1 and 0.1 nbar, about 1000 km above the cloud tops.

Ionization and dissociation of atmospheric constituents is also caused by electrons precipitating from the magnetosphere, but unlike solar photons, whose spectrum is fairly well understood, there are large uncertainties in the energy spectrum of precipitating particles. The aeronomy of the atmosphere is strongly affected by the energy spectrum of the electrons because it determines the altitude profile and relative importance of electron-induced reactions. The reader is referred to the paper by Dalgarno *et al.* (1999) for a review of electron processes in an H_2/He/H gas. The range of electron-induced reactions is analogous to that for photons, as shown in Table 9.3. The modeling of particle precipitation has concentrated on the impact of electrons with energies of 0.1 to $>$ 100 keV. Precipitation of energetic ions has been postulated from time to time (Horanyi *et al.* 1988, Waite

Table 9.3. Chemical Reactions

	Reaction											Rate	Reference
						Photon Reactions							
R1a	H_2	+	hν		$\rightarrow$	H_2^+	+	e				2.48×10^{-9}	Yan *et al.* (1998)
R1b					$\rightarrow$	H^+	+	H	+	e		8.26×10^{-10}	Yan *et al.* (1998)
R2	H_2	+	hν		$\rightarrow$	H	+	H					
R3	H	+	hν		$\rightarrow$	H^+	+	e				4.40×10^{-9}	Hummer & Seaton (1963)
R4	He	+	hν		$\rightarrow$	He^+	+	e				2.39×10^{-9}	Yan *et al.* (1998)
						Electron Reactions							
R5a	H_2	+	e		$\rightarrow$	H_2^+	+	e					
R5b					$\rightarrow$	H^+	+	H	+	e			
R6	H_2	+	e		$\rightarrow$	H	+	H					
R7	H	+	e		$\rightarrow$	H^+	+	e					
R8	He	+	e		$\rightarrow$	He^+	+	e					
						Chemical Reactions							
R9	H_2^+	+	H_2		$\rightarrow$	H_3^+	+	H				2.0×10^{-15}	Thread and Huntress (1974)
R10	H_3^+	+	H		$\rightarrow$	H_2^+	+	H_2				2.0×10^{-15}	Estimated
R11	H_2^+	+	H		$\rightarrow$	H^+	+	H_2				6.4×10^{-16}	Kapras *et al.* (1979)
R12	H^+	+	H_2(v $\geq$ 4)		$\rightarrow$	H_2^+	+	H				$1.0\times10^{-15}e^{-21960/T}$	Estimated (see text)
R13a	He^+	+	H_2		$\rightarrow$	HeH^+	+	H				4.2×10^{-19}	Schauer *et al.* (1989)
R13b					$\rightarrow$	H^+	+	H	+	He		8.8×10^{-20}	
R14	HeH^+	+	H_2		$\rightarrow$	H_3^+	+	He				1.5×10^{-15}	Bohme *et al.* (1980)
R15	HeH^+	+	H		$\rightarrow$	H_2^+	+	He				9.1×10^{-16}	Kapras *et al.* (1979)
						Recombination Reactions							
R16	H	+	H	+ M	$\rightarrow$	H_2	+	M				$8.0\times10^{-45}(300/T)^{0.6}$	Ham *et al.* (1970)
R17	H^+	+	e		$\rightarrow$	H	+	hν				$6.3\times10^{-15}(300/T_e)^{0.64}$	Storey and Hummer (1995)
R18	He^+	+	e		$\rightarrow$	H	+	hν				$7.2\times10^{-15}(300/T_e)^{0.64}$	Storey and Hummer (1995)
R19	H_2^+	+	e		$\rightarrow$	H	+	H				$2.3\times10^{-13}(300/T_e)^{0.4}$	Auerbach *et al.* (1977)
R20a	H_3^+	+	e		$\rightarrow$	H_2	+	H				$2.9\times10^{-14}(300/T_e)^{0.65}$	Sundström *et al.* (1994)
R20b					$\rightarrow$	H	+	H	+	H		$8.6\times10^{-14}(300/T_e)^{0.65}$	Datz *et al.* (1995)
R21	HeH^+	+	e		$\rightarrow$	He	+	H				$1.0\times10^{-14}(300/T_e)^{0.6}$	Yousif & Mitchell (1989)

Two body reaction rates in m^3s^{-1}, and three body reaction rates in m^6s^{-1}. Photon reactions rates are optically thin values at 5.2 AU in s^{-1}

et al. 1988, Morrissey *et al.* 1997), but as yet there is no evidence for involvement of energetic ions in the UV aurora. Trafton *et al.* (1998) has determined limits of 13% and 50% on the contribution to the total precipitation energy by O and S ions. We thus concentrate on electron precipitation. The precipitating electrons themselves cause few reactions in the atmosphere. Rather, they create secondary electrons through ionization of atmospheric constituents, that act as the agents for further ionization and dissociation. Roughly 40 eV is lost by the primary in an ionization event, implying that a 1 keV primary can create 25 secondary electrons, thus secondary processes dominate.

The ions and radicals created by solar radiation and precipitating particles react with the ambient species to create new chemical species. The reactions that are important above the homopause and their rate coefficients are presented in Table 9.3. Though it is the primary ion produced, H_2^+ densities are low, because it is quickly converted to H_3^+ through R9. H_3^+ does not react with the other neutral or ion species and therefore builds up to fairly large densities. The primary loss for H_3^+ is recombination (R20), which produces either 1 or 3 H atoms. H^+ has the second largest production rate and is especially significant at high altitudes where the large H abundance enhances the H^+ production rate. H^+ ions, in contrast to H_2^+, do not readily react with other thermospheric species. Moreover, their radiative recombination rate is very slow. As a consequence, although it represents only ~20% of the ions produced, H^+ is the most abundant ion in most models of the non-auroral ionosphere. There is one possibility for removing H^+ more rapidly than through radiative recombination. McElroy (1973) pointed out that the reaction of H^+ with H_2 becomes exothermic if H_2 is in vibrational level 4 or higher (R12). This possibility has been explored in several modeling studies and will be discussed further below.

Estimates of the rate coefficient for recombination of H_3^+ have varied greatly over the last 30 years. Early measurements by Leu *et al.* (1973) found a large rate coefficient of $2.3\times10^{-13}\,m^3s^{-1}$, typical of that expected for dissociative recombination. Similar results were obtained by Peart and Dodler (1974), Auerbach *et al.* (1977), McGowan *et al.* (1979) Mathur *et al.* (1978), and Macdonald *et al.* (1984). However, measurements by Adams and Smith (1987, 1988, 1989) implied that the rapid rate was for vibrationally excited H_3^+ and that recombination of ground state H_3^+ proceeded at an extremely slow rate ($k < 10^{-17}\,m^3s^{-1}$). This conclusion received theoretical support from quantum mechanical calculations that indicated an absence of level crossings through which recombination could proceed (Michels and Hobbs, 1984). The possibility of a slow H_3^+ recombination rate spawned several investigations into the consequences for the jovian ionosphere (McConnell *et al.* 1987,

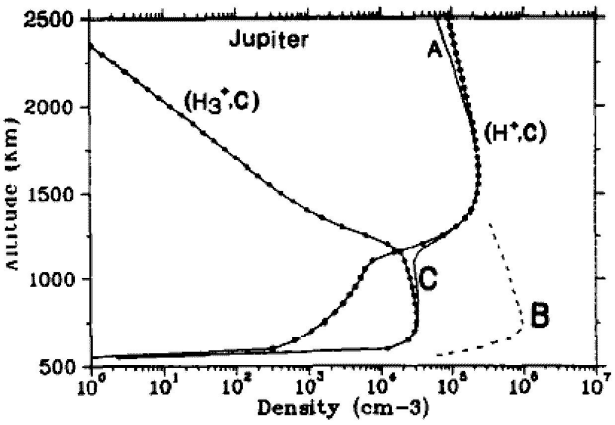

Figure 9.13. A comparison between the models for Jupiter's ionosphere and the V1 Ingress measurements (Curve A). Curve B is a model with no vertical winds or enhanced H_2 vibrational temperature. Curve B has a vertical wind of $25\,\mathrm{m\,s^{-1}}$ and k_2=$2.15\times10^{-20}\mathrm{m^3s^{-1}}$. (From Majeed and McConnell 1991.)

Majeed and McConnell 1991). If the rate were as low as some of the suggested values, it was possible that H_3^+ rather than H^+ would be the main constituent of the non-auroral ionosphere. However, several later laboratory measurements that cleanly separated vibrational levels indicated a rapid recombination coefficient for the ground state (Amano 1988, Canos *et al.* 1992, Larsson *et al.* 1993, Sundstrom *et al.* 1994, Datz *et al.* 1995) and further theoretical work, aided by a greatly improved understanding of the H_3^+ spectrum, indicated rapid pathways for recombination (Bates 1992, Bates *et al.* 1993). The preponderance of evidence now favors rapid H_3^+ recombination and we will consider the consequences of a slow rate no further.

H atoms are produced by photon and electron induced dissociation (R1b and R2) and dissociative ionization (R5b, R6), and by recombination of H_3^+ (R20). H atoms are not lost at significant rates through chemical means in the thermosphere but diffuse downward to the lower atmosphere, where they undergo three-body recombination (R16) or catalytic recombination enabled by hydrocarbons, producing H_2. In either case, loss is rapid below the homopause and the H density quickly becomes small. Diffusion is very rapid in the upper thermosphere and models show that the H density distribution is close to a diffusive equilibrium profile. It follows that diurnal variation in H density should be small because the thermospheric H profile is connected by diffusion to the upper mesosphere where diurnal variations are small.

1D Non-Auroral Ionosphere Models

The chemistry described above is fairly simple, yet the electron density profiles measured by *Pioneer*, *Voyager*, and *Galileo* have defied easy explanation. Not only do the electron densities exhibit large variability, but the individual profiles are different from that predicted by photochemical models. The first comprehensive study of the jovian ionosphere was published by McConnell *et al.* (1982), who demonstrated that models of the jovian ionosphere incorporating solar ionization, chemistry, and diffusion failed to match any of the measured electron density profiles. Generally, the observed ionospheric peaks occurred at higher altitude than predicted and the densities were smaller than predicted. Figure 9.13 shows a typical comparison of observed and calculated electron densities. Obviously, there are physical processes at work that are not included in the photochemical models.

McConnell *et al.* (1982) offer two remedies to overcome the shortcomings mentioned above. They note that H^+ is the main ion in the standard models and that it has a long lifetime because radiative recombination (R17) is a slow process. Because H^+ is so long lived, the jovian ionosphere is especially sensitive to plasma flow. McConnell *et al.* (1982) suggest that the mismatch between the measured ionospheric peak and that predicted by the photochemical models is evidence for flow of plasma along field lines. Where the flow is upward the ionospheric peak will move to higher altitude and where the flow is downward the ionospheric peak will move to lower altitude. Although plasma flow is able to explain the altitude of the peak, the flow does not bring the calculated magnitude of the ionospheric peak into accord with observations. To solve this problem, McConnell *et al.* (1982) examine loss of H^+ through reaction with vibrationally excited H_2. If this reaction is sufficiently rapid it results in lower electron densities. Utilizing both plasma flow and enhanced H_2 vibrational densities, McConnell *et al.* (1982) are able to construct ionospheric models that adequately match most of the observations. More recently, Majeed *et al.* (1999) have analyzed the *Galileo*/0 electron density profiles using the same approach. These authors are able to find combinations of vibrational excitation and vertical drifts that reproduce the observed ionosphere, though the ingress profile requires oppositely directed winds in different altitude regions. Although the existence of these winds have yet to be verified, it is fair to say that the ionospheric models can generally be made to work. The question then becomes whether the required winds and vibrational excitation levels are physically plausible.

Vertical plasma flow in an ionosphere can be induced by rapid escape processes or by neutral winds. The latter possibility is more likely in the jovian ionosphere. Horizontal neutral winds force vertical plasma motion when the ions are tied to slanted magnetic field lines. This requires an ion gyro frequency larger than the ion-neutral collision frequency. The ion gyro frequency is given by $\omega = eB/mc$, which is equal to 4.1×10^4 and 1.4×10^4 Hz for H^+ and H_3^+, respectively. The ion-neutral collision frequency is given by $\omega = kN$, where N is the neutral density and k a collision rate approximately equal to 2.9×10^{-15} and $2.1\times10^{-15}\,\mathrm{m^3s^{-1}}$ for H^+ and H_3^+ (Banks and Kockarts 1970). The gyro frequency is greater than the collision frequency at pressures less than 1 and $0.5\,\mu$bar for H^+ and H_3^+; thus, the ions are tied to the field lines throughout the bulk of the ionosphere. In this case the flux of ions is given by

$$\phi_i = -D_{in}\sin^2 I\left(\frac{\partial N_i}{\partial z} + \frac{N_i}{H_i} + \frac{N_iT_i}{N_eT_e}\frac{\partial N_e}{\partial z} + \frac{N_i}{T_i}\frac{\partial(T_i+T_e)}{\partial z}\right) + N_iW_D \quad (5)$$

where W_D is the vertical drift velocity given by

$$W_D = W_N \sin^2 I - V_n \sin I \cos I \quad (6)$$

with V_N and W_N the velocity of the neutral atmosphere in the northward and vertical directions and I is the angle made by the magnetic field with the vertical, i.e. the dip angle. Equation (6) ignores the possibility of flows driven by electric fields. For a dip angle of 45°, a neutral wind of $1\,\mathrm{km\,s^{-1}}$ implies a vertical plasma flow of $0.5\,\mathrm{km\,s^{-1}}$. Velocities this large cause quite substantial changes to the ionosphere (McConnell *et al.* 1982). To progress further requires measurements and/or models of the neutral winds in Jupiter's thermosphere. This subject is discussed in Section 9.3.5.

The vibrational distribution of H_2 has been studied by Cravens (1974), Atreya *et al.* (1979), Atreya and Donahue (1982), Waite *et al.* (1983), Cravens (1987), Majeed *et al.* (1991), and Kim *et al.* (1992). H_2 has 14 vibrational levels in its electronic ground state. The first few levels are separated by ∼0.5 eV while the separation between levels 13 and 14 is 0.75 eV. If the vibrational distribution were in LTE at a temperature of 1000 K less than 10^{-10} of the molecules would be in the $v \geq 4$ levels. This value is so low that H_2(v) has a negligible effect on ionospheric densities. Thus, the importance of H_2(v) rests on the possibility that the fraction of molecules in $v \geq 4$ is much greater than the LTE population. Non-LTE populations are a possibility because the V-T collision rates in the thermosphere are too low to ensure LTE. The population of the vibrational levels must be determined by calculating the sources and sinks for H_2(v) molecules.

The important sources of H_2(v) in the upper atmosphere of Jupiter are electron excitation of H_2, by both electron and solar photon excitation of the Lyman and Werner bands which fluoresce to vibrationally excited levels in the ground state, and through H_3^+ recombination (R20A), which may produce H_2(v). Primary loss processes include de-excitation through collisions with H and H_2, and reaction with H^+. In addition, vibrational quanta may be redistributed among molecular levels through V-V collisions and may be redistributed in altitude through diffusion.

Cravens (1987) presented the first detailed model for H_2(v). His solar only models, which may be appropriate for low latitudes where electron precipitation is negligible, show that H_3^+ recombination was the main source of H_2(v). The density of H_2(v ≥ 4) at high altitudes was equal to that expected for a Boltzmann distribution at ∼1700 K. This modest enhancement in H_2(v) relative to LTE did cause a decrease in the calculated electron density but only by a factor of two, so the models still predicted much higher electron densities than inferred from the radio occultation experiments. Auroral simulations by Cravens (1987) showed a larger effect with H_2(v ≥ 4) densities corresponding to vibrational temperatures of ∼2500 K and model electron densities reduced by a factor of 10. This brings the models into agreement with the observations at high altitudes but the auroral models still predict an order of magnitude too many electrons near the ionospheric peak (Hinson *et al.* 1999).

Majeed *et al.* (1991) considered only low-latitude solar input cases but added vibrational excitation due to solar fluorescence in the H_2 electronic bands. Majeed *et al.* calculated vibrational temperatures for H_2(v=4) of 1600 K and 1200 K with and without fluorescence. Though the enhanced H_2(v ≥ 4) densities do lead to a reduction in electron densities, the altitude of the electron density computed by Majeed *et al.* (1991) still failed to match the observations. When Majeed *et al.* (1991) imposed vertical winds to raise the altitude of the peak, the calculated electron density becomes much higher than observed.

Kim *et al.* (1992) computed detailed profiles of the H_2(v) concentrations in the auroral regions as a function of altitude, including all the effects listed above except solar fluorescence. They found that H_2(v=1)/H_2(v=0) concentrations were close to LTE, but, crucially, H_2(v=4) populations increased by several orders of magnitude above the expected LTE value from the 0.5 μbar level upward to higher altitudes in the thermosphere. The net result was that the charge exchange reaction between H^+ and H_2(v) to form H_2^+ kept H_3^+ concentrations higher than expected even at high altitudes where H^+ was the dominant ion. Detailed comparison with the radio occultation measurements were not considered in Kim *et al.* (1992), so it is unclear what their results imply for the difficulty in explaining the electron density profiles.

In general, calculations of H_2(v ≥ 4) appear to fall short of that needed to bring the computed electron densities into agreement with observations. It is not clear if this reflects inadequacies in the H_2(v ≥ 4) models or if some other process is responsible for depressing H^+ densities.

The 1D models discussed above are computed for the steady state and do not calculate the diurnal variation of electron density. Chen (1982) has presented time dependent calculations of the jovian ionosphere but predicted small H_3^+ densities (in contrast to later calculations and observations) and so the calculated diurnal variations were small. However, several aspects of the measured profiles suggest that diurnal variations could be important. As mentioned above, the *Voyager* 1 and *Galileo*/0 electron density profiles are similar in the sense that the ionospheric peak is often at higher altitude at dawn than at dusk. The recombination lifetime of the ionosphere is shortest at low altitudes because this region of the ionosphere is dominated by H_3^+, which recombines rapidly compared with H^+. For the *Galileo*/0 ingress the electron density peaks at 900 km where the temperature is 800 K, implying a recombination coefficient of $6\times10^{-14}\,\mathrm{m^3 s^{-1}}$. The electron density is $1\times10^{9}\,\mathrm{m^{-3}}$ and the resulting lifetime is only 160 seconds, much shorter than a jovian day. As a consequence, most of the H_3^+ should have recombined during the night. On the other hand, the recombination time for H^+ is very long, implying that the electron densities at high altitude should not vary during a jovian day. This is in rough agreement with the trends in the data and is also seen in the 3D simulations of Achilleos *et al.* (1998). The time constant arguments presented above do not explain why the electron densities for the *Voyager* 2 and *Galileo*/0 egress are larger than the ingress densities at high altitude or why the *Galileo*/4 dusk densities are lower than the dawn densities, neither does it explain the altitudes of the electron peaks, so clearly other factors are involved.

Matcheva *et al.* (2001) have investigated the effects of gravity waves on ionospheric structure and show that waves modify the ionosphere in two important ways. The authors provide convincing evidence that the sharp ionization layers seen below the main electron density peak are due to compression and rarefraction of plasma by the waves. Cal-

culations presented by Matcheva *et al.* (2001) show that the characteristics of the observed ionization layers are roughly consistent with effects that would be caused by the observed gravity waves in Jupiter's atmosphere. Matcheva *et al.* (2001) also show that upward propagating waves induced a downward flux of plasma that depletes electron density at high altitude and enhances it at low altitude. This effect may contribute to the production of low altitude electron density peaks seen in some of the radio occultation results. Finally, Matcheva *et al.* (2001) point out that the ionosphere in the presence of waves is unlikely to be in steady state and this fact, along with variability in wave sources, may help to explain the observed variability of the electron density profiles.

Interpretation of the global maps of H_3^+ column density inferred from the IR observations have focused not on the detailed chemistry and vertical structure of the ionosphere, but on horizontal variations. Miller *et al.* (1997) points out that the H_3^+ emission rate at latitudes below ∼50 degrees is larger than predicted by models that rely soley upon solar energy deposition (Achilleos *et al.* 1998). In fact, there is a general increase in emission intensity with latitude, contrary to the decreasing profile expected from solar input. Miller *et al.* (1997) interpret these characteristics as evidence for electron precipitation equatorward of the main auroral oval.

The H_3^+ temperature and column density maps were interpreted further by Rego *et al.* (2000), who attempted to separate contributions due to the aurora, diffuse emission from the polar cap, solar input, and a 4th contribution which they labeled MTL (for Mid-to-Low Latitudes). The solar input was specified by assuming that the H_3^+ emission rate was equal at all latitudes to the value at the equator. The MTL component was found to be necessary because the emission rate begins increasing with latitude approximately 5 arc-seconds equatorward of the auroral oval. Assuming the spin axis of Jupiter to lie in the plane of the sky implies that the emissions are confined largely to latitudes poleward of 45 degrees. The MTL emissions also track the variations of aurora with longitude. Rego *et al.* (2000) interpret these characteristics as evidence that the MTL component is auroral in nature, but more diffuse in latitude than the main auroral oval. In essence, they argue that there is some relatively weak electron precipitation from the inner magnetosphere that augments the intense precipitation in the auroral zone. The energy associated with the MTL component is roughly equal in magnitude to solar EUV but is deposited primarily at higher latitudes.

Rego *et al.* (2000) derive energy input rates by assuming that they are linearly related to the emission rate. This is not necessarily the case, given the complex and poorly understood structure of the ionosphere. Emission rate variations could be due to other factors, such as changes in the H^+ density, which would alter the electron density and hence the H_3^+ recombination rate. On the other hand, it is not clear that anything more complicated than a linear approximation is justified until our knowledge of the ionosphere is better established.

9.3.2 H Densities

Analysis of H Lyα emissions constrains primarily the H distribution in the vicinity of and above the CH_4 homopause. The H density depends on the net production of H by chemical processes in the thermosphere and the rate of diffusion to the lower atmosphere. Gladstone *et al.* (1996) examined the dependence of H column densities on the production rate through specification of a downward flux at the upper boundary of the calculation (Hunten 1969, Wallace and Hunten 1973). This downward flux can account for both local production of H and transport of H from auroral zones, as long as the meridional transport occurs mostly at high altitudes. As discussed earlier, the speed of diffusion ensures a diffusive equilibrium profile regardless of the location of the sources and sinks, so the approximation should be accurate. Gladstone *et al.* (1996) computed H column densities of 7.2×10^{19}, 6.0×10^{20}, 1.3×10^{21}, and $5.2\times10^{21}\,\mathrm{m}^{-2}$ for fluxes of 0, 4×10^9, 8×10^9, and $4\times10^{10}\,\mathrm{m}^{-2}\mathrm{s}^{-1}$, respectively. Column densities of 1×10^{21}, 2×10^{21}, and $4\times10^{21}\,\mathrm{m}^{-2}$ have been inferred by investigators (Rego *et al.* 2001, Ben Jaffel *et al.* 1993, Gladstone *et al.* 1996). Adopting a value of $2\times10^{21}\,\mathrm{m}^{-2}$ implies that a flux of roughly $3\times10^{10}\,\mathrm{m}^{-2}\mathrm{s}^{-1}$ is required to explain the Lyα observations; however, the H production rate due to solar processes is only $3\times10^9\,\mathrm{m}^{-2}\mathrm{s}^{-1}$(Waite *et al.* 1983). Alternatively, H at low latitude on Jupiter might be transported down from high production regions in the auroral zones. Estimates of the total power dissipated in the auroral zones vary from 10^{13} to 10^{14} Watts. Using the results on energy partitioning in Waite *et al.* (1983), we calculate H production rates of 4×10^{30} to $4\times10^{31}\,\mathrm{s}^{-1}$ or globally-averaged column production rates of 6×10^9 to $6\times10^{10}\,\mathrm{m}^{-2}$, respectively. Thus, it seems that most of the H in the jovian thermosphere must be produced in the auroral zones, a fact that was realized shortly after the discovery of the intense jovian aurora (Yung and Strobel 1980, Broadfoot *et al.* 1981, Waite *et al.* 1983).

If the aurorae are supplying most of the H in Jupiter's upper atmosphere, then it follows that the H density in the auroral regions should be relatively large. This question was first addressed by Waite *et al.* (1983). Their calculations considered the effects of precipitating electrons on equatorial and auroral model atmospheres. The equatorial models are calculated by assuming that absorption of solar radiation drives chemical changes in the atmosphere, but the precipitating electrons do not, while the auroral models are a fully self-consistent calculation. The rationale behind this approach is that meridional transport may carry away many of the products of auroral chemistry and so the electrons could be depositing their energy into something similar to an equatorial atmosphere, even in the auroral zones. Waite *et al.* (1983) calculate H column integrated production rates of 1.6×10^{15} and $4.1\times10^{15}\,\mathrm{m}^{-2}\mathrm{s}^{-1}$ for precipitation of $10\,\mathrm{mW\,m}^{-2}$ of 1 and 10 keV electrons into an auroral atmosphere. Utilizing the model atmosphere of Atreya *et al.* (1981) and Festou *et al.* (1981) and adopting a constant eddy diffusion coefficient of $K(z) = 20\,\mathrm{m}^2\mathrm{s}^{-1}$, Waite *et al.* (1983) calculate H columns of 3.7×10^{22} and $4.2\times10^{22}\,\mathrm{m}^{-2}$, for the 1 and 10 keV cases. The H density becomes comparable to H_2 at a pressure of roughly 3×10^{-2} nbar in these models.

Perry *et al.* (1999) have also presented calculations of H profiles in the auroral zones for electrons of energy 20, 50, and 100 keV and a flux of $11\,\mathrm{mW\,m}^{-2}$. To calculate the composition of the atmosphere, Perry *et al.* (1999) adopt models in which the eddy diffusion coefficient varies as the

inverse square root of number density and consider values at the homopause of $K_H = 180$, 990, and 7600 $m^2 s^{-1}$. Perry *et al.* mention that their CH_4 profiles disagree with the Festou *et al.* (1981) analysis but do not discuss how they relate to more recent determinations of CH_4 density. An H column density of 1×10^{21} m^{-2} is adopted for the background atmosphere, motivated by the relatively low H density derived by Prangé *et al.* (1997), and the ASI measurements are used to defined the temperature profile. Perry *et al.* (1999) compute H column densities of 3×10^{22}, 1.5×10^{22}, and 6×10^{21} m^{-2} for fluxes of 11 mW $m^{-2}$of 20, 50 and 100 keV electrons into the model atmosphere with $K = 990\,m^2 s^{-1}$. These values are considerably lower than the column density of 4×10^{22} m^{-2} calculated by Waite *et al.* (1983) for a flux of 10 mW m^{-2} of 10 keV electrons, yet the H densities in Perry *et al.*'s models become larger than H_2 at a pressure of ∼2 nbar. It is not clear if the divergent results are due to differences in the temperature profile, eddy coefficient, or some other aspect of the model.

Achilleos *et al.* (1998) took the first steps toward calculating the auroral and low-latitude H densities in a self-consistent manner using a Thermospheric General Circulation Model (TGCM). These authors calculate H production rates for an assumed flux of 8 mW m^{-2} of 10 keV electrons. Achilleos *et al.* (1998) adopt an eddy diffusion coefficient that varies as the inverse square root of number density with values of 500 $m^2 s^{-1}$ in the auroral regions and 100 $m^2 s^{-1}$ in low-latitude regions at a pressure of 2 μbar. The model atmosphere is calculated self-consistently, but the calculations have not yet been run to convergence so the results also depend on the initial guess, which is taken from Rego *et al.* (1994). Achilleos *et al.* (1998) find large densities with H becoming the dominant constituent at pressures less than 1 nbar. Interestingly, the build-up of H in the auroral zones is a significant driver of meridional winds because it lowers the mean molecular weight, thereby increasing the scale height.

Although there seems to be general agreement that the jovian aurorae are copious sources of H, it is difficult to draw other general conclusions from the studies described above. The models are characterized by a variety of assumptions regarding input electron fluxes, thermal profiles, eddy diffusion profiles, and H densities in the background atmosphere. In many cases, the assumptions are at odds with results from analysis of other observations. There do appear to be enough observations available to tightly constrain the problem. The spectrum of precipitating electrons can be inferred through analysis of H_2 emissions (*c*f. Ajello *et al.* 2000), the H densities through analysis of Lyα profiles, the thermal profile through analysis of H_3^+ and H_2 emissions, and the CH_4 profile through analysis of CH_4 fluorescence. An investigation that took all these constraints into account and made the smallest number of ad hoc assumptions would be worthwhile.

There remains the interesting problem of what causes the changes in line shape responsible for the Lyα bulge. Ben Jaffel *et al.* (1993) argue that the observed broadening of the line cores is evidence for supersonic turbulence in Jupiter's upper atmosphere. In order to fit the line profile, Ben Jaffel *et al.* (1993) require turbulence with a characteristic velocity of 9 km s^{-1} over a column of 2×10^{19} m^{-2}, which is roughly 1% of the total H column in the upper atmosphere. This hypothesis is further explored in Sommeria *et al.* (1995), who suggest that the supersonic turbulence is caused by the collision in the equatorial region of two high speed jets emanating from the polar regions. Emerich *et al.* (1996) argue that the rapidly changing and complex line profiles observed with the GHRS/HST support the supersonic turbulence explanation, but the arguments in its favor do not appear strong.

The supersonic jet explanation for the Lyα bulge fails to explain several of its primary characteristics. As noted by Sommeria *et al.* (1995), the correlation of the bulge with the magnetic dip equator must be viewed as a coincidence in their theory and this is less than satisfying. Moreover, Sommeria *et al.* (1995) show that initial horizontal velocities in the auroral zone must be 20 km s^{-1} for the jets to reach the equator. In principle, winds could be driven by meridional temperature gradients or by the auroral electrojet. The maximum velocity produced by temperature gradients is of order the sound speed, or 2 km s^{-1}, which is much smaller than that required by Sommeria *et al.* (1995). The maximum velocity that can be produced by the auroral electrojet is equal to the rotation velocity of the planet at the latitude of the auroral oval, or 6 km s^{-1}, which is a factor of several less than required. In the absence of significant drag forces, meridional velocities greater than the rotational velocity are required to overcome the Coriolis force, but the electrojet can only produce velocities less than the rotation velocity. Forces due to viscosity or ion drag can cause can cause meridional winds even in the presence of a strong Coriolis force, but the existence of significant drag forces is likely in itself to prohibit development of supersonic winds. In fact, a potentially serious problem with the supersonic wind hypothesis is the neglect of molecular viscosity. According to Sommeria *et al.* (1995), the bulge is caused by a small column of supersonic H flowing through or above a stationary background atmosphere. The deceleration due to viscous drag is given by $(1/\rho)\partial/\partial z\ (\mu\partial U/\partial z)$, which we approximate as $\mu\Delta U/\rho H^2$. Assuming a velocity difference of $\Delta U = 20$ km s^{-1} over a distance of $H = 150$ km, a viscosity coefficient of $\mu = 3\times10^{-1}$ kg $m^{-1} s^{-1}$ and a density of $\rho = 6\times10^{-14}$ kg m^{-3} implies a viscous deceleration of $4\times10^2 m\,s^{-2}$, and a stopping distance of 500 km, much smaller than a jovian radius. In order to avoid this viscous deceleration the column of supersonic H would have to be detached from the main atmosphere in some fashion. Finally, winds of 20 km s^{-1} in the jovian upper atmosphere should appear as Doppler shifted Lyα profiles at high and mid latitudes, but this has not been observed.

9.3.3 Thermal Structure

Possible sources of heating in the upper atmosphere of Jupiter include absorption of solar energy, precipitation of charged particles, dissipation of kinetic energy in winds and waves, as well as redistribution of energy by dynamical processes. Possible sources of cooling include the divergence of the thermal conduction flux, dynamical cooling by waves or large scale motions, and radiation by atmospheric molecules.

H_2 is the most abundant species in the upper atmosphere but is an inefficient coolant. The small A values for ro-vibrational transitions imply negligible radiative cooling rates. Pure rotational transitions in H_2 are also extremely

weak and can be neglected on Jupiter, though they may important on Uranus (Trafton *et al.* 1999). Rotational transitions of H_3^+ are likewise forbidden and unimportant in cooling; however, as noted in Section 9.2.2, the vibrational spectrum of H_3^+ is permitted and unusually strong. Moreover blackbody emission peaks near 3 μm at the temperatures of the jovian thermosphere, close to where H_3^+ radiates. Thus, on Jupiter, H_3^+ radiation is important to the thermal balance, especially in auroral regions where temperatures are elevated.

Heating associated with absorption of solar energy or energetic charged particles is a complicated affair. To accurately calculate the heating rate requires an accounting of the numerous processes that increase the translational energy of atoms, molecules or ions. Such calculations have been carried out by Waite *et al.* (1983) and Grodent *et al.* (2001). Chemical reactions are the primary means for heating the neutral atmosphere. The products of exothermic chemical reactions, such as H_3^+ recombination, have excess energy that is thermalized through collisions with the background atmosphere. Second in importance are collision between ambient molecules and vibrationally and rotationally excited H_2 that convert vibrational (VT) and rotational (RT) energy in the excited molecule to translational energy of the collision partner. Heating by this process requires vibrational and rotational level populations above their LTE values. Excess vibrational and rotational excitation is produced by electron impact excitation and scattering in the Lyman and Werner bands. Also important is dissociation of H_2 by electron impact and solar radiation. By tabulating all these processes Waite *et al.* (1983) calculated column-averaged heating efficiencies of 53%, 51%, and 53%, for solar EUV absorption, 1 and 10 keV electrons precipitating into an unconverged equatorial atmosphere. For electron precipitation into a converged atmosphere, which has a higher H density, Waite *et al.* (1983) calculated heating efficiencies of 33 and 46%, for 1 and 10 keV electrons.

Temperatures in the thermospheres of the terrestrial planets and Titan can be understood primarily as a balance between thermal conduction and heating by solar EUV and energetic particles. When these models are applied to low latitude regions on Jupiter and the other giant planets they predict that temperatures in upper thermosphere only tens of kelvin higher than at the mesopause (Strobel and Smith, 1973), yet the observed temperatures are hundred of kelvins greater than mesopause temperatures. We can gain insight into this problem with some simple estimates first applied to Jupiter by Hunten and Dessler (1977). We assume that the solar energy is deposited in a thin layer at pressure p_1 and radiated away in a thin layer at pressure $p_\circ$ near the mesopause. Thermal conduction carries the energy between the layers. Under these assumptions, the exospheric temperature is given by

$$T^s = T_\circ^s + \frac{sH_\circ F_\lambda}{A} ln\big(p_\circ/p_1\big) \tag{7}$$

where F_λ is the thermal conduction flux, defined to be positive downward. (Derivation of this equation requires the use of pressure as the vertical coordinate, rather than altitude). To compute values we adopt a solar EUV flux at 1 A.U. of 4 mW m^{-2}, a heating efficiency of 50%, and $\log(p_\circ/p_1) = 5$, which is a typical value for Earth. The thermal conductivity is given by $\lambda = AT^s$, where $A = 252\,\mathrm{mW\,m^{-2}K^{-(s+1)}}$ and $s = 0.751$ (Hanley *et al.* 1970). The results are presented in Table 9.4 for all four giant planets along with measured exospheric temperatures. The calculations do not include cooling from H_3^+ radiation and the temperatures are therefore upper limits. Nevertheless, the observed temperature differences are much larger than the calculated values. Clearly, some process other than absorption of solar energy is heating the thermospheres of the outer planets, and this process is not specific to Jupiter. Possibilities investigated to date include energetic particle precipitation in the equatorial regions, dissipation of upward propagating gravity waves, and redistribution of energy deposited in the auroral regions to low latitudes. We will discuss each in turn.

Low-Latitude Particle Precipitation

Energetic particle precipitation at low latitudes was suggested shortly after discovery of the high temperatures on Jupiter (Hunten and Dessler 1977, Broadfoot et al. 1981). For a while, this possibility received some support from the belief that precipitating particles were required to explain the UV emissions from Jupiter and that the heating associated with these particles was approximately that necessary to explain the high thermospheric temperatures (Shemansky 1985) However, since the UV emissions are adequately explained by a combination of solar fluorescence and photoelectron excitation (Yelle *et al.* 1987, Yelle 1988, Liu and Dalgarno 1996a), this argument no longer applies. Waite *et al.* (1997) discovered X-ray emission from low latitudes on Jupiter, suggesting energetic particle precipitation. Analysis of these data using models for the precipitation of energetic ions into the jovian atmosphere showed that the observed X-ray intensity was consistent with column integrated heating rates from 0.08 to 3.0 mW m^{-2}, with a preferred value of 0.2 mW m^{-2}. Energy fluxes in this range could plausibly explain the observed temperatures. However, Maurelis *et al.* (2000) demonstrated that a significant fraction of the X-ray emissions are due to scattering of solar X-rays, which is not associated with any heating of the upper atmosphere. More recent observations of jovian X-rays with Chandra (Gladstone *et al.* 2002) show that the low-latitude emissions vary smoothly over the disc of Jupiter and in particular show no correlation with the magnetic field. This supports the solar scattering hypothesis (T. Cravens, personal communication 2002) and it seems doubtful that low-latitude particle precipitation at the levels postulated by Waite *et al.* (1997) is required to explain the observed X-rays. We note that smaller levels of particle precipitation are not ruled out by either the UV or X-ray data.

As discussed in Section 9.3.1, Miller *et al.* (1997) have shown that enhanced H_3^+ emission rates are not strictly confined to the auroral ovals but there is a weaker component that extends to lower latitudes. Presumably, this enhanced emission is also related to heating and ionization associated with electron precipitation, as are the H_3^+ emissions from the main auroral oval. Rego *et al.* (2000) has estimated that the energy deposition implied by this emission is of the same order as solar EUV and much less than the energy deposited in the auroral zones. The energy is deposited at lower lati-

Table 9.4. Exospheric Temperatures

Planet	Jupiter	Saturn	Uranus	Neptune
Heliocentric Distance (A.U.)	5.20	9.57	19.19	30.07
Absorbed Solar Flux ($\mathrm{mW\,m^{-2}}$)	3.7×10^{-2}	1.1×10^{-2}	2.7×10^{-3}	1.1×10^{-3}
Mean Molecular Mass (amu)	2.26	2.12	2.30	2.38
Gravity ($\mathrm{cm\,s^{-2}}$)	2312.	896.	869.	1110.
$T_\circ$ (kelvins)	160.	143.	130.	130.
$H_\circ$ (km)	25.5	62.6	54.1	40.9
T_∞ (observed)	940.	420.	800.	600.
ΔT (observed)	780.	280.	670.	470.
T_∞ (calculated)	202.7	177.1	137.9	132.3
ΔT (calculated)	42.7	34.1	7.9	2.3

tudes than the energy forming the main oval and therefore it may be easier to transport to low latitudes. On the other hand, since the energy involved is only of the same order as solar EUV it cannot have a large effect on the thermospheric temperature.

Gravity Wave Dissipation

The gravity waves inferred from the ASI temperature profile (Young *et al.* 1997) carry substantial amounts of energy and have a significant effect on the temperature profile in the thermosphere. These waves are likely generated in the lower atmosphere and their amplitudes grows approximately as $1/\sqrt{\rho}$ as they travel to the thermosphere. Waves with small wavelengths are effectively damped and only waves with long wavelengths that also avoid critical levels in the stratosphere survive to the thermosphere. Thus, we expect that only a small fraction of the waves deposit their energy in the thermosphere. On the other hand, only 4×10^{-5} of Jupiter's internal energy flux is required to heat the thermosphere to observed levels.

Young *et al.* (1997) compared the energy flux carried by the waves with the thermal conduction flux inferred from a smoothed version of the ASI temperature profile. They found that the two fluxes were in good agreement if the wave flux was multiplied by 0.65, presumably accounting for the fact that not all the wave energy would be deposited as heat. This resulted in a net wave heating flux of $0.5\,\mathrm{mW\,m^{-2}}$. The heating effects of the two waves were considered separately and it was found that wave 2 (see Table 9.2) was far more important to the thermal balance.

Matcheva and Strobel (1999) re-examined the question of wave heating in Jupiter's thermosphere and showed that the expression for the wave energy flux derived by French and Gierasch (1974) and used by Young *et al.* (1997) was incorrect. The error can be traced to the fact that French and Gierasch (1974) assumed a stationary background atmosphere in their derivation. However, a wave in the presence of damping transports mass. The mass flux is second order in the perturbation velocity and must be balanced by a flux in the background atmosphere to satisfy mass conservation; thus, the background atmosphere cannot be stationary. Though the induced velocity is second order in the perturbation variables it cannot be neglected as it was in French and Gierasch (1974) because the energy flux is also second order in the perturbation variables. As a consequence, the induced velocity has a significant effect on the wave heating rates. This effect was first realized by Walterscheid (1981).

Matcheva and Strobel (1999) derive the following expression for wave heating

$$\frac{\partial}{\partial z}\left(\overline{\rho u}\,\overline{w'u'} + \overline{w'p'} + \rho c_p \overline{w'T'} - \lambda\frac{\partial \overline{T}}{\partial z}\right) = Q_R \qquad (8)$$

where primes indicate perturbations due to the wave and the overbar indicates an average over a wave period. The vertical velocity is w, u is the horizontal velocity, and λ is the thermal conduction coefficient. The first term in equation (8) represents heating due to the interaction between the wave and the horizontal wind field. Matcheva and Strobel (1999) consider only cases for which this term is zero. The second term represents the work done by pressure forces. Matcheva and Strobel (1999) refer to the third term as the divergence of sensible heat flux. The fourth term is the thermal conduction flux and the sum of all these terms is equal to the radiative heating rate, Q_R, which for Jupiter is simply cooling by H_3^+. A term describing viscous heating of the background atmosphere has also been dropped from equation (8), though it is also of second order in the perturbation variables.

The wave heating terms are shown in Figure 9.14 for waves with the characteristics identified by Young *et al.* (1997). The $\overline{w'p'}$ term is positive at all altitudes but the $\rho_\circ c_p \overline{w'T'}$ term changes from positive below the location of maximum wave amplitude to negative at higher altitudes. The column-integrated heating rate of the wave is still positive but its effect on the temperature profile is reduced. Matcheva and Strobel (1999) calculate a thermospheric temperature rise of ∼200 K for waves with the inferred characteristics, which, though significant, is a factor of 3 smaller than required. Matcheva and Strobel (1999) also consider waves with larger amplitudes than those observed by the ASI experiment and show that these waves can heat the thermosphere to 700 K. Because of the cooling effect of waves, the exospheric temperature may be smaller than the maximum temperature in the thermosphere (Matcheva and Strobel, 1999). We mentioned earlier that Sieff *et al.* (1998) showed that a temperature decrease of 100 K in the upper thermosphere is consistent with the ASI data. Verification of the existence of a temperature drop in the upper thermosphere would help determine the wave heating rates, but at present there are no observations that strongly constrain temperatures in this region.

Strobel (2002) has derived an expression for the maxi-

mum energy flux carried by a gravity wave in the thermosphere. His approach is to estimate the maximum energy flux as that carried by a wave with an amplitude equal to the breaking amplitude. Mathematically, this is equivalent to requiring $k_z \Delta T < g/c_p$, at the maximum wave amplitude where k is the vertical wavenumber and ΔT the amplitude. Strobel (2002) derives an expression for the wave flux at the location where ΔT is maximum. However, the wave is already significantly damped by the time it reaches it maximum amplitude and a significant amount of thermospheric heating has already occurred. This energy must be included in the estimate because Strobel (2002) is comparing his calculations to the outward flux of energy at the base of the thermosphere. Following the procedure outlined in Strobel (2002), it can be shown that the unattenuated flux for a wave that is at saturation where its amplitude is maximum is

$$F = 1.35 g \frac{\gamma - 1}{\gamma} \left(\mu + \frac{\lambda}{c_p} \right) \tag{9}$$

where γ is the specific heat index, μ the coefficient of viscosity, and λ the thermal conduction coefficient. In addition to a factor of 2.7, this differs from the expression given by Strobel (2002) because we consider damping by both viscosity and thermal conduction. Equation (9) gives the wave flux in the lower thermosphere, whereas Strobel's (2002) expression gives the wave flux at the altitude of maximum amplitude. Using $\lambda/c_p = 2.9 \times 10^{-6}\ \mathrm{kg\,m^{-1}\,s^{-1}}$, $\mu = 2.0 \times 10^{-6}\ \mathrm{kg\,m^{-1}\,s^{-1}}$, $g = 23\ \mathrm{m\,s^{-2}}$, and $\gamma = 1.4$ gives $F = 0.43\ \mathrm{mW\,m^{-2}}$, which is a factor of 3.3 larger than estimated by Strobel (2002) and approximately equal to thermal conduction flux inferred from the ASI temperature profile.

The estimates above neglect several factors in order to simplify the problem and the quantitative results should not be treated as precise. As mentioned by Strobel (2002), the strong temperature gradient in the thermosphere helps to stabilize waves against convective instability and permits larger fluxes. Moreover, the energy input into the thermosphere can be enhanced by the presence of additional waves, although these may interact to cause wave breaking at lower levels, limiting the increase in wave energy. Finally, equation (9) assumes that waves are damped by viscosity and thermal conduction, but other processes such as ro-vibrational relaxation, molecular diffusion, and ion drag can damp waves as well.

Matcheva and Strobel (1999) used a semi-analytic WKB approximation to calculate the growth of wave amplitudes and phase. A full numerical simulation was carried out by Hickey *et al.* (2000). Rather than calculating a temperature rise due to wave heating, Hickey *et al.* (2000) calculate wave propagation through a model atmosphere based on the ASI observations and the wave properties derived by Young *et al.* (1997). The observational constraints on the wave properties are the apparent vertical wavelength along the probe trajectory and the altitude of maximum amplitude (see Table 9.2). In order to have wave 2 reach its maximum amplitude at 710 km, Hickey *et al.* (2000) require a vertical wavelength of 338 km, more than a factor of 3.7 larger than the vertical wavelength of 92 km derived by Young *et al.* (1997) and Matcheva and Strobel (1999). Hickey *et al.* (2000) attribute this large difference to the neglect of dissipative effects in the approximate dispersion relations used in the WKB approximations, but these terms are included by Matcheva and Strobel (1999) and, although there is an effect, it is not large and does not explain a factor of 3.7 increase in wavelength. Hickey *et al.* (2000) also suggest that wave reflection by the increase of kinetic viscosity with altitude may explain the differences in derived wavelength.

Hickey *et al.* (2000) determine the net heating rate in the thermosphere by calculating the divergence of the thermal conduction flux from a smoothed version (with waves removed) of the ASI temperature profile. Hickey *et al.* then calculate a new temperature profile from the difference between the net heating rate and the wave heating rate. They find that the temperature profile calculated in this manner is only slightly warmer (tens of kelvins) and, in some cases, cooler than the ASI profile. Thus, the Hickey *et al.* (2000) results differ significantly from Matcheva and Strobel (1999).

The differences may be due to the more sophisticated numerical treatment used by Hickey *et al.* (2000). As these authors point out, WKB calculations overestimate wave fluxes because they do not account for reflection. On the other hand, there is reason to be skeptical of Hickey *et al.*'s approach for relating heating rates and temperatures. Because the relationship between heating rates and temperature is highly non-linear and non-local, it is not clear how to interpret a temperature difference calculated from a difference in heating rates. The conclusion that the waves can cause a net cooling is particulary problematic. At the base of the thermosphere, where damping is unimportant, the upward wave flux must be balanced by the thermal conduction flux

$$\lambda \frac{d\overline{T}}{dz} = \overline{w'p'} \tag{10}$$

The wave energy flux is $\overline{w'p'} \sim 0.4\ \mathrm{mW\,m^{-2}}$, implying a positive temperature gradient of ~2 K/km. While the magntitude of the flux may be altered by reflection, the reflection cannot reasonably be expected to cause a downward energy flux or a negative temperature gradient.

The wave heating models employed by Young *et al.* (1997), Matcheva and Strobel (1999), and Hickey *et al.* (2000) are highly idealized. The interaction of waves with the horizontal wind field is neglected, even though the waves deposit momentum as well as energy. The atmospheres are treated as if composed of a single constituent, even though the effects of multi-species diffusion on wave damping and heating can be large (del Genio *et al.* 1979). The atmosphere is assumed to be in LTE, but the interaction of waves with the internal degrees of freedom on molecules can effect the energetics substantially (Hines 1977a, 1977b). The effects of ion drag are ignored even though this is an important damping process for some waves on Earth (Klostermeyer, 1972). It is essential to examine these processes before definitive conclusions are formed on the importance of wave heating on Jupiter.

Redistribution of Auroral Energy

The altitude derivative of the ASI temperature profile indicates a downward thermal conduction flux of $0.6\ \mathrm{mW\,m^{-2}}$ (Young *et al.* 1997). If we assume that this is the energy flux

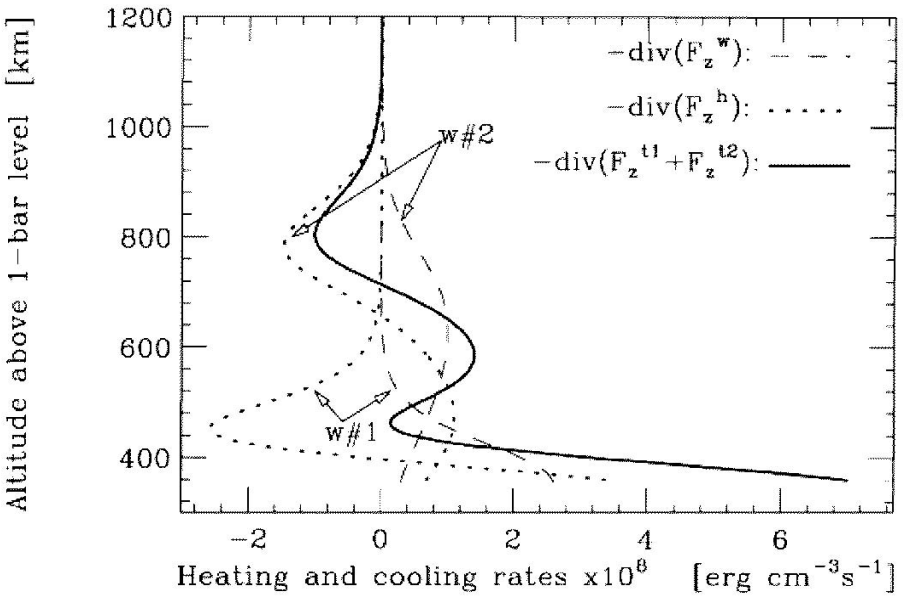

Figure 9.14. Gravity wave heating rates in Jupiter's upper atmosphere for the wave characteristics determined by Young *et al.* (1987). The 'sensible heat flux' studied by Matcheva and Strobel (2001) causes a cooling of the upper thermosphere. (From Matcheva and Strobel 1999).

required to raise the thermospheric temperature to 940 K and that it applies at all latitudes and longitudes then a total power of 4×10^{13} W is implied. This is within the range of 10^{13}-10^{14} W inferred for the jovian aurora. However, in order for the auroral energy to be important on global scales, the meridional transport of this energy must be more efficient than local loss processes, such as conduction down to the hydrocarbon layer or radiative cooling by H_3^+. Dynamical simulations, such as those described in section 9.3.5, are needed to fully address this problem. However, we can gain some insight into the problem with some general observations.

The time constant for vertical energy transport by thermal conduction can be expressed as

$$\frac{1}{t_\lambda} = \frac{\gamma}{\gamma - 1}\frac{F_\lambda}{Hp} \tag{11}$$

where γ is the ratio of specific heats, F_λ is the thermal conduction flux, H is the atmospheric scale height, and p an estimate of the pressure at which high temperatures are reached. We adopt $\gamma = 1.4$, $F_\lambda = 0.6\,\mathrm{mW\,m^{-2}}$, $H = 100\,\mathrm{km}$, and $p = 10^{-2}\,\mu$bar and estimate $t_\lambda = 6\times10^5$ s. Thus, to compete with thermal conduction, meridional wind speeds in the upper atmosphere need to be of order $u \sim R_J/t_\lambda \sim 0.1\,\mathrm{km\,s^{-1}}$, which is not unreasonable and is, for example, of roughly the same speed as meridional winds in the Earth's thermosphere. Moreover this estimate of the wind speed is smaller than the velocities in the electrojet measured by Stallard *et al.* (2002).

The time constant for radiative cooling of the thermosphere is given by

$$\frac{1}{t_R} = \frac{q_R}{\rho H c_p T} \tag{12}$$

where q_R is the column integrated cooling rate due to H_3^+, ρ the mass density, and c_p the specific heat at constant pressure. For $q_R = 0.1\,\mathrm{mW\,m^{-2}}$, $\rho = 4\times10^{-10}\,\mathrm{kg\,m^{-3}}$, and $T = 600$ K (the values at 0.01 μbar), we have $t_R = 4\times10^6$ s. This is larger than the thermal conduction time constant, so H_3^+ radiation at mid-latitudes should not choke off meridional flow; however, the H_3^+ radiation rate is highly temperature sensitive and time constants are significantly shorter in the auroral regions. Lam *et al.* (1997) infers a H_3^+ cooling rate of $\sim1\,\mathrm{mW\,m^{-2}}$ in the main auroral oval, implying a time constant of $t_R = 4\times10^5$ s, which is comparable to the thermal conduction time constant, but still likely to be longer than the dynamical time constant. Thus, these simple estimates indicate that some of the auroral energy may be carried away horizontally. The most important barrier to meridional transport of auroral energy is likely to be the Coriolis force. However, simple calculations of this effect, in the highly viscous upper atmosphere, are difficult and complete dynamical simulations are necessary to further study the question.

Summary

The explanation for the high thermospheric temperatures at low and mid-latitudes on Jupiter is still uncertain. Redistribution of auroral energy is a possibility, but this has yet to be demonstrated with calculations. If non-auroral X-rays are produced by solar scattering, then precipitation of energetic ions at low latitudes is unlikely to be a significant source of thermospheric heating. Neither is precipitation of low energy electrons required to explain the UV emissions from non-auroral regions. Moreover, we must remember that the high thermospheric temperatures occur also on Saturn, Uranus, and Neptune and it is sensible to search for an explanation common to all 4 giant planets. Energetic particle precipitation is even less likely on Saturn, Uranus, and Neptune

than on Jupiter and redistribution of auroral energy is not a possibility except on Jupiter. The only energy source available on all 4 giant planets is upwardly propagating gravity waves. This, of course, does not argue that processes related to the intense magnetosphere are not important on Jupiter, but rather that if waves are important on Saturn, Uranus and Neptune, then then should be important on Jupiter as well.

With the properties for waves deduced from the ASI observations, gravity wave heating does not appear sufficient to account for the thermospheric temperatures on Jupiter, and it is unclear if even larger waves would be sufficient. Nevertheless, the ASI profile represents a single trace through the thermosphere at a single time and it may be unwise to conclude that it represents average conditions. Moreover, calculations of gravity wave heating to date have been highly simplified. The observed waves do appear to carry sufficient energy but a better understanding of their dissipation is needed. Finally, we note that meridionally propagating gravity waves, generated by aurora, may transport energy to lower latitudes, combining these two possibilities.

9.3.4 Auroral Temperature profile

It is clear that the high thermospheric temperatures in the auroral zone are caused by energetic particle precipitation. The most recent examination of this question is by Grodent *et al.* (2001) who calculated heating by precipitating electrons, with a detailed accounting of the heating processes, radiation by H_3^+, and thermal conduction. The calculations were constrained by comparison with temperatures and color ratios inferred from the H_2 Lyman and Werner bands, H_2 quadrupole emission rates, and H_3^+ emission rates. The spectrum of precipitating electrons used by Grodent *et al.* (2001) is similar to that inferred by Ajello *et al.* (2001), however adjustments are made so that the calculated temperature profile matches the observational constraints. Results are shown in Fig 15. Grodent *et al.* (2001) found that the ∼100 eV electrons argued for by Ajello *et al.* (2001) are important for heating the upper thermosphere and establishing the exospheric temperature. The energy deposited by these electrons is balanced primarily by thermal conduction. The 100 keV electrons deposit their energy mostly below the homopause, where it is efficiently radiated away by hydrocarbons. Grodent *et al.* (2001) find that a flux of 3 keV electrons is needed to heat the thermosphere just above the homopause and explain the temperatures derived from the H_2 Lyman and Werner bands. Interestingly, they find that thermal conduction plays a small role in this region and heating is balanced primarily by H_3^+ cooling.

The H_3^+ cooling rates used by Grodent *et al.* (2001) are actually a factor of 5 larger than those observed in the auroral zones by Lam *et al.* (1997). The rationale for this is that the Lam *et al.* observations had a pixel size of $3'' \times 3''$, which is larger than the area of the auroral region modeled by Grodent *et al.* (2001). Thus, Grodent *et al.* (2001) postulated that the average brightness observed by Lam *et al.* (1997) is due to dilution of a higher emission rate from a smaller area. But, Stallard *et al.*'s (2002) study made use of a $0.2'' \times 0.5''$ pixel size, with the $0.2''$ dimension in the east-west direction. Their spatial resolution was therefore much better matched to the auroral oval dimensions seen in HST images (e.g. Clarke *et al.* 1998, Pallier and Prangé, 2001). More detailed examination of Stallard's results show that for individual east-west emission profiles across the auroral/polar region the DPR was never less than 40% of the brightest part of the auroral oval. And the BPR intensity was ∼60% of auroral. So although the oval itself only extended over 0.5" - i.e. 1/6 of Lam *et al.*'s (1997) pixel size - in good agreement with Grodent *et al.*'s (2001) estimate, the rest of the pixel was filled with diffuse, but still considerable, emission from the rest of the polar cap. Thus, the correction for the differences in spatial resolution in probably closer to a factor of 2 than the factor of 5 adopted by Grodent *et al.* (2001).

9.3.5 Dynamics of the Thermosphere

The previous sections have emphasized that atomic hydrogen in Jupiter's upper atmosphere may be synthesized primarily in the auroral zones and that energy deposited in the auroral zones may be important on a global scale. Moreover, as discussed in Section 9.2.2, we have direct evidence from the Doppler shift of H_3^+ emissions of high winds in auroral regions. To study these phenomena requires an investigation into the dynamics of the upper atmosphere. We first discuss how winds in the auroral region can be driven by coupling between the ionosphere and magnetosphere and then review models for dynamics on a global scale.

Jupiter's middle magnetosphere, between the orbit of Io at 5.9 R_J and ∼60 R_J, is dominated by an equatorial plasmasheet. Plasma is continuously supplied by the eruption of volcanoes on Io, and the subsequent photo-ionization of the gas produced. This plasma is accelerated toward co-rotation with the planet by the jovian magnetic field. Freshly formed plasma orbits roughly at the angular velocity of Io, once every 42.46 hours, but the jovian field is rotating with the planet, once every 9.93 hrs, over a factor of 4 faster. As plasma is accelerated, it also drifts radially outward. Hill (1979) showed that at distances greater than ∼20 R_J the jovian magnetic field became too weak, and the required torque too large, to maintain effective plasmasheet co-rotation. He linked the rate at which the plasmasheet fell behind co-rotation to the intensity of currents generated along magnetic field lines. These Birkeland, or field-aligned, currents flow outward through the plasmasheet from the point of significant co-rotation breakdown to the point where the plasma is orbiting Jupiter more or less at the Keplerian velocity. Thus the currents are upward along field lines close to the planet and downward along those further out. Later work by Hill (2001) and Cowley and Bunce (2001) showed that these currents could be responsible for producing the bright auroral ovals observed on Jupiter (e.g. Clarke *et al.* 1998, Satoh and Connerney 1999): the upward current around 20 R_J corresponds to downward precipitating, high energy electrons, accelerated by megavolt plasmasheet electric potentials (Cowley and Bunce, 2001).

The field aligned currents have to close through the ionosphere, between the footprints of the regions spanned by the upward and downward current carrying field lines. Megavolt potential differences may again be involved to drive the necessary currents through the ionosphere. In the northern hemisphere, the magnetic field at the auroral oval is nearly vertically upward and the electric field is southward; in the

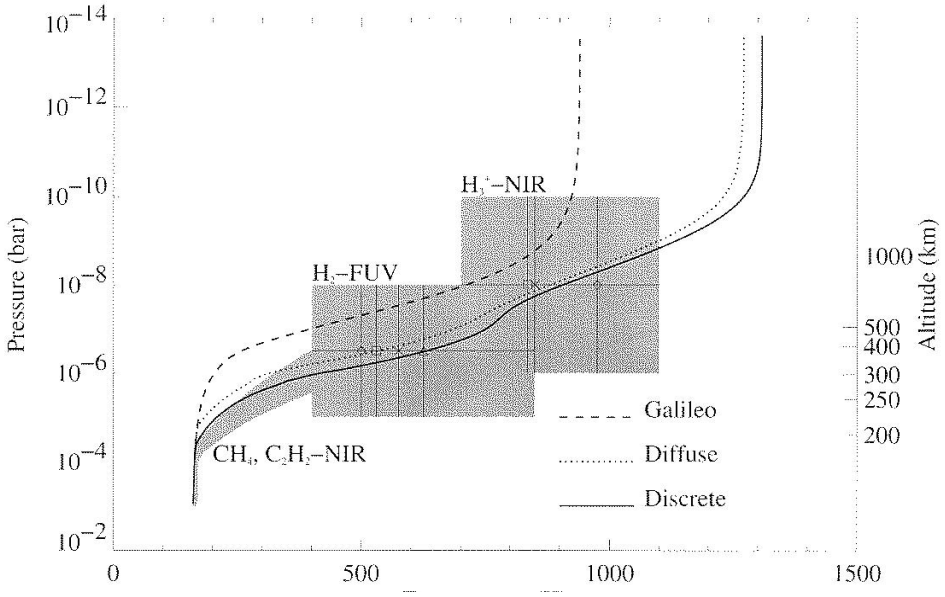

Figure 9.15. A model for the temperature profile in the northern auroral region that satisfies constraints due to H_2 UV and quadrapole emissions and H_3^+ emissions. (From Grodent *et al.* 2001).

south the polarity of both the magnetic and electric fields is the opposite. In both hemispheres, these fields interact to produce an ion wind that flows around the auroral oval, against the rotation of the planet. This ion wind also drags the neutral atmosphere with it. Thus a part of the jovian upper atmosphere is forced into rotation against the rest of the atmosphere, creating frictional forces, which may, in turn, drive an upper atmosphere wind system. Looked at another way, plasma originally generated by Io's volcanoes needs to be accelerated into co-rotation with Jupiter as the planet's magnetic field sweeps through it. Since the plasma is also drifting radially outward as a result of centrifugal forces, this process is occurring at all locations in the plasmasheet, and clearly requires considerable transfer of angular momentum. This angular momentum is in fact being transferred from Jupiter itself, via the magnetic field lines dragging through the upper atmosphere. With Io producing about 1 ton of plasma per second, the planet transfers 7×10^{13} W of rotational energy to the plasmasheet if one approximates the sheet to be in complete co-rotation out to 30 R_J and at the Keplerian velocity thereafter. As far as Jupiter is concerned, the net effect of this process is to slow the planet's rotation down. At the present rate, however, Jupiter will not be brought to a halt by this process until the Universe is several times older than its current age. In summary, this theory predicts zonal winds at auroral latitudes in the anti-rotation direction with speeds a fraction of the rotation velocity. These are just the characteristics observed by Rego *et al.* (1999) and Stallard *et al.* (2001) from H_3^+ observations.

Groups at the University College London (Achilleos *et al.* 1998) and the University of Michigan (Bougher *et al.* 2001) have developed Thermospheric General Circulation Models (TGCMs) of Jupiter's upper atmosphere to study the coupling between the upper atmosphere and magnetosphere and the implications of auroral activity on lower latitudes. Both models solve the primitive equations on a rotating planet, including ion-neutral collision terms. Chemical and physical properties are calculated on a grid of altitude/latitude/longitude points at regular time intervals. These models are computationally expensive, since time intervals need to be short to satisfy dynamical stability requirements and grids need to be fine-scaled enough to simulate the observed properties in sufficient detail to be insightful. Compounding the problem is the fact that thermal time constants on Jupiter, especially at the base of the thermosphere, are long (Achilleos *et al.* 1998). For this reason the models have not yet been run to convergence.

The UCL model is also called the Jovian Ionosphere Model or JIM and is based on the terrestrial Coupled Thermosphere-Ionosphere Model (Fuller-Rowell *et al.* 1996), itself the product of coupled the UCL Thermosphere Model (Fuller-Rowell and Rees, 1980) and the Sheffield ionospheric model of Quegan *et al.* (1982). The JIM grid consists of 40 longitude resolution elements and 91 latitude elements. The altitude grid is expressed on a logarithmic pressure scale with 2.5 levels per scale height. A total of 30 pressure levels are included that extend from 2 μbar to 0.02 nbar. JIM calculates the chemical composition continuously, so as to be able to respond to changing inputs, the time step is set to 4 s. This means that 9000 time steps are required to simulate a jovian day. Full details of the dynamics, which includes hydrostatic equilibrium, Coriolis forces and viscosity, and the chemical reaction scheme are given in Achilleos *et al.* (1998). The model makes use of a simplified magnetic field, an offset tilted dipole (OTD), where the boundaries of the auroral oval are set to match as closely as possible those given by the model of Connerney (1993). Precipitation of auroral electrons is simulated by a single incident energy flux; originally this was set at 10 keV, with a total energy of 8 mW m^{-2}. Additionally, later runs of the model included some low-latitude electron precipitation (Achilleos *et al.* 2000), as well as a polar cap flux. In the polar region a "two-cell" electric field, as used by Quegan *et al.* (1982)

for the Earth has been adopted. Across the auroral oval it is possible to input an electric potential to simulate effects due to plasmasheet generated fields (Achilleos *et al.* 2000; Miller *et al.* 2000). JIM is thus an approximation to Jupiter that simulates basic features and is particularly useful for dealing with rapidly changing inputs.

A somewhat complementary approach to JIM has been taken by Bougher and co-workers at the University of Michigan in producing a jovian TGCM that is a more specific match with Jupiter (Bougher *et al.* 2001). This model extends lower into the jovian atmosphere, to around 20 μbar, so that coupling between the stratosphere and thermosphere/ionosphere may be simulated; this is particularly important for understanding the auroral EUV emission of Jupiter and the cooling effect of stratospheric hydrocarbons. The Michigan model also uses a more realistic magnetic field model, due to Connerney *et al.* (1998), as well as polar cap potentials derived from *Voyager* data, and a more sophisticated electron precipitation spectrum of energies. This model does not work out the detailed chemistry at each time step, however.

In the absence of full details of the Michigan model (at the time this writing), this section will concentrate on what has been learned so far from the JIM model. This model was developed in particular to simulate the effects of energy inputs in the production of ions, especially H_3^+. At the equator, solar EUV at midday produces column densities of H_3^+ of $\sim 7\times10^{15}$ m^{-2}, which fall to less than 1×10^{15} m^{-2} shortly before dawn. H^+ concentrations, on the other hand, vary only by a factor of two, from 5×10^{15}m^{-2} at noon to 2.5×10^{15}m^{-2} in the midnight to dawn sector. This shows the importance for the diurnal variation of the ionosphere of the relatively rapid dissociative recombination of H_3^+ with electrons. In the auroral regions, an 8 mW m^{-2} flux of 10 keV electrons produces N(H_3^+) of several x 10^{16}m^{-2}, with peak local densities of 2.5×10^{11}m^{-3} occurring around the 0.3 μbar level. Corresponding N(H^+) values are similarly of several 10^{16}m^{-2}. But the local density profile is far less peaked, with three maxima of $\sim 4\times10^{10}$m^{-3} occurring at pressures of 0.3 μbar, 1 nbar and 0.1 nbar. Without any MTL precipitation, JIM produces N(H_3^+) latitudinal profiles that have peak densities on the equator and the aurorae, but distinct minima at sub-auroral latitudes, in contrast with the observations (Lam *et al.* 1997, Rego *et al.* 2000). For this reason, MTL precipitation was added, reaching 0.1 of the auroral value at the footprint of the (OTD) L=5 magnetic footprint, and 0 at L=2. With this additional input, the model does match the observed values (Achilleos *et al.* 2000).

The detection by Rego et al. (1999b) of the auroral electrojet prompted a series of studies of the effect of imposing an equatorward voltage across the auroral oval (Achilleos et al., 2000). Results show that ions reach velocities of between 500 m s^{-1} and 1 km s^{-1} for voltages of $\sim$1 MV across the oval. Additionally, neutrals in the auroral oval can be accelerated to between 30% and 70% of the ion velocities, for potentials up to 1MV. These accelerated auroral neutrals, in turn, generate neutral winds in the atmosphere immediately surrounding the ovals, which have considerable meridional components. None, however, appear strong enough to reach all the way to the equator. The ratio between the ion and neutral velocities is an important parameter in models of magnetospheric-ionospheric coupling. Cowley and Bunce (2001) have defined a parameter:

$$k = (\Omega_J - \Omega_N)/(\Omega_J - \Omega_I) \quad (13)$$

where Ω_J is the angular velocity of the planet, in the inertial frame of reference, Ω_N is the angular velocity of the neutral atmosphere in the auroral oval, and Ω_I that of the ions. This parameter modifies the ionospheric conductivity, the height-integrated Pedersen conductivity, Σ_p, as experienced by voltages generated in the magnetosphere: the effective conductivity is given by:

$$\Sigma_p' = (1-k)\Sigma_p \quad (14)$$

This conductivity reduction, in turn, feeds back into the level of Birkeland current that can be produced along the field lines. And, since the field-aligned current is responsible for generating ions and electrons, and thus conductivity, the feedback loop is closed by a further modification of Σ_p' in response to the precipitating electrons. In theory, therefore, it should be possible to combine the results of JIM studies and magnetospheric theory to produce a self-consistent, dynamic picture of the magnetosphere-ionosphere coupling. At present, JIM is being used to simulate varying fluxes of a range of input electron energies, and coupling them with the imposition of equatorward auroral oval voltages up to 10 MV, equivalent to $\sim$10 V m^{-1} in the JIM grid. The model is producing values of $\Sigma_p' \sim 10$ mho, for 100 mW m^{-2} fluxes of 60 keV electrons, with ion velocities of $\sim$1.5 km s^{-1}and k 0.65 for 10 MV potentials (Millward et al., work in progress).

In the runs to date, JIM produces thermally driven auroral ion winds of $\sim$35 m s^{-1} (Achilleos *et al.* 1998). Such relatively slow meridional winds are soon turned in a zonal direction by the strong Coriolis force on Jupiter. It seems unlikely that this will change as the model is run for longer times. If this is the case then the auroral energy may remain confined at high latitudes, contributing in only a minor way to the upper atmospheric energy balance at low latitudes. It also remains possible that energy is carried from the auroral zones to lower latitudes by atmospheric waves rather than meridional winds.

The auroral electrojet and its associated neutral winds are an important source of heating in the auroral atmosphere that has not been taken into account previously, although the Joule heating effect has been well known (see, e.g. Waite *et al.* 1983). Miller *et al.* (2000) showed that a relatively quiet electrojet, produced by a 1 MV potential and the original modest JIM inputs, entrained the neutral atmosphere such that in the auroral oval some 8×10^{15} J of rotational energy was engendered. When they switched off the electric field - the equivalent of bringing the plasmasheet into complete co-rotation - the neutral wind dissipated with a half-life of $\sim$1000 s. Assuming that this energy is eventually converted into heat, this is equivalent to heating the atmosphere at a rate of 8×10^{12} W, a not inconsiderable fraction of the 10^{13}-10^{14} W assumed to power the UV and IR aurorae. Such impulsive changes to the plasmasheet must be rare, if they ever occur, but the observation by Stallard *et al.* (2001) of a doubling of the electrojet velocity over a period of a few days shows that major changes can take place on relatively short timescales. And there has to be continuous frictional generation of heat as a result of the constant acceleration

of neutrals entrained in the electrojet with the surrounding atmosphere. In the steady state, this can also add to the heating of the upper atmosphere planet wide. The relative importance of this effect is an area of active investigation.

9.4 SUMMARY AND OUTLOOK

The most striking aspect of investigations into jovian aeronomy revealed by this review is the variety of powerful techniques for probing Jupiter's upper atmosphere that have become available over the last 15 years. These techniques touched upon virtually every aspect of atmospheric structure. Ion temperatures and densities can be determined through analysis of H_3^+ emissions, and neutral temperatures through analysis of H_2 spectra. The CH_4 density profile can be inferred from CH_4 fluorescence. The spectrum of precipitating electrons in the auroral zone can be inferred from analysis of the H_2 spectrum. The Lyα line profile constrains the H density at low latitudes and the location of electron energy deposition in auroral regions. In principle, it seems possible to obtain a fairly complete characterization of upper atmospheric structure.

Impressive strides have been made through utilization of the new techniques. These include the measurement of ion and (possibly) neutral winds in Jupiter's upper atmosphere, providing a direct means to study the energy flow from magnetosphere to auroral regions and possible lower latitudes. A high quality temperature profile from the *Galileo* probe has provided sufficient information that reasonably constrained investigations into gravity wave heating are possible. The agreement between temperatures determined through analysis of H_2 emission spectra and the *Galileo* probe results verifies the former technique and provides an as yet unexploited means to study global neutral temperature variations. Currently available maps of H_3^+ density and temperature have raised the possibility of a more diffuse aurora than previously suspected and, in conjunction with more sophisticated analysis, should help constrain the enigmatic ionosphere. Finally, the growing sophistication of electron deposition and radiative transfer codes in conjunction with ever-improving spectroscopic and imaging observations have led to the possibility of comprehensive constraints on auroral energy deposition rates.

To take full advantage of these developments will require increased co-ordination among different observations and between observations and models. The primary challenge to the co-ordination of observations is the difficulty of scheduling ground-based and Earth-orbital telescopic observations. The primary tool for the co-ordination of models and observations are the newly developed TGCMs. These models contain sufficient physics to relate diverse observations within a comprehensive framework with a single set of assumptions, while in turn the observations have become sufficiently global in character to adequately constrain the models. Thus, though we have as yet no definitive answers on such major questions as the upper atmospheric energy source or the reason for the variability and vertical structure of electron density. We anticipate substantial progress on these topics in the years to come.

Acknowledgements. RY would like to acknowledge support by NASA's Planetary Atmospheres Program. The authors thank J. McConnell and D. Strobel for helpful reviews.

REFERENCES

Abgrall, H., E. Roueff, F. Launay, J. Y. Roncin, and J. L. Subtil, Table of the Lyman Band system of molecular hydrogen, *A&AS* **101**, 273, 1993a.

Abgrall, H., E. Roueff, F. Launay, J. Y. Roncin, and J. L. Subtil, Table of the Werner Band system of molecular hydrogen, *A&AS* **101**, 323, 1993b.

Achilleos, N., S. Miller, J. Tennyson, A. D. Aylward, I. Mueller-Wodarg, and D. Rees, JIM: A time-dependent, three-dimensional model of Jupiter's thermosphere and ionosphere, *J. Geophys. Res.* **103**, 20,089–20,112, 1998.

Achilleos, N., S. Miller, R. Prangé, G. Millward, and M. K. Dougherty, A dynamical model of Jupiter's auroral electrojet, *New J. Phys.* **3**, 3, 2001.

Adams, N. G. and D. Smith, Recent advances in the studies of reaction rates relevant to interstellar chemistry, in *Astrochemistry*, p. 1, 1987.

Adams, N. G. and D. Smith, Laboratory studies of dissociative recombination and mutual neutralisation and their relevance to interstellar chemistry, in *Rate Coefficients in Astrochemistry*, p. 173, 1988.

Adams, N. G. and D. Smith, FALP studies of positive ion/electron recombination, in *Dissociative recombination: Theory, experiment and applications*, pp. 124–140, 1989.

Ajello, J. M., D. E. Shemansky, W. R. Pryor, A. I. Stewart, K. E. Simmons, T. Majeed, J. H. Waite, G. R. Gladstone, and D. Grodent, Spectroscopic evidence for high-altitude aurora at Jupiter from Galileo Extreme Ultraviolet Spectrometer and Hopkins Ultraviolet Telescope observations, *Icarus* **152**, 151–171, 2001.

Amano, T., Is the dissociative recombination of H_3^+ really slow? A new spectroscopic measurement of the rate constant, *ApJ* **329**, L121–L124, 1988.

Atreya, S. K., *Atmospheres and Ionospheres of the Outer Planets and their Satellites*, Springer-Verlag, 1986.

Atreya, S. K. and T. M. Donahue, Model ionospheres of Jupiter, in *Jupiter, T. Gehrels (ed), University of Arizona Press*, pp. 304–318, 1976.

Atreya, S. K. and T. M. Donahue, Models of the Jovian Upper Atmosphere, *Reviews of Geophysics and Space Physics* **17**, 388–396, 1979.

Atreya, S. K., T. M. Donahue, B. R. Sandel, A. L. Broadfoot, and G. R. Smith, Jovian upper atmospheric temperature measurement by the Voyager 1 UV spectrometer, *Geophys. Res. Lett.* **6**, 795–798, 1979.

Atreya, S. K., T. M. Donahue, and M. Festou, Jupiter - Structure and composition of the upper atmosphere, *ApJ* **247**, L43–L47, 1981.

Atreya, S. K., R. B. Kerr, W. L. Upson, M. C. Festou, T. M. Donahue, E. S. Barker, W. D. Cochran, and J. L. Bertaux, Copernicus measurement of the Jovian Lyman-alpha emission and its aeronomical significance, *ApJ* **262**, 377–387, 1982.

Banks, P. M. and G. Kockarts, *Aeronomy, Part B*, Academic Press, 1973.

Baron, R., R. D. Joseph, T. Owen, J. Tennyson, S. Miller, and G. E. Ballester, Imaging Jupiter's aurorae from H_3^+ emissions in the 3-4 micron band, *Nature* **353**, 539–542, 1991.

Baron, R. L., T. Owen, J. E. P. Connerney, T. Satoh, and J. Harrington, Solar wind control of Jupiter's H_3^+ auroras, *Icarus* **120**, 437–442, 1996.

Bates, D. R., Dissociative recombination when potential energy

curves do not cross , *J. Phys. B Atomic Mol. Phys.* **25**, 5479–5488, 1992.

Bates, D. R., M. F. Guest, and R. A. Kendall, Enigma of H_3^+ dissociative recombination, *Planet. Space Sci.* **41**, 9–15, 1993.

Ben Jaffel, L., J. T. Clarke, R. Prange, G. R. Gladstone, and A. Vidal-Madjar, The Lyman alpha bulge of Jupiter - Effects of non-thermal velocity field, *Geophys. Res. Lett.* **20**, 747–750, 1993.

Ben Jaffel, L., A. Vidal-Madjar, G. R. Gladstone, J. C. McConnell, C. Emerich, R. Prange, and J. T. Clarke, GHRS Detection of the Fossil Deuterium of Jupiter, in *The Scientific Impact of the Goddard High Resolution Spectrograph*, p. 366, 1998.

Bertaux, J. L., M. Festou, E. S. Barker, and E. B. Jenkins, Copernicus measurements of the Lyman-alpha albedo of Jupiter, *ApJ* **238**, 1152–1159, 1980.

Bisikalo, D. V., V. I. Shematovich, J.-C. Gérard, G. R. Gladstone, and J. H. Waite, The distribution of hot hydrogen atoms produced by electron and proton precipitation in the Jovian aurora, *J. Geophys. Res.* **101**, 21,157–21,168, 1996.

Bohme, D. K., G. I. Mackay, and H. I. Schiff, Determination of proton affinities from the kinetics of proton transfer reactions. VII. The proton affinities of O_2, H_2, Kr, O, N_2, Xe, CO_2, CH_4, N_2O, and CO, *J. Chem. Phys.* **73**, 4976–4986, 1980.

Broadfoot, A. L., M. J. Belton, P. Z. Takacs, B. R. Sandel, D. E. Shemansky, J. B. Holberg, J. M. Ajello, H. W. Moos, S. K. Atreya, T. M. Donahue, J. L. Bertaux, J. E. Blamont, D. F. Strobel, J. C. McConnell, R. Goody, A. Dalgarno, and M. B. McElroy, Extreme ultraviolet observations from Voyager 1 encounter with Jupiter, *Science* **204**, 979–982, 1979.

Broadfoot, A. L., B. R. Sandel, D. E. Shemansky, J. C. McConnell, G. R. Smith, J. B. Holberg, S. K. Atreya, T. M. Donahue, D. F. Strobel, and J. L. Bertaux, Overview of the Voyager ultraviolet spectrometry results through Jupiter encounter, *J. Geophys. Res.* **86**, 8259–8284, 1981.

Broadfoot, A. L., F. Herbert, J. B. Holberg, D. M. Hunten, S. Kumar, B. R. Sandel, D. E. Shemansky, A. J. Dessler, S. Linick, and R. Springer, Ultraviolet spectrometer observations of Uranus, *Science* **233**, 74–79, 1986.

Caldwell, J., F. C. Gillett, and A. T. Tokunaga, Possible infrared aurorae on Jupiter, *Icarus* **44**, 667–675, 1980.

Caldwell, J., A. T. Tokunaga, and G. S. Orton, Further observations of 8-micron polar brightenings of Jupiter, *Icarus* **53**, 133–140, 1983.

Canosa, A., J. C. Gomet, B. R. Rowe, J. B. A. Mitchell, and J. L. Queffelec, Further measurements of the H_3^+ (v = 0,1,2) dissociative recombination rate coefficient, *J. Chem. Phys.* **97**, 1028–1037, 1992.

Carlson, R. W. and D. L. Judge, Pioneer 10 ultraviolet photometer observations at Jupiter encounter, *J. Geophys. Res.* **79**, 3623–3633, 1974.

Chen, R. H., Time-dependent calculations of Jupiter's ionosphere, *J. Geophys. Res.* **87**, 167–170, 1982.

Clarke, J. T. and G. R. Gladstone, The center to limb variation in Jupiter's H LY alpha emission, *J. Geophys. Res.* **95**, 21,281–21,284, 1990.

Clarke, J. T., H. A. Weaver, P. D. Feldman, H. W. Moos, W. G. Fastie, and C. B. Opal, Spatial imaging of hydrogen Lyman-alpha emission from Jupiter, *ApJ* **240**, 696–701, 1980.

Clarke, J. T., J. Trauger, and J. H. Waite, Doppler shifted H LY alpha emission from Jupiter's aurora, *Geophys. Res. Lett.* **16**, 587–590, 1989.

Clarke, J. T., G. R. Gladstone, and L. Ben Jaffel, Jupiter's dayglow H LY alpha emission line profile, *Geophys. Res. Lett.* **18**, 1935–1938, 1991.

Clarke, J. T., L. Ben Jaffel, A. Vidal-Madjar, G. R. Gladstone, J. H. J. Waite, R. Prange, J. Gerard, J. Ajello, and G. James, Hubble Space Telescope Goddard high-resolution spectrograph H2 rotational spectra of Jupiter's aurora, *ApJ* **430**, L73–L76, 1994.

Clarke, J. T., G. Ballester, J. Trauger, J. Ajello, W. Pryor, K. Tobiska, J. E. P. Connerney, G. R. Gladstone, J. H. Waite, L. Ben Jaffel, and J. Gérard, Hubble Space Telescope imaging of Jupiter's UV aurora during the Galileo orbiter mission, *J. Geophys. Res.* **103**, 20,217–20,236, 1998.

Cochran, W. D. and E. S. Barker, Variability of Lyman-alpha emission from Jupiter, *ApJ* **234**, L151–L154, 1979.

Connerney, J. E. P., Magnetic fields of the outer planets, *J. Geophys. Res.* **98**, 18,659, 1993.

Connerney, J. E. P., R. Baron, T. Satoh, and T. Owen, Images of Excited H_3^+ at the Foot of the Io Flux Tube in Jupiter's Atmosphere, *Science* **262**, 1035–1038, 1993.

Connerney, J. E. P., M. H. Acuña, N. F. Ness, and T. Satoh, New models of Jupiter's magnetic field constrained by the Io flux tube footprint, *J. Geophys. Res.* **103**, 11,929–11,940, 1998.

Cowley, S. W. H. and E. J. Bunce, Origin of the main auroral oval in Jupiter's coupled magnetosphere- ionosphere system, *Planet. Space Sci.* **49**, 1067–1088, 2001.

Cravens, T. E., Vibrationally excited molecular hydrogen in the upper atmosphere of Jupiter, *J. Geophys. Res.* **92**, 11,083–11,100, 1987.

Cravens, T. E., E. Howell, J. H. Waite, and G. R. Gladstone, Auroral oxygen precipitation at Jupiter, *J. Geophys. Res.* **100**, 17,153–17,162, 1995.

Dalgarno, A., M. Yan, and W. Liu, Electron energy deposition in a gas mixture of atomic and molecular hydrogen and helium, *ApJS* **125**, 237–256, 1999.

Datz, S., G. Sundström, C. Biedermann, L. Broström, H. Danared, S. Mannervik, J. R. Mowat, and M. Larsson, Branching processes in the dissociative recombination of H_3^+, *Phys. Rev. Lett.* **74**, 896–899, 1995.

del Genio, A. D., J. M. Straus, and G. Schubert, Effects of wave-induced diffusion on thermospheric acoustic-gravity waves, *Geophys. Res. Lett.* **5**, 265–267, 1978.

del Genio, A. D., G. Schubert, and J. M. Straus, Characteristics of acoustic-gravity waves in a diffusively separated atmosphere, *J. Geophys. Res.* **84**, 1865–1879, 1979a.

del Genio, A. D., G. Schubert, and J. M. Straus, Gravity wave propagation in a diffusively separated atmosphere with height-dependent collision frequencies, *J. Geophys. Res.* **84**, 4371–4378, 1979b.

Dessler, A. J., B. R. Sandel, and S. K. Atreya, The Jovian hydrogen bulge - Evidence for co-rotating magnetospheric convection, *Planet. Space Sci.* **29**, 215–224, 1981.

Dols, V., J. C. Gérard, J. T. Clarke, J. Gustin, and D. Grodent, Diagnostics of the Jovian Aurora Deduced from Ultraviolet Spectroscopy: Model and HST/GHRS Observations, *Icarus* **147**, 251–266, 2000.

Drossart, P., B. Bezard, S. Atreya, J. Lacy, and E. Serabyn, Enhanced acetylene emission near the north pole of Jupiter, *Icarus* **66**, 610–618, 1986.

Drossart, P., J.-P. Maillard, J. Caldwell, S. J. Kim, J. K. G. Watson, W. A. Majewski, J. Tennyson, S. Miller, S. K. Atreya, J. T. Clarke, J. H. Waite, and R. Wagener, Detection of H_3^+ on Jupiter, *Nature* **340**, 539–541, 1989.

Drossart, P., B. Bezard, S. K. Atreya, J. Bishop, J. H. Waite, and D. Boice, Thermal profiles in the auroral regions of Jupiter, *J. Geophys. Res.* **98**, 18,803, 1993a.

Drossart, P., J.-P. Maillard, J. Caldwell, and J. Rosenqvist, Line-resolved spectroscopy of the Jovian H_3^+ auroral emission at 3.5 micrometers, *ApJ* **402**, L25–L28, 1993b.

Drossart, P., T. Fouchet, J. Crovisier, E. Lellouch, T. Encrenaz, H. Feuchtgruber, and J. P. Champion, Fluorescence in the 3μm bands of methane on Jupiter and Saturn from ISO/SWS observations, in *ESA SP-427: The Universe as Seen by ISO*, p. 169, 1999.

Dungey, J. W., Interplanetary Magnetic Field and the Auroral Zones , *Phys. Rev. Lett.* **6**, 47–48, 1961.

Emerich, C., L. Ben Jaffel, and R. Prange, On the analysis of the H Lyman-alpha dayglow of Jupiter, Saturn and Uranus, *Planet. Space Sci.* **41**, 363–371, 1993.

Emerich, C., L. Ben Jaffel, J. T. Clarke, R. Prange, G. R. Gladstone, J. Sommeria, and G. Ballester, Evidence for supersonic turbulence in the upper atmosphere of Jupiter, *Science* **273**, 1085–1087, 1996.

Eshleman, V. R., G. L. Tyler, G. E. Wood, G. F. Lindal, J. D. Anderson, G. S. Levy, and T. A. Croft, Radio science with Voyager at Jupiter - Initial Voyager 2 results and a Voyager 1 measure of the Io torus, *Science* **206**, 959–962, 1979.

Feldman, P. D. and W. G. Fastie, Fluorescence of Molecular Hydrogen Excited by Solar Extreme- Ultraviolet Radiation., *ApJ* **185**, L101+, 1973.

Feldman, P. D., M. A. McGrath, H. W. Moos, S. T. Durrance, D. F. Strobel, and A. F. Davidsen, The spectrum of the Jovian dayglow observed at 3 A resolution with the Hopkins ultraviolet telescope, *ApJ* **406**, 279–284, 1993.

Festou, M. C., S. K. Atreya, T. M. Donahue, B. R. Sandel, D. E. Shemansky, and A. L. Broadfoot, Composition and thermal profiles of the Jovian upper atmosphere determined by the Voyager ultraviolet stellar occultation experiment, *J. Geophys. Res.* **86**, 5715–5725, 1981.

Fjeldbo, G., A. Kliore, B. Seidel, D. Sweetnam, and D. Cain, The Pioneer 10 radio occultation measurements of the ionosphere of Jupiter, *A&A* **39**, 91–96, 1975.

French, R. G. and P. J. Gierasch, Waves in the jovian upper atmosphere, *J. Atmos. Sci.* **31**, 1707–1712, 1974.

Frommhold, L., R. Samuelson, and G. Birnbaum, Hydrogen dimer structures in the far-infrared spectra of Jupiter and Saturn, *ApJ* **283**, L79–L82, 1984.

Fuller-Rowell, T. J. and D. Rees, A three-dimensional time-dependent global model of the thermosphere, *J. Atmos. Sci.* **37**, 2545–2567, 1980.

Gerard, J., V. Dols, R. Prange, and F. Paresce, The morphology of the north Jovian ultraviolet aurora observed with the Hubble Space Telescope, *Planet. Space Sci.* **42**, 905–917, 1994.

Gerard, J.-C. and V. Singh, A model of energy deposition of energetic electrons and EUV emission in the Jovian and Saturnian atmospheres and implications, *J. Geophys. Res.* **87**, 4525–4532, 1982.

Giles, J. W., H. W. Moos, and W. R. McKinney, The far ultraviolet /1200-1900 A/ spectrum of Jupiter obtained with a rocket-borne multichannel spectrometer, *J. Geophys. Res.* **81**, 5797–5806, 1976.

Gladstone, G. R., UV resonance line dayglow emissions on earth and Jupiter, *J. Geophys. Res.* **93**, 14,623–14,630, 1988.

Gladstone, G. R., Auroral resonance line radiative transfer, *J. Geophys. Res.* **97**, 1377–1387, 1992.

Gladstone, G. R., D. T. Hall, and J. H. J. Waite, EUVE observations of Jupiter during the impact of Comet Shoemaker- Levy 9, *Science* **268**, 1595–1597, 1995.

Gladstone, G. R., M. Allen, and Y. L. Yung, Hydrocarbon Photochemistry in the Upper Atmosphere of Jupiter, *Icarus* **119**, 1–52, 1996.

Gladstone, G. R., J. H. Waite, D. Grodent, W. S. Lewis, F. J. Crary, R. F. Elsner, M. C. Weisskopf, T. Majeed, J.-M. Jahn, A. Bhardwaj, J. T. Clarke, D. T. Young, M. K. Dougherty, S. A. Espinosa, and T. E. Cravens, A pulsating auroral X-ray hot spot on Jupiter, *Nature* **415**, 1000–1003, 2002.

Grodent, D., J. H. J. Waitè, and J. Gérard, A self-consistent model of the Jovian auroral thermal structure, *J. Geophys. Res.* **106**, 12,933–12,952, 2001.

Gross, S. H. and S. I. Rasool, The upper atmosphere of Jupiter, *Icarus* **3**, 311, 1964.

Herbert, F., B. R. Sandel, R. V. Yelle, J. B. Holberg, A. L. Broadfoot, D. E. Shemansky, S. K. Atreya, and P. N. Romani, The upper atmosphere of Uranus: EUV occultations observed by Voyager 2, *J. Geophys. Res.* **92**, 15,093–15,109, 1987.

Hickey, M. P., R. L. Walterscheid, and G. Schubert, Gravity wave heating and cooling in Jupiter's thermosphere, *Icarus* **148**, 266–281, 2000.

Hill, T. W., Inertial limit on corotation, *J. Geophys. Res.* **84**, 6554–6558, 1979.

Hill, T. W., The Jovian auroral oval, *J. Geophys. Res.* **106**, 8101–8108, 2001.

Hill, T. W. and A. J. Dessler, Plasma motions in planetary magnetospheres, *Science* **252**, 410–415, 1991.

Hines, C. O., Relaxational dissipation in atmospheric waves. I - Basic formulation. II - Application to earth's upper atmosphere, *Planet. Space Sci.* **25**, 1045–1074, 1977.

Hinson, D. P., F. M. Flasar, A. J. Kliore, P. J. Schinder, J. D. Twicken, and R. G. Herrera, Jupiter's ionosphere: Results from the first Galileo radio occultation experiment, *Geophys. Res. Lett.* **24**, 2107, 1997.

Hinson, D. P., J. D. Twicken, and E. Tuna Karayel, Jupiter's ionosphere: New results from Voyager 2 radio occultation measurements, *J. Geophys. Res.* **103**, 9505–9520, 1998.

Holberg, J. B., W. T. Forrester, D. E. Shemansky, and D. C. Barry, Voyager absolute far-ultraviolet spectrophotometry of hot stars, *ApJ* **257**, 656–671, 1982.

Horanyi, M., T. E. Cravens, and J. H. Waite, The precipitation of energetic heavy ions into the upper atmosphere of Jupiter, *J. Geophys. Res.* **93**, 7251–7271, 1988.

Hubbard, W. B., V. Haemmerle, C. C. Porco, G. H. Rieke, and M. J. Rieke, The occultation of SAO 78505 by Jupiter, *Icarus* **113**, 103–109, 1995.

Hunten, D. M. and A. J. Dessler, Soft electrons as a possible heat source for Jupiter's thermosphere, *Planet. Space Sci.* **25**, 817–821, 1977.

Judge, D. L. and R. W. Carlson, Pioneer 10 observations of the ultraviolet glow in the vicinity of Jupiter, *Science* **183**, 317–318, 1974.

Karayel, E. T. and D. P. Hinson, Sub-Fresnel-scale vertical resolution in atmospheric profiles from radio occultation, *Radio Science* **32**, 411–424, 1997.

Kim, S. and W. Maguire, Two micron quadrupole line emission of H2 from the Jovian auroral zone, in *Jovian Atmospheres*, pp. 95–98, 1986.

Kim, S., P. Drossart, J. Caldwell, and J.-P. Maillard, Temperatures of the Jovian auroral zone inferred from 2-micron H2 quadrupole line observations, *Icarus* **84**, 54–61, 1990.

Kim, S. J., J. Caldwell, A. R. Rivolo, R. Wagener, and G. S. Orton, Infrared polar brightening on Jupiter. III - Spectrometry from the Voyager 1 IRIS experiment, *Icarus* **64**, 233–248, 1985.

Kim, S. J., P. Drossart, J. Caldwell, J. Maillard, T. Herbst, and M. Shure, Images of aurorae on Jupiter from H_3^+ emission at 4 microns, *Nature* **353**, 536–539, 1991.

Kim, Y. H., J. L. Fox, and H. S. Porter, Densities and vibrational distribution of H_3^+ in the Jovian auroral ionosphere, *J. Geophys. Res.* **97**, 6093–6101, 1992.

Kim, Y. H., J. J. Caldwell, and J. L. Fox, High-resolution ultraviolet spectroscopy of Jupiter's aurora with the Hubble Space Telescope, *ApJ* **447**, 906, 1995.

Kim, Y. H., J. L. Fox, and J. J. Caldwell, Temperatures and altitudes of Jupiter's ultraviolet aurora inferred from GHRS observations with the Hubble Space Telescope, *Icarus* **128**, 189–201, 1997.

Lam, H. A., N. Achilleos, S. Miller, J. Tennyson, L. M. Trafton, T. R. Geballe, and G. E. Ballester, A baseline spectroscopic study of the infrared auroras of Jupiter, *Icarus* **127**, 379–393, 1997.

Lellouch, E., B. Bézard, T. Fouchet, H. Feuchtgruber, T. Encre-

naz, and T. de Graauw, The deuterium abundance in Jupiter and Saturn from ISO-SWS observations, *A&A* **370**, 610–622, 2001.

Leu, M. T., M. A. Biondi, and R. Johnsen, Measurements of recombination of electrons with H_3^+ and H_5^+ Ions, *Phys. Rev. A* **8**, 413–419, 1973.

Liu, W. and A. Dalgarno, The ultraviolet spectra of the Jovian aurora, *ApJ* **467**, 446, 1996a.

Liu, W. and A. Dalgarno, The ultraviolet spectrum of the Jovian dayglow, *ApJ* **462**, 502, 1996b.

Liu, W. and D. R. Schultz, Jovian x-ray aurora and energetic oxygen ion precipitation, *ApJ* **526**, 538–543, 1999.

Mahaffy, P. R., T. M. Donahue, S. K. Atreya, T. C. Owen, and H. B. Niemann, Galileo Probe Measurements of D/H and 3He/4He in Jupiter's Atmosphere, *Space Sci. Rev.* **84**, 251–263, 1998.

Maillard, J., P. Drossart, J. K. G. Watson, S. J. Kim, and J. Caldwell, H_3^+ fundamental band in Jupiter's auroral zones at high resolution from 2400 to 2900 inverse centimeters, *ApJ* **363**, L37–L41, 1990.

Majeed, T. and J. C. McConnell, The upper ionospheres of Jupiter and Saturn, *Planet. Space Sci.* **39**, 1715–1732, 1991.

Majeed, T., J. C. McConnell, and G. R. Gladstone, A model analysis of Galileo electron densities on Jupiter, *Geophys. Res. Lett.* **26**, 2335, 1999.

Majewski, W. A., P. A. Feldman, J. K. G. Watson, S. Miller, and J. Tennyson, Laboratory observation of the $2\nu 2$ band of the H_3^+ molecular ion, *ApJ* **347**, L51–L54, 1989.

Matcheva, K. I. and D. F. Strobel, Heating of Jupiter's thermosphere by dissipation of gravity waves due to molecular viscosity and heat conduction, *Icarus* **140**, 328–340, 1999.

Matcheva, K. I., D. F. Strobel, and F. M. Flasar, Interaction of gravity waves with ionospheric plasma: Implicationsfor jupiter's ionosphere, *Icarus* **152**, 347–365, 2001.

Mathur, D., S. U. Khan, and J. B. Hasted, Collision processes of electron with molecular hydrogen ions, *J. Phys. B Atomic Mol. Phys.* **12**, 2043–2050, 1979.

Maurellis, A. N., T. E. Cravens, G. R. Gladstone, J. H. Waite, and L. W. Acton, Jovian x-ray emission from solar x-ray scattering, *Geophys. Res. Lett.* **27**, 1339, 2000.

McConnell, J. C. and T. Majeed, H_3^+ in the Jovian ionosphere, *J. Geophys. Res.* **92**, 8570–8578, 1987.

McConnell, J. C., B. R. Sandel, and A. L. Broadfoot, Airglow from Jupiter's nightside and crescent - Ultraviolet spectrometer observations from Voyager 2, *Icarus* **43**, 128–142, 1980.

McConnell, J. C., B. R. Sandel, and A. L. Broadfoot, Voyager U.V. spectrometer observations of He 584 A dayglow at Jupiter, *Planet. Space Sci.* **29**, 283–292, 1981.

McConnell, J. C., J. B. Holdberg, G. R. Smith, B. R. Sandel, D. E. Shemansky, and A. L. Broadfoot, A new look at the ionosphere of Jupiter in light of the UVS occultation results, *Planet. Space Sci.* **30**, 151–167, 1982.

McElroy, M. B., The ionospheres of the major planets, *Space Sci. Rev.* **14**, 559, 1973.

McGowan, J. W., P. M. Mul, V. S. D'Angelo, J. B. A. Mitchell, P. Defrance, and H. R. Froelich, Energy dependence of dissociative recombination below 0.08 eV measured with (electron-ion) merged-beam technique, *Phys. Rev. Lett.* **42**, 373–375, 1979.

McGrath, M. A., An unusual change in the Jovian Lyman-alpha bulge, *Geophys. Res. Lett.* **18**, 1931–1934, 1991.

McGrath, M. A., P. D. Feldman, G. E. Ballester, and H. W. Moos, IUE observations of the Jovian dayglow emission, *Geophys. Res. Lett.* **16**, 583–586, 1989.

McKellar, A. R. W., Possible identification of sharp features in the Voyager far- infrared spectra of Jupiter and Saturn, *Canadian J. Phys.* **62**, 760–763, 1984.

Metzger, A. E., D. A. Gilman, J. L. Luthey, K. C. Hurley, H. W. Schnopper, F. D. Seward, and J. D. Sullivan, The detection of x-rays from Jupiter, *J. Geophys. Res.* **88**, 7731–7741, 1983.

Michels, H. H. and R. H. Hobbs, Low-temperature dissociative recombination of $e^- + H_3^+$, *ApJ* **286**, L27–L29, 1984.

Miller, S. and J. Tennyson, Calculated rotational and rovibrational transitions in the spectrum of H_3^+, *ApJ* **335**, 486–490, 1988.

Miller, S., J. Tennyson, and R. D. Joseph, Infrared emissions of H_3^+ in the atmosphere of Jupiter in the 2.1 and 4.0 micron region, *ApJ* **360**, L55–L58, 1990.

Miller, S., N. Achilleos, G. E. Ballester, H. A. Lam, J. Tennyson, T. R. Geballe, and L. M. Trafton, Mid-to-Low Latitude H_3^+ Emission from Jupiter, *Icarus* **130**, 57–67, 1997.

Miller, S., N. Achilleos, G. E. Ballester, T. R. Geballe, R. D. Joseph, R. Prange, D. Rego, T. Stallard, J. Tennyson, L. M. Trafton, and J. H. Waite, The role of H_3^+ in planetary atmospheres, *Royal Society of London Philosophical Transactions Series A* **358**, 2485–2502, 2000.

Mitchell, J. B. A., J. L. Forand, C. T. Ng, D. P. Levac, R. E. Mitchell, P. M. Mul, W. Claeys, A. Sen, and J. W. McGowan, Measurement of the branching ratio for the dissociative recombination of H_3^++e, *Physical Review Letters* **51**, 885–888, 1983.

Moos, H. W., W. G. Fastie, and M. Bottema, Rocket measurement of ultraviolet spectra of Venus and Jupiter between 1200 and 1800 Å, *ApJ* **155**, 887, 1969.

Morrissey, P. F., P. D. Feldman, J. T. Clarke, B. C. Wolven, D. F. Strobel, S. T. Durrance, and J. T. Trauger, Simultaneous spectroscopy and imaging of the jovian aurora with the Hopkins Ultraviolet Telescope and the Hubble Space Telescope, *ApJ* **476**, 918, 1997.

Nagy, A. F., W. L. Chameides, R. H. Chen, and S. K. Atreya, Electron temperatures in the Jovian ionosphere, *J. Geophys. Res.* **81**, 5567–5569, 1976.

Oka, T., Observation of the infrared spectrum of H_3^+, *Phys. Rev. Lett.* **45**, 531–534, 1980.

Oka, T. and T. R. Geballe, Observations of the 4 micron fundamental band of H_3^+ in Jupiter, *ApJ* **351**, L53–L56, 1990.

Pan, F.-S. and T. Oka, Calculated forbidden rotational spectra of H_3^+, *ApJ* **305**, 518–525, 1986.

Parkinson, C. D., E. Griffioen, J. C. McConnell, L. B. Jaffel, A. Vidal-Madjar, J. T. Clarke, and G. R. Gladstone, Estimates of atomic deuterium abundance and lyman-alpha airglow in the thermosphere of Jupiter, *Geophys. Res. Lett.* **26**, 3177, 1999.

Peart, B. and K. T. Dolder, The production of de-excited H_3^+ ions and measurements of the energies of two electronically-excited states , *Journal of Physics B Atomic Molecular Physics* **7**, 1567–1573, 1974.

Perry, J. J., Y. H. Kim, J. L. Fox, and H. S. Porter, Chemistry of the Jovian auroral ionosphere, *J. Geophys. Res.* **104**, 16,451, 1999.

Prange, R., D. Rego, L. Pallier, L. Ben Jaffel, C. Emerich, J. Ajello, J. T. Clarke, and G. E. Ballester, Detection of self-reversed Ly alpha lines from the jovian aurorae with the Hubble Space Telescope, *ApJ* **484**, L169+, 1997.

Quegan, S., G. J. Bailey, R. J. Moffett, R. A. Heelis, T. J. Fuller-Rowell, D. Rees, and R. W. Spiro, A theoretical study of the distribution of ionization in the high- latitude ionosphere and the plasmasphere - First results on the mid-latitude trough and the light-ion trough, *J. Atmos. Terr. Phys.* **44**, 619–640, 1982.

Rego, D., R. Prange, and J. Gerard, Auroral Lyman alpha and H_2 bands from the giant planets: 1. Excitation by proton precipitation in the jovian atmosphere, *J. Geophys. Res.* **99**, 17,075–17,094, 1994.

Rego, D., R. Prangé, and L. Ben Jaffel, Auroral Lyman α and H_2 bands from the giant planets 3. Lyman α spectral profile

including charge exchange and radiative transfer effects and H_2 color ratios, *J. Geophys. Res.* **104**, 5939–5954, 1999.

Rego, D., S. Miller, N. Achilleos, R. Prangé, and R. D. Joseph, Latitudinal profiles of the jovian IR emissions of H_3^+ at 4 μm with the NASA Infrared Telescope Facility: Energy inputs and thermal balance, *Icarus* **147**, 366–385, 2000.

Rego, D., J. T. Clarke, L. B. Jaffel, G. E. Ballester, R. Prangé, and J. McConnell, The analysis of the H Lyman α emission line profile from Jupiter's aurora, *Icarus* **150**, 234–243, 2001.

Sandel, B. R., A. L. Broadfoot, and D. F. Strobel, Discovery of a longitudinal asymmetry in the H Lyman-alpha brightness of Jupiter, *Geophys. Res. Lett.* **7**, 5–8, 1980.

Satoh, T. and J. E. P. Connerney, Jupiter's H_3^+ emissions viewed in corrected jovimagnetic coordinates, *Icarus* **141**, 236–252, 1999.

Satoh, T., J. E. P. Connerney, and R. L. Baron, Emission source model of Jupiter's H_3^+ aurorae: A generalized inverse analysis of images, *Icarus* **122**, 1–23, 1996.

Schauer, M. M., S. R. Jefferts, S. E. Barlow, and G. H. Dunn, Reactions of H_2 with He^+ at temperatures below 40 K, *J. Chem. Phys.* **91**, 4593–4596, 1989.

Seiff, A., D. B. Kirk, T. C. D. Knight, L. A. Young, F. S. Milos, E. Venkatapathy, J. D. Mihalov, R. C. Blanchard, R. E. Young, and G. Schubert, Thermal structure of Jupiter's upper atmosphere derived from the Galileo probe, *Science* **276**, 102–104, 1997.

Seiff, A., D. B. Kirk, T. C. D. Knight, R. E. Young, J. D. Mihalov, L. A. Young, F. S. Milos, G. Schubert, R. C. Blanchard, and D. Atkinson, Thermal structure of Jupiter's atmosphere near the edge of a 5- micron hot spot in the north equatorial belt, *J. Geophys. Res.* **103**, 22,857–22,890, 1998.

Shemansky, D. E., An explanation for the H Ly-alpha longitudinal asymmetry in the equatorial spectrum of Jupiter - an outcrop of paradoxical energy deposition in the exosphere, *J. Geophys. Res.* **90**, 2673–2694, 1985.

Shemansky, D. E. and J. M. Ajello, The Saturn spectrum in the EUV - Electron excited hydrogen, *J. Geophys. Res.* **88**, 459–464, 1983.

Shemansky, D. E. and D. L. Judge, Evidence for change in particle excitation of Jupiter's atmosphere 1968-1979, *J. Geophys. Res.* **93**, 21–28, 1988.

Shemansky, D. E. and G. R. Smith, The implication for the presence of a magnetosphere on Uranus in the relationship of EUV and radio emission, *Geophys. Res. Lett.* **13**, 2–5, 1986.

Skinner, T. E., M. T. Deland, G. E. Ballester, K. A. Coplin, P. D. Feldman, and H. W. Moos, Temporal variation of the jovian H I Lyman alpha emission (1979- 1986), *J. Geophys. Res.* **93**, 29–34, 1988.

Smith, G. R. and D. M. Hunten, Study of planetary atmospheres by absorptive occultations, *Rev. Geophys.* **28**, 117–143, 1990.

Sommeria, J., L. Ben Jaffel, and R. Prange, On the existence of supersonic jets in the upper atmosphere of Jupiter., *Icarus* **118**, 2–24, 1995.

Southwood, D. J. and M. G. Kivelson, A new perspective concerning the influence of the solar wind on the Jovian magnetosphere, *J. Geophys. Res.* **106**, 6123–6130, 2001.

Stallard, T., S. Miller, G. Millward, and R. D. Joseph, On the dynamics of the jovian ionosphere and thermosphere. i. the measurement of ion winds, *Icarus* **154**, 475–491, 2001.

Stallard, T., S. Miller, G. Millward, and R. D. Joseph, On the dynamics of the jovian ionosphere and thermosphere. ii. the measurement of H_3^+ vibrational temperature, column density, and total emission, *Icarus* **156**, 498–514, 2002.

Storey, P. J. and D. G. Hummer, Recombination line intensities for hydrogenic ions-IV. Total recombination coefficients and machine-readable tables for Z=1 to 8, *MNRAS* **272**, 41–48, 1995.

Strobel, D. F., Aeronomic systems of planets, moons, and comets, in *Atmospheres of the Solar System*, pp. 7–22, AGU, 2002.

Strobel, D. F. and S. K. Atreya, Ionosphere, in *Physics of the Jovian Magnetosphere, A.J. Dessler (ed), cambridge University Press*, pp. 51–67, 1983.

Trafton, L., Uranus' (3-0) H_2 quadrupole line profiles, *Icarus* **70**, 13–30, 1987.

Trafton, L., D. F. Lester, and K. L. Thompson, Unidentified emission lines in Jupiter's northern and southern 2-micron aurorae, *ApJ* **343**, L73–L76, 1989.

Trafton, L. M. and J. K. G. Watson, Occurrence of global-scale emissions on Jupiter - Proposed identification of jovian dimer H_2 emission, *ApJ* **385**, 320–326, 1992.

Trafton, L. M., J. C. Gerard, G. Munhoven, and J. H. Waite, High-resolution spectra of Jupiter's northern auroral ultraviolet emission with the Hubble Space Telescope, *ApJ* **421**, 816–827, 1994.

Trafton, L. M., S. Miller, T. R. Geballe, J. Tennyson, and G. E. Ballester, H_2 quadrupole and H_3^+ emission from Uranus: The Uranian thermosphere, ionosphere, and aurora, *ApJ* **524**, 1059–1083, 1999.

Vervack, R. J., B. R. Sandel, G. R. Gladstone, J. C. McConnell, and C. D. Parkinson, Jupiter's He 584 A dayglow: New results., *Icarus* **114**, 163–173, 1995.

Waite, J. H., T. E. Cravens, J. Kozyra, A. F. Nagy, S. K. Atreya, and R. H. Chen, Electron precipitation and related aeronomy of the Jovian thermosphere and ionosphere, *J. Geophys. Res.* **88**, 6143–6163, 1983.

Waite, J. H., J. T. Clarke, T. E. Cravens, and C. M. Hammond, The Jovian Aurora - Electron or ion precipitation?, *J. Geophys. Res.* **93**, 7244–7250, 1988.

Waite, J. H., F. Bagenal, F. Seward, C. Na, G. R. Gladstone, T. E. Cravens, K. C. Hurley, J. T. Clarke, R. Elsner, and S. A. Stern, ROSAT observations of the Jupiter aurora, *J. Geophys. Res.* **99**, 14,799, 1994.

Waite, J. H., G. R. Gladstone, W. S. Lewis, P. Drossart, T. E. Cravens, A. N. Maurellis, B. H. Mauk, and S. Miller, Equatorial x-ray emissions: Implications for Jupiter's high exospheric temperatures, *Science* **276**, 104–108, 1997.

Wallace, L. and D. M. Hunten, The Lyman-alpha albedo of Jupiter, *ApJ* **182**, 1013, 1973.

Walterscheid, R. L., Dynamical cooling induced by dissipating internal gravity waves, *Geophys. Res. Lett.* **8**, 1235–1238, 1981.

Wolven, B. C. and P. D. Feldman, Self-absorption by vibrationally excited H_2 in the Astro-2 Hopkins Ultraviolet Telescope spectrum of the jovian aurora, *Geophys. Res. Lett.* **25**, 1537, 1998.

Yelle, R. V., H_2 emissions from the outer planets, *Geophys. Res. Lett.* **15**, 1145–1148, 1988.

Yelle, R. V., B. R. Sandel, A. L. Broadfoot, and J. C. McConnell, The dependence of electroglow on the solar flux, *J. Geophys. Res.* **92**, 15,110–15,124, 1987.

Yelle, R. V., L. A. Young, R. J. Vervack, R. Young, L. Pfister, and B. R. Sandel, Structure of Jupiter's upper atmosphere: Predictions for Galileo, *J. Geophys. Res.* **101**, 2149–2162, 1996.

Yousif, F. B. and J. B. A. Mitchell, Recombination and excitation of HeH^+, *Phys. Rev. A* **40**, 4318–4321, 1989.

Yung, Y. L. and D. F. Strobel, Hydrocarbon photochemistry and Lyman alpha albedo of Jupiter, *ApJ* **239**, 395–402, 1980.

Yung, Y. L., G. R. Gladstone, K. M. Chang, J. M. Ajello, and S. K. Srivastava, H_2 fluorescence spectrum from 1200 to 1700 A by electron impact - Laboratory study and application to Jovian aurora, *ApJ* **254**, L65–L69, 1982.